VIBRATIONAL SPECTRA OF SOME DODECABORATE SALTS

Abdel-Fattah

VIBRATIONAL SPECTRA OF SOME ICOSAHEDRAL DODECABORATE SALTS

BY

Mohamed Abdel-Fattah

A thesis submitted to the Faculty of Graduate Studies and research in partial fulfilment of the requirements for the degree of Master of Science

Department of Chemistry,
McGill University,
Montreal, Quebec,
CANADA.

September 1976

ABSTRACT

M.Sc. Mohamed Abdel-Fattah Chemistry

VIBRATIONAL SPECTRA OF SOME
ICOSAHEDRAL DODECABORATE SALTS

This thesis is concerned chiefly with an analysis of the vibrational spectra of solid icosahedral dodecaborate salts, $M_2[B_{12}X_{12}]$ (M=K, Cs, Me_4N and X=H, D, Cl, Br, I), and the double salt $Cs_2[B_{12}H_{12}]\cdot CsCl$. The spectra have been assigned on the basis of factor group analyses for the known crystal structures of the compounds. In addition, icosahedral molecules in chemistry are reviewed briefly, as are the physiochemical properties of the $[B_{12}H_{12}]^{2-}$ ion and its perhalogenated derivatives.

RESUME

M.Sc. Mohamed Abdel-Fattah Chimie

SPECTRES VIBRATIONNELS DE QUELQUES SELS ICOSAHEDRIQUES DE DODECABORATES

Le sujet de cette thèse se rattache principalement à l'analyse des spectres vibrationnels des sels cristallins des dodécaborates icosahédriques de structure, $M_2[B_{12}H_{12}]$, (M=K, Cs, Me_4N; X-H, D, Cl, Br, I) et du double sel $Cs_2[B_{12}H_{12}\cdot CsCl$. L'interprétation des spectres est en accord avec les analyses des groupes facteurs de structures cristallines connues. En plus, les molécules icosahédriques en chimie sont briévement examinées, d'ailleurs les propriétées physiochimiques de l'ion $[B_{12}H_{12}]^{2-}$ aussi bien que leurs derivés perhalogènes ont été rapportés.

ACKNOWLEDGEMENTS

I would like to express my sincere appreciation to my supervisor, Dr. Ian S. Butler, for his invaluable assistance, guidance and patience throughout all phases of this work.

I am also grateful to Dr. W.H. Knoth (E.I. DuPont De Nemours and Co., Inc.) for supplying the chemicals $Cs_2B_{12}Cl_{12}\cdot H_2O$, $Cs_2B_{12}Br_{12}\cdot H_2O$, $Cs_2B_{12}H_{12}$ and $[Me_4N]_2B_{12}I_{12}$ used in this work.

As well, I would like to thank Mr. Roland Haddad for his assistance with the low temperature equipment and Ms. Renee Charron who took great care in typing this manuscript.

I am indebted also to my fellow lab. workers for their discussions and suggestions.

The financial support of McGill University is gratefully acknowledged.

To my parents, and especially to my wife, Anne,

who supported and encouraged me throughout this endeavour.

TABLE OF CONTENTS

LIST OF FIGURES

LIST OF TABLES

GENERAL INTRODUCTION

The use of symmetry in chemistry and physics has led to a more thorough understanding of many of the physio-chemical properties of molecules. One particular area in which symmetry plays a vital role is the prediction and analysis of molecular spectra, especially for molecules of high symmetry.

The icosahedron or, as it is formally called, the double pyramidal pentagonal antiprism, is shown in Fig. 1. It is one of the five regular polyhedra commonly referred to as the Platonic solids[1]. This geometry is the most efficient way to pack 12 particles around a point[2]. With the exception of a sphere, the icosahedron is the most symmetrical shape known. It consists of 20 equilateral triangular faces, 12 vertices and 30 edges, with every five triangle having a common vertix. There are ten symmetry classes - E, $12C_5$, $12C_5^2$, $20C_3$, $15C_2$, i, $12S_{10}$, $12S_{10}^3$, $20S_6$, 15σ - giving in all 120 symmetry elements[1]. These together constitute the I_h point group. Examples of each of the ten symmetry classes are indicated in Fig. 2.

The icosahedron was first recognized as a structural unit in 1941 during the X-ray analysis of boron carbide (B_4C)[3]. Subsequently, this geometry has been identified in numerous boron-rich compounds. There are four types of elementary boron, all of which contain icosahedral B_{12} units. In the

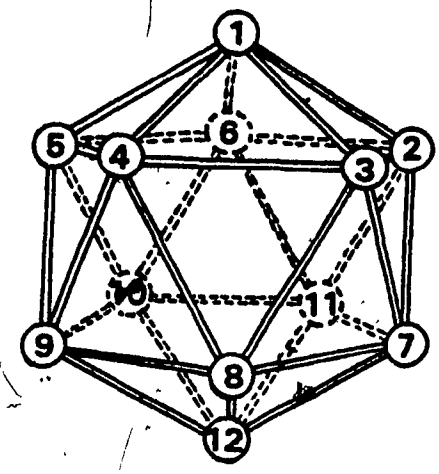

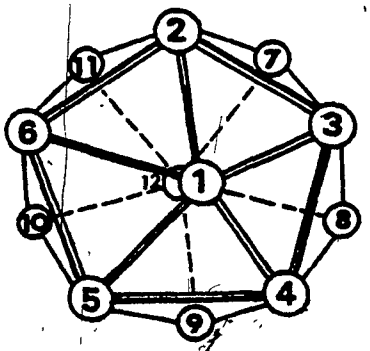

FIGURE 1: The icosahedron

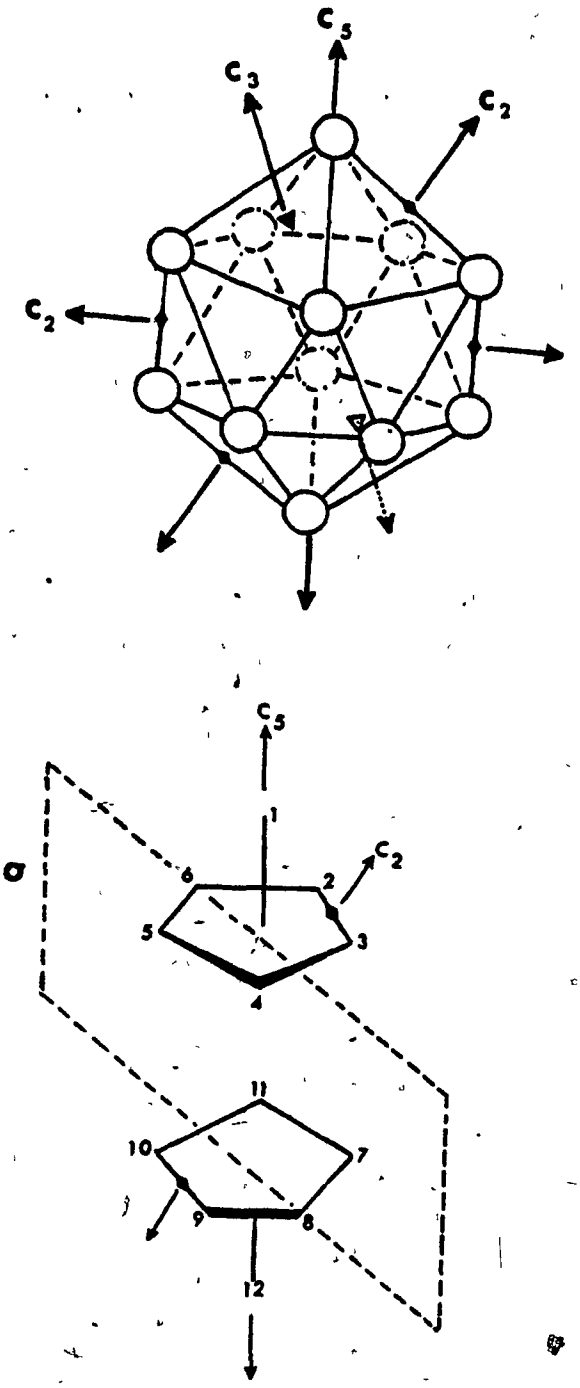

FIGURE 2: Examples of symmetry classes of the icosahedron

relatively simple α-rhombohedral[4] and α-tetragonal forms[5], the B_{12} icosahedra are joined together to give cross-linked sheet-like frameworks[6]. In the more complex polymeric β-tetragonal[7] and β-rhombohedral[8] forms, and in compounds based on their networks, the structures are derived from giant icosahedral units such as B_{84} or B_{156} which are composites of many icosahedra. The B_{156} unit is generated when twelve B_{12} icosahedra are bonded to a central icosahedron. When the central icosahedron is radially bonded to twelve pentagonal pyramids, i.e., twelve half-icosahedra, the B_{84} unit is produced. Both the B_{84} and the B_{156} units possess full icosahedral symmetry (Fig. 3).

Many boranes can be considered as fragments of icosahedra and they are described as <u>nido</u> (nest-like) or <u>arachno</u> (spider-web like) depending on their shape[9]. Boranes with the general formula B_nH_{n+4} give <u>nido</u> structures, while those represented by the formula B_nH_{n+6} adopt <u>arachno</u> structures (Fig. 4).

Although boron is particularly prone to form compounds adopting icosahedral arrangements, the geometry is not restricted to this element. There are many examples of hydrides, alloys, metal complexes and even viruses with this structure. Some examples are described below.

Icosahedral symmetry has been found to arise from the orientation of 12 atoms attached to a central heavy atom, e.g., $Mg_3Ce_2(NO_3)_{12}$, where the cerium atoms are sur-

1

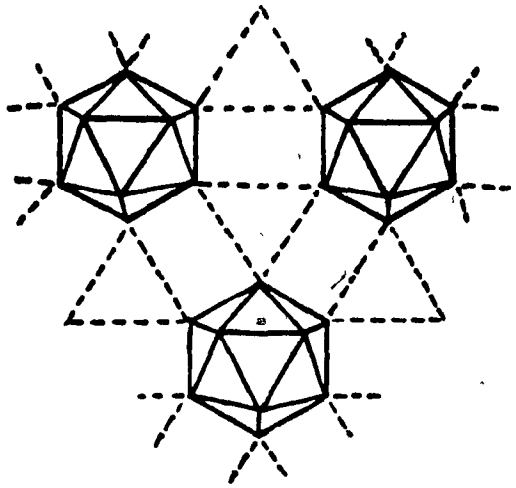

2

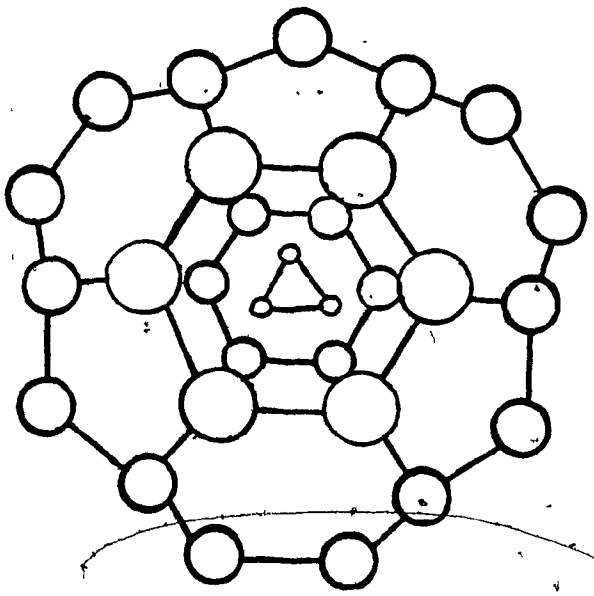

FIGURE 3: Complex icosahedral structures
(1) α-rhombohedral boron
(2) β-rhombohedral boron

rounded by cages of 12 oxygen atoms[10]. A similar situation occurs in $Ba(NO_3)_6$, $La_2(SO_4)_3 \cdot 9H_2O$, $Mg(H_2O)_6 \cdot Th(NO_3)_6 \cdot 2H_2O$ and $Ba(ClO_4)_2 \cdot 3H_2O$[11]. In the latter, the 12 oxygen atoms forming the cage are drawn from the two perchlorate groups as well as from six water molecules[12]. In the case of $BaSiF_6$ and $BaGeF_6$, the icosahedral cage is formed by the fluorine atoms of eight neighbouring hexafluorometallate(II) ions[13]. In $Zr(BH_4)_4$ and possibly the analogous compounds of uranium and hafnium, the heavy atom is enclosed in a cage of 12 hydrogen atoms[14].

Among the many viruses that apparently crystallize in icosahedral arrangements is the polio virus[15]. The high symmetry may play an important role in the biochemical action of these viruses.

The only discrete monomeric molecules possessing I_h symmetry are the $[B_{12}X_{12}]^{2-}$ ions, where X=H, Cl, Br, I[16].

Table I summarizes the known examples of molecules adopting icosahedral geometry. The structural information given is based on a comparison with the prototype structures of elementary boron.

This thesis is concerned particularly with the study of the vibrational spectra of the $[B_{12}X_{12}]^{2-}$ anions and their salts. Over the past 15 years, only cursory attention has been paid to the spectra of these interesting molecules and a detailed analysis has not yet been reported. This was one of the main objectives of the present study.

FIGURE 4: Examples of icosahedral structures

(a) Closo structures
(b) Nido structures
(c) Arachno structures
(d) Miscellaneous structures

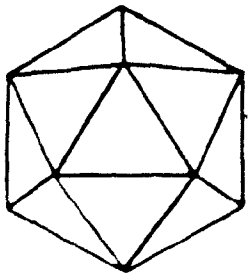

$B_{12}H_{12}^{-2}$

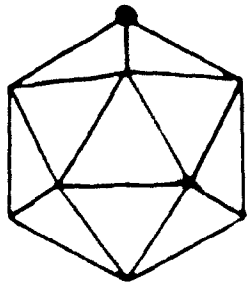

$C\,B_{11}H_{12}^{-}$

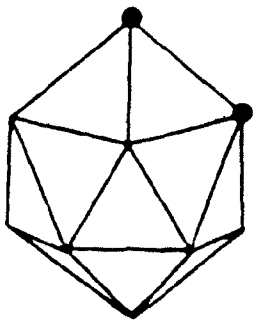

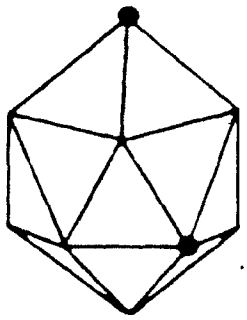

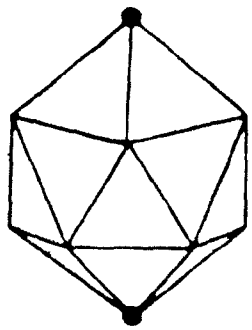

Isomers of $C_2B_{10}H_{12}$

Fig. 4

(A) Closo Structures

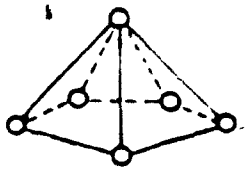

B_6H_{10}

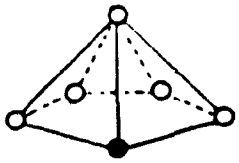

CB_5H_9

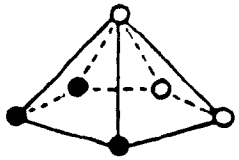

$C_2B_3H_7$

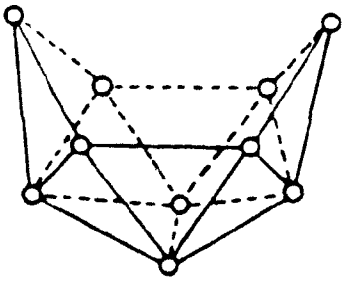

$B_{10}H_{14}$

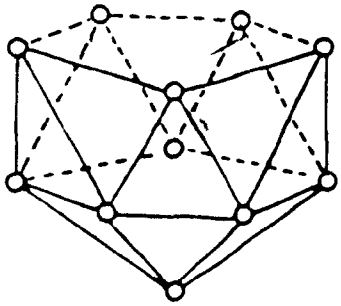

$B_{11}H_{14}^-$

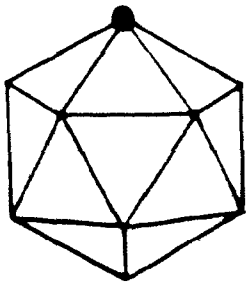

$SB_{11}H_{11}$

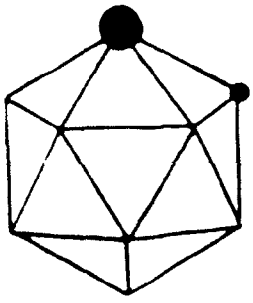

$CB_{10}H_{11}M$

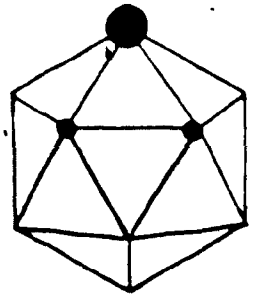

$C_2B_9H_{11}M$

(B) Nido Structures

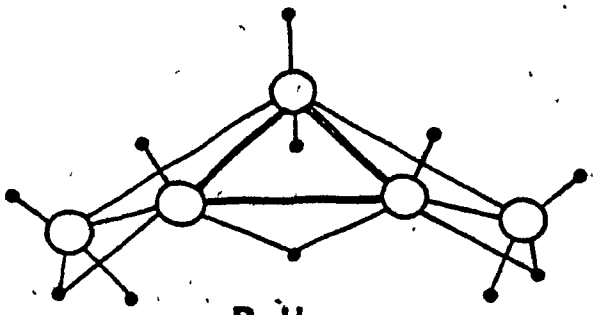

B_5H_{11}

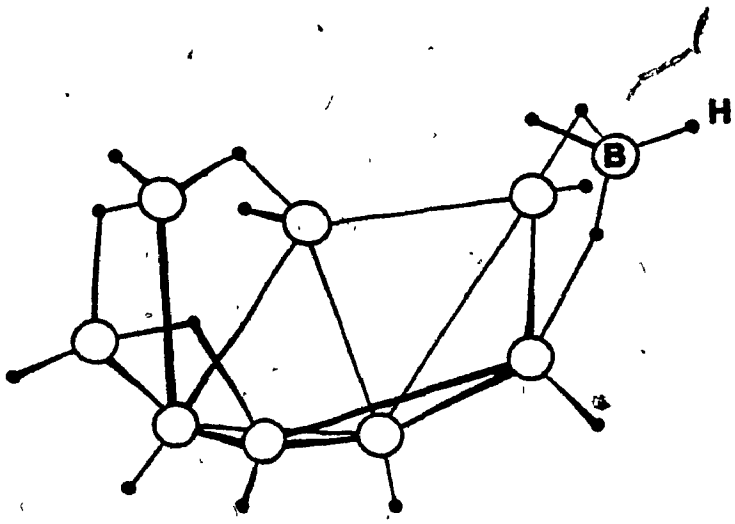

B_9H_{15}

○ Boron

• Hydrogen

(C) Arachno Structures

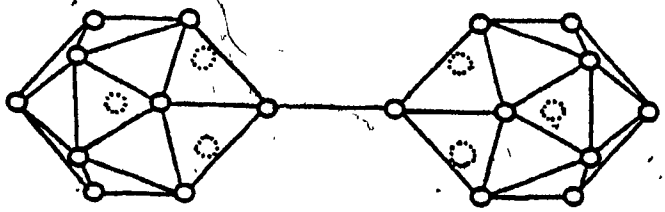

$B_{24}H_{23}^{-2}$

Coupled

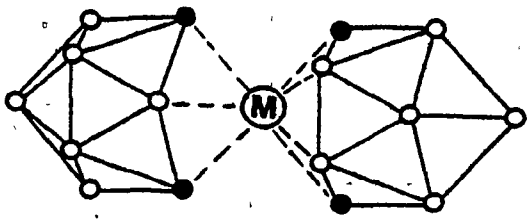

$(C_2B_9H_{11})_2M$

Fused

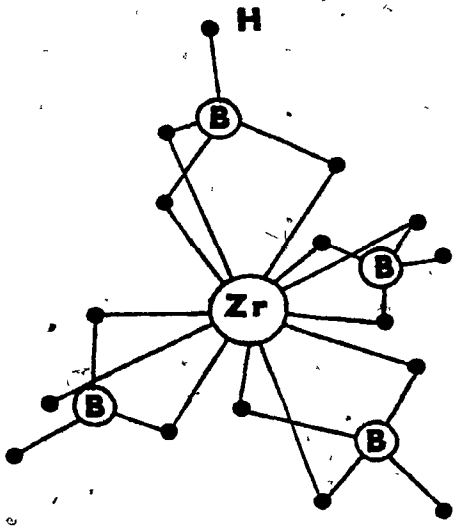

$Zr(BH_4)_4$

(D) Miscellaneous Structures

There are four chapters and two appendices in the thesis. In Chapter I, there is a general review of the chemistry of $[B_{12}H_{12}]^{2-}$ and the related halogenated derivatives. This review deals principally with the synthesis, physiochemical properties and uses of these compounds. Chapter II describes the experimental procedures used in the present work. The results are presented and discussed in Chapter III. In Chapter IV, there is a conclusion and some suggestions for future study. Finally, Appendix I summarizes the group theoretical treatment for icosahedral species of the type $[B_{12}X_{12}]^{2-}$, while Appendix II deals with the isotopic substitution study.

TABLE I: Compounds having icosahedral symmetry

Class of compounds	Chemical formula	Structure type	Icosahedral Units [ ]	Ref.
Elementary Boron:	B			
α-Rhombohedral		α-Rh	B_{12}	4
β-Rhombohedral		β-Rh	$[B_{84}]^a + 2B_{10} + B$	8
α-Tetragonal		α-Tet	$4[B_{12}] + 2B$	5,6
β-Tetragonal		β-Tet	$[B_{84}]$	7
Boron Carbides	B_4C, $B_{12}C_3$	α-Rh	$[B_{12}]$ or $[B_{11}C]$	3,17
	$B_{13}C_2$	α-Rh	$[B_{12}]$	18
Boron Silicides	B_3Si, $(B_{10.5}Si_{1.5})Si_2$	α-Rh	$[B_{11}Si]$, $B_{10}Si_2$	19
Boron Sulphides	$B_{12}S$	α-Rh	$[B_{12}] + S$	20
	$B_{13}S$, $B_{12}SB$	α-Rh	$[B_{12}] + SB$	
Boron Phosphides	$B_{12}P_2$	α-Rh	$2[B_{12}] + 2P$	21
Boron Sub-oxides	B_7O, $B_{13}O_2$	α-Tet	$4[B_{12}] + 2B$	22
	$B_{12}OBO$			
Boron Arsenides	$B_{12}As_2$	α-Rh	$[B_{12}] + 2As$	23
Metal Borides:				
Aluminum	AlB_{10}, $AlB_{24}C_4$, $AlB_{26}C_4$	α-Tet	$4[B_{12}] + 2Al + 4CBC$	24,25
	AlB_{12}	β-Rh	$[B_{84}]^a + 2B_{10} + B(Al)$	26
Magnesium[c]	MgB_{12}	β-Rh	$[B_{84}]$	2
Beryllium	BeB_{12}, $Be(BeB_{24})$	α-Tet	$4[B_{12}] + 2Be$	27
	BeB_6	β-Tet	$[B_{84}]$	28
Nickel	NiB_{25}	α-Tet	$4[B_{12}] + 2Ni$	29
Tantalum	TaB_{25}	α-Tet	$4[B_{12}] + 2Ta$	25
Yttrium[d]	YB_{70}	β-Rh	$[B_{156}]^b + 4B_{10} + 2B$	30
Lanthanides[d]	LnB_{70}, Ln=Ho, Yb, Tb,...	β-Rh	$[B_{156}]^b$	31
	LnB_{100}, Ln=Gd, Yb,...	β-Rh	$[B_{156}]$	32
Polyhedral Boranes (Boron Hydrides)	B_5H_{11}	Arachno-	Quasi $[B_{12}]$ icosahedra	33
	B_6H_{10}	Nido-		34
	B_9H_{15}	Arachno-		35
	$B_{10}H_{14}$	Nido-		36
	$[B_{11}H_{13}]^{2-}$	Nido-		37
	$[B_{11}H_{14}]^-$	Nido-		37
	$[B_{12}H_{12}]^{2-}$	Discrete	$[B_{12}]$, $[H_{12}]$	38
	$[B_{12}X_{12}]^{2-}$, X=Cl, Br, I	Discrete	$[B_{12}]$, $[X_{12}]$	39
	$B_{18}H_{22}$	Fused[e]	$2[B_{12}]$	40
	$B_{20}H_{16}$	Fused[e]	$2[B_{12}]$	41
	$[B_{24}H_{23}]^{3-}$	Coupled[f]	$2[B_{12}]$	42
Carboranes and Neocarboranes	$B_{10}C_2H_{12}$	Simple[g]	$[C_2B_{10}]$, $[H_{12}]$	43
	$B_{10}C_2X_{12}$, X=Cl, Br, I	Simple[g]	$[C_2B_{10}]$, $[X_{12}]$	44
	$B_{10}H_{10}C_2H_2$	Simple[g]	$[C_2B_{10}]$, $[H_{12}]$	
	$B_{10}X_{10}C_2H_2$	Simple[g]	$[C_2B_{10}]$, $[H_2X_{10}]$	45
	$[B_{11}CH_{12}]^-$	Simple[g]	$[CB_{11}]$, $[B_{12}]$	46
Thioboranes	$B_{11}H_{11}S$ and derivatives e.g., $B_{11}H_{10}SPh$	Simple[g]	$[SB_{11}]$	47

TABLE I: (continued)

Class of compounds	Chemical formula	Structure type	Icosahedral units [ ]	Ref.
Metalo-carboranes[h] and Nido-carboranes	$M(B_9H_{11}C_2)$, M=Co, Fe, Ni	Fused[e]	$[B_9C_2M]$	48,49
	$M(B_{10}H_{11}C)_2$, M=Co, Ni	Fused[e]	$[B_{10}CM]$	50
	$MB_9C_2H_{11}$, $M=Ge^{2+}$, Sn^{2+}, Pb^{2+}, $[Be \leftarrow L]^{2+}$	Simple	$[B_9C_2M]$	51,52
	$MB_{10}CH_{11}$, M=P, As, Sb, GeR	Simple	$[B_{10}CM]$	51,52
Metalo-thioboranes[h]	$M(B_{10}SH_{10})_2$, M=Co, Fe, Ni, Pt, Ru	Coupled[f]	$[B_{10}SM]$	47
Carbophosphoboranes	$B_{10}CPH_{11}$	Simple[g]	$[B_{10}CP]$	53
	$B_{11}PH_{11}Ph$	Simple	$[B_{11}P]$	
Metal Hydrides[i]	δ-UH_3-δ-UH_{12}	Simple[g]	$M[H_{12}]$	54
Metal Hydroborates[i]	$M(BH_4)_4$ M=Zr, U, Th	Simple	$M[H_{12}]$	14,55
Coordination Compounds or Metal Complexes[i]	$La(SO_4)_3 \cdot 9H_2O$	Simple	$M[O_{12}]$	56
	$Th(SO_4)_6^{8-}$	Simple	$M[O_{12}]$	57
	$Mg(H_2O)_6 \cdot Th(NO_3)_6 \cdot 2H_2O$	Simple	$Th[O_{12}]$	58
	$Ca_2Mg_3(NO_3)_{12} \cdot 24H_2O$	Simple	$Ca[O_{12}]$	10
	$Ba(NO_3)_2$	Simple	$Ba[O_{12}]$	59
	$Ba(ClO_4)_2 \, 3H_2O$	Simple	$Ba[O_{12}]$	12
	$BaSiF_6$	Simple	$Ba[F_{12}]$	13
	$BaGeF_6$	Simple	$Ba[F_{12}]$	13
Complex Alloys[i,j]	Transition Elements of GV, VI/GI, II	Complex	$[M_{12}]$	60
	β-Tungsten	Complex	$[M_{12}]$	61
	M_3M' M=Mo, Cr, V M'=Al, Si e.g., $(AlMo_{12})$, $(SiCr_{12})$	Complex	$[M'M_{12}]$	61
Viruses	Polio virus	Complex		15

[a] B_{24} = 12 radial $[\frac{1}{2}B_{12}]$ + central $[B_{12}] = 7[B_{12}]$

[b] B_{156} = 12 radial $[B_{12}]$ + central $[B_{12}] = 13[B_{12}]$

[c] Borides of Mg, Na and Li should have structures similar to that of aluminum borides[2].

[d] The structures of these boron-rich borides seem to be stabilized by the presence of a small number of heavy atoms[4].

[e] The two icosahedra share a common atom, edge or face.

[f] The two icosahedra are joined by an external bond.

[g] Simple structures are those composed of isolated icosahedra as opposed to the complex structures of elementary boron or complex alloys.

[h] The metal atom is centrally located over the pentagonal face of the anion thus closing the cage structure. Without the metal, these anions $[B_9C_2H_{11}]^{2-}$ etc., become quasi-icosahedral of the nido type.

[i] In these structures, the icosahedron is formed around a central heavy metal atom.

[j] The icosahedron is one of the four coordination polyhedra utilized in the complex alloy systems[60].

CHAPTER I REVIEW OF THE CHEMISTRY OF THE DODECAHYDRODODECABORATE ION, $[B_{12}H_{12}]^{2-}$

As mentioned in the Introduction, $[B_{12}H_{12}]^{2-}$ is one of the few known examples of species possessing discrete icosahedral symmetry. The following review is focussed chiefly on the chemical and physical properties of this ion and is considered to be complete up to June 1976.

A. SYNTHESIS

In 1960, Pitochelli and Hawthorne[62] reported the formation of $[Et_3NH]_2B_{12}H_{12}$ as a minor product in the reaction of 2-iododecaborane-14 with triethylamine in benzene. Three years later, several research groups independently discovered routes to $[B_{12}H_{12}]^{2-}$. For instance, Miller et al.[63] obtained a very high yield (79%) of $[B_{12}H_{12}]^{2-}$ salts from the reaction of diborane (B_2H_6) with either $[BH_4]^-$ or amine-borane complexes at high temperatures and under pressure (Eqs. 1, 2).

$$5B_2H_6 + 2NaBH_4 \xrightarrow[100\text{-}180°]{Et_3N} Na_2B_{12}H_{12} + 13H_2 \qquad (1)$$

$$5B_2H_6 + Et_3N{:}BH_3 \xrightarrow{100\text{-}180°} [Et_3NH]_2B_{12}H_{12} + 11H_2 \qquad (2)$$

In their investigation, Ellis et al.[64] produced $[B_{12}H_{12}]^{2-}$ in

65% yield by refluxing B_2H_6 and $NaBH_4$ in ethereal solution at 180-200° for 16 hr. Finally, Greenwood and Morris[65] reacted decaborane-14 with triethylamine-borane under reflux in an evacuated vessel; $[B_{12}H_{12}]^{2-}$ was obtained in 76% yield as the triethylammonium salt.

In 1970, Harzdarf et al.[66] reported an unusual synthesis for $Na_2[B_{12}H_{12}]$ from aluminum (or silicon) powder, dehydrated borax and metallic sodium heated at 620° for 2 hr under 3 atmospheres hydrogen pressure.

Miller et al.[67] have now used several different boron hydrides and various Lewis bases and by isolating the intermediates they have established a general equation for the reactions (Eq. 3):

$$aH^- + bB_xH_y \longrightarrow [B_{bx}H_{by+a-z}]^{a-} + Z/2\ H_2 \qquad (3)$$

They have also obtained $[B_{12}H_{12}]^{2-}$ from the thermal disproportionation of the triborohydride ion (Eq. 4):

$$5NaB_3H_8 \xrightarrow{\Delta} Na_2B_{12}H_{12} + 3NaBH_4 + 8H_2 \qquad (4)$$

Greenwood and Morris[65] have suggested that conversion of decaborane-14 into $[B_{12}H_{12}]^{2-}$ may occur first by dissociation of the triethylamine-borane complex, followed by slow formation of the triethylamine adduct of decaborane and finally rapid electrophilic attack on this molecule by two

BH_3 groups (Eqs. 5-8):

$$\text{Base} + \tfrac{1}{2}B_2H_6 \longrightarrow H_3B - \text{Base} \qquad (5)$$

$$Et_3N{:}BH_3 \rightleftharpoons Et_3N + BH_3 \qquad (6)$$

$$2Et_3N + B_{10}H_{14} \longrightarrow (Et_3N)_2B_{10}H_{12} + H_2 \qquad (7)$$

$$2BH_3 + (Et_3N)_2B_{10}H_{12} \longrightarrow (Et_3NH)_2B_{12}H_{12} + 2H_2 \qquad (8)$$

Miller et al.[67] have shown that the base-borane reactions appear to be governed by the strength of the base. Strong bases such as amines give primarily ammonium salts of $[B_{12}H_{12}]^{2-}$; weaker bases such as phosphines, sulphides and arsines afford $[H_2B(Base)_2]^+[B_{12}H_{11}(Base)]^-$ as the major product together with varied amounts of $[B_{12}H_{10}(Base)_2]$. Another important controlling factor in these reactions is the degree of steric hinderance around the donor atom. In this context, the hindered Et_3N molecule affords $[B_{12}H_{12}]^{2-}$ as the major product, whereas less hindered amines produce $[H_2B(NR_3)_2]^+$ and $[B_{12}H_{11}(NR_3)]^-$ as well as $[B_{12}H_{12}]^{2-}$.

Adams et al.[68] have investigated the reactions of decaborane-14 and $[BH_4]^-$ in ethereal solutions. They proposed the following stepwise mechanism for the reaction since they were able to isolate the intermediates (Eqs. 9-11):

$$B_{10}H_{14} + [BH_4]^- + R_2O \longrightarrow [B_{10}H_{13}]^- + R_2OBH_3 + H_2 \quad (9)$$

$$[B_{10}H_{13}]^- + R_2OBH_3 \xrightarrow{90°} [B_{11}H_{14}]^- + R_2O + H_2 \quad (10)$$

$$[B_{11}H_{14}]^- + [BH_4]^- \xrightarrow{160°} [B_{12}H_{12}]^{2-} + 3H_2 \quad (11)$$

The du Pont research group[67] headed by Muetterties has established the steps from $[BH_4]^-$ to $[B_2H_7]^-$ to $[B_3H_8]^-$. They generallized that the reaction involves chiefly attack of the strongly electrophilic boron hydride on a nucleophilic species such as the hydride or borohydride ions, subsequently building the icosahedral boron structure.

B. PHYSICAL PROPERTIES

1. General

Salts of $[B_{12}H_{12}]^{2-}$ are usually high melting, colourless crystalline solids. However, the Ni^{2+}, Eu^{3+} salts and those containing ammonia or water, e.g., $[ML_6]_2B_{12}H_{12}$, (M=Co, Cr, Ni; L=NH_3, H_2O), are coloured[69]. When the cation is small (e.g., Na^+, Ca^{2+}), the salts are water soluble; however when it is large (e.g., Cs^+, Tl^+, R_3NH^+, R_4N^+), the salts are insoluble[69]. Overall, the salts are thermally stable, even at very high temperatures. For example, $Cs_2[B_{12}H_{12}]$ can be heated to 600° in air without any apparent decomposition; it is also unchanged when heated in a sealed quartz tube at 810°[2].

The $[B_{12}H_{12}]^{2-}$ cage is strongly resistant to oxidation. Polarographic studies on the Na^+ salt show a very high oxidation potential, the half-wave potential ($E_{\frac{1}{2}}$) is greater than +1.4 V[69]. Potassium permanganate at 80° oxidizes the dodecaborate ion via $[B_{12}H_{11}OH]^{2-}$ and $[B_{12}H_{10}(OH)_2]^{2-}$ to boric acid[70,71] and this reaction is recommended as a titration method for the ion[66].

The $[B_{12}H_{12}]^{2-}$ ion has exceptional stability toward acids or bases[2]. For instance, neither 3N HCl nor 3N NaOH at 95° for 16 hr has any observable effect. Further confirmation of the extraordinary kinetic stability of these ions is derived from the fact that the hydronium ion $(H_3O)^+$ salt, obtained by passing solutions of $[B_{12}H_{12}]^{2-}$ salts on a strongly acidic ion exchange resin, is a stronger acid than H_2SO_4.

All 12 hydrogen atoms are replaced by deuterium when $[B_{12}H_{12}]^{2-}$ is treated with D_2O in an acid medium (DCl).

The toxicity of dodecahydrododecaborate salts is very low and almost comparable to that of NaCl. $Na_2B_{12}H_{12}$ in large doses has no apparent effect on humans and is excreted unchanged in the urine[95]. The lethal dose of $Na_2[B_{12}H_{12}]$ for rats is more than 7.5 g/Kg of body weight[69]. The low toxicity must be attributable to the great stability of the anion since boron hydrides usually have a high toxicity level[71].

2. Crystal Structures of $[B_{12}H_{12}]^{2-}$ Salts

The icosahedron is a non-crystallographic point group since it has more symmetry elements than can be used in the crystal lattice. Also, the five-fold rotation axis is forbidden in crystal symmetry. Other symmetry elements of the icosahedron may be chosen to build the crystal lattice. Depending on which symmetry elements are in use, the resulting crystal system could be cubic, orthorhombic, trigonal, monoclinic or any of their subgroups.

Potassium dodecahydrododecaborate(2-) crystallizes in the face-centered cubic space group Fm3 (T_h^3) with four molecules per unit cell and a cell edge a=10.64 Å[72]. This space group contains the following symmetry sites: $C_1(96)$, $C_s(48)$, $C_2(48)$, $C_3(32)$, $C_{2v}(24)$, $C_{2h}(24)$, T(8), $2T_h(4)$. The K^+ ions occupy the T(8) sites having the coordinates (¼,¼,¼) and are located in the tetrahedral holes between four adjacent icosahedra (Fig. 5). The hydrogen and boron atoms are in the site group $C_s(48)$ with different coordinates.

The X-ray diffraction study[72] ruled out the closely related cubo-octahedron because of the absence of a four-fold rotation axis. At the same time, it confirmed the icosahedral structure of the $[B_{12}H_{12}]^{2-}$ anion. The B_{12} icosahedron is slightly distorted since there are two types of B-B bond lengths, 1.780 and 1.755 Å. This distortion is attributed to steric interaction between the K^+ ion and the 24 hydrogens of the encircling icosahedron. The B-H bond length (1.07 Å) is

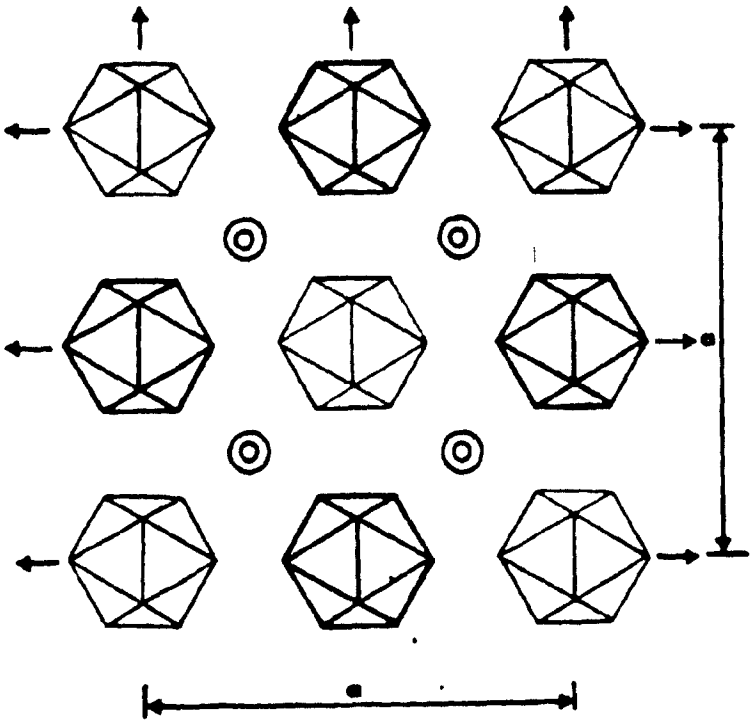

FIGURE 5: The unit cell of $K_2B_{12}H_{12}$. Icosahedra at level zero are indicated by lighter lines. Those in heavier lines are at level 1/2. The K^+ ions (◎) are at levels 1/4 and 3/4.

shorter than that found in most boron hydrides (~1.21 Å). The K^+ - H distance is 2.29 Å.

X-ray diffraction has also been used to determine the structure of other dodecaborate salts. The Cs^+ and Rb^+ salts crystallize in the cubic system as hexaoctahedra[73]. The unit cells contain four molecules and are face-centered in the space group Fm3m (O_h^5)* with cell edges, a=11.28 and 10.85 Å for the Cs^+ and Rb^+, respectively. The double salt $Cs_2B_{12}H_{12} \cdot CsOH$ crystallizes in the space group Pnma(D_{2h}^{16}) of the orthorhombic class[73]. The unit cell contains four molecules with the icosahedra occupying the C_s symmetry sites. The edge lengths of the unit cell are a=14.27, b=9.85 and c=10.36 Å.

3. Bonding and Electronic Structure

The 12 boron atoms needed to form the icosahedron possess 48 atomic orbitals. Longuet-Higgins and Roberts[75]

---

*While this thesis was being prepared for publication, the same workers reported a new X-ray analysis of Cs^+ and Rb^+ salts[74]. In this work they found that these salts are isostructural with the K^+ salt, viz., Fm3(T_h^3). While this change does not affect the number of optically-active bands expected, it does play a role in the activity of the associated lattice modes and also changes the symmetry labels of some species (vide infra, Chapter III).

subdivided these orbitals according to their spacial orientations, viz.,

(a) Twelve 2s orbitals with their maximum amplitudes lying outside the icosahedron.

(b) Twelve 2p orbitals oriented in such a way that their axes pass through the centre of the cage. These are called "radial orbitals".

(c) Twenty-four 2p orbitals having their maximum extension in the pseudospherical surface of the cage. These are called "surface or tangential orbitals".

The 2s and 2p radial orbitals have their maximum amplitudes in the same direction. Therefore, they can combine to give two sets of sp hybrid orbitals at 180° to each other. These orbitals are described as "radial" or "external" depending on whether they point inward toward the centre of, or outward from the icosahedron. The external orbitals easily overlap with the 1s orbitals of hydrogen atoms to form 12 equivalent covalent B-H bonds at the vertices of the icosahedron. The 24 electrons required to fill the external orbitals are supplied equally by the hydrogen and boron atoms.

The twelve sp radial orbitals, together with the 24 tangential orbitals, constitute the "internal orbitals" of the $[B_{12}H_{12}]^{2-}$ icosahedron. These 36 internal orbitals are conventionally subdivided into "bonding" and "antibonding" orbitals. On the basis of molecular orbital calculations,

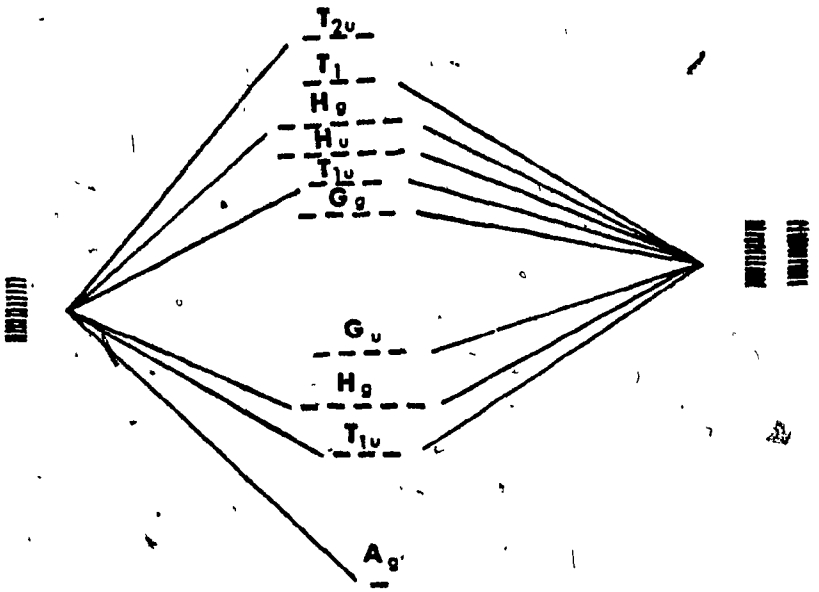

12 radial (sp) orbitals — 36 molecular orbitals — 24 tangential p-orbitals

FIGURE 6: Relative energy levels of the 13 bonding and 23 antibonding molecular orbitals of the icosahedral $[B_{12}H_{12}]^{2-}$ ion.

13 bonding orbitals are necessary in order to have a closed-shell electronic configuration. Twenty-four electrons, out of the 26 required to fill these orbitals, come from the skeletal boron atoms, while the extra pair of electrons has to be supplied by an external cation. For this reason, the neutral $B_{12}H_{12}$ which will provide only 24 electrons, was eliminated as a stable ground-state species. The remaining 23 orbitals are antibonding orbitals. They are vacant since they are energetically unfavourable.

In the molecular orbital treatment of Longuet-Higgins and Roberts[75], the atomic orbitals were combined to form the symmetry orbitals that belong to the same irreducible representation of the I_h point group. Using these symmetry orbitals, the energy parameters of the molecular orbitals were calculated and the ordering of the orbitals was established. The resulting molecular orbital diagram for the dodecahydrododecaborate anion is shown in Fig. 6.

Although the bonding in $[B_{12}H_{12}]^{2-}$ can be explained in terms three-centre bonds, it is impossible to find a single canonical structure that fully describes the anion. The structure is better considered as a composite of many resonance forms, each containing 10 three-centre BBB bonds and 3 covalent B-B bonds. Lipscomb[38] has established rules to limit the number of these resonance structures, $[B_{12}H_{12}]^{2-}$ is best described by 70 such resonance structures[14]. The result of this large number of resonance structures is the

complete delocalization of electrons over the entire cage. Therefore, the resonance stabilization energy is considered to be at a maximum and the B_{12} cage is comparable to aromatic systems[70]. In fact, Muetterties has described these compounds as superaromatic[77]. Moreover, the volume of the $[B_{12}H_{12}]^{2-}$ cage is said to be of the same order of magnitude as that produced by a benzene molecule spinning around its two-fold rotation axis[16]. This three-dimensional aromaticity results in unusually large diamagnetic susceptibility and polarizability[78]. Also, it is responsible for the unique stability of these boron compounds mentioned earlier.

4. Spectroscopic Properties

a. Electronic spectra

The electronic structure of the dodecaborate(2-) ion had been predicted prior to its synthesis[75]. Data are now available[80] for bond orders, ionization potentials, charge distribution, orbital energies, etc. The energy difference between the bonding and the antibonding orbitals is about 14 eV[38]. The result of this substantial energy gap is that the dodecahydrododecaborate anion has no absorption maxima in either the visible or the uv region down to 200 nm where a strong end-absorption appears. On the other hand, the closely-related perhalogen derivatives $[B_{12}X_{12}]^{2-}$ (X=Cl, Br, I) do exhibit uv absorption bands[81] as shown in Table II:

TABLE II: UV absorptions for $[B_{12}X_{12}]^{2-}$ ions

Anion	Cation	Solvent	λ_{max} (nm)	ϵ_{max} & $mole^{-1}cm^{-1}$
$[B_{12}Cl_{12}]^{2-}$	$[Me_4N]^+$	MeCn	243	110
$[B_{12}Br_{12}]^{2-}$	Cs^+	H_2O	260	100
$[B_{12}I_{12}]^{2-}$	Na^+	H_2O	267	4600

b. Nuclear magnetic resonance spectra

A powerful tool in the study of the structures of boron hydrides and their substituted products is nmr spectroscopy. Two distinct types of nmr are applied to these compounds, viz., ^1H and ^{11}B nmr. The latter is of more use in the study of this class of compounds, since it gives less complicated spectra and at the same time differentiates between the boron atoms[14].

i. ^1H nmr spectra

Spin coupling of covalently bonded hydrogen ($I=\frac{1}{2}$) and ^{11}B ($I=3/2$) will produce four different orientations. Therefore, for every hydrogen, there should be four equally spaced, equally intense bands. Since all the hydrogens are equivalent in the $[B_{12}H_{12}]^{2-}$ icosahedron, the hydrogen peaks will be superimposed and the only feature of the spectra

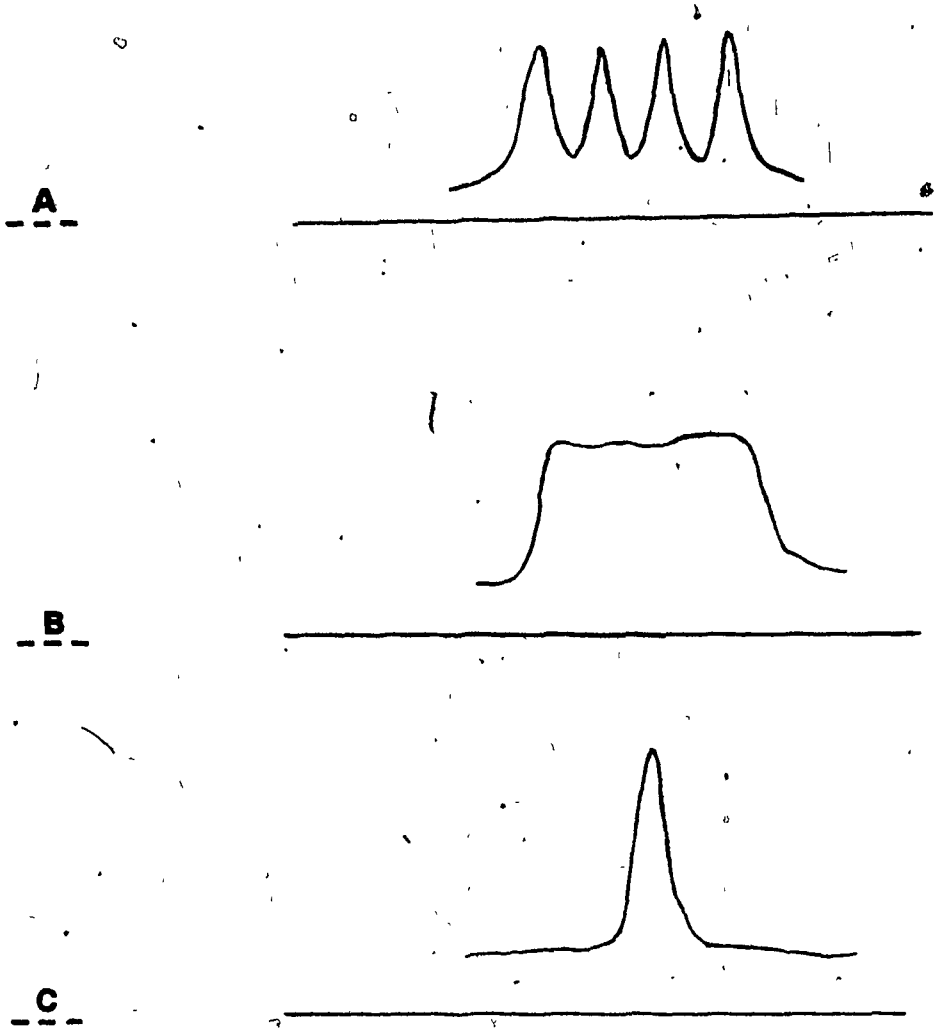

FIGURE 7: ^{1}H nmr spectrum of $K_2B_{12}H_{12}$ (in H_2O). (A) theoretical spectrum. (B) actual spectrum. (C) after irradiation with ^{11}B resonance frequency.

should be these four bands (Fig. 7). If the spectra are observed while irradiating with the resonance frequency of ^{11}B, the boron atoms will be decoupled from the hydrogens and the nmr spectrum should consist of a singlet. Theoretically, spin-coupling of ^{10}B-^{1}H nuclei should afford seven bands, but these will be of low intensity owing to the relatively low natural abundance of ^{10}B and can be ignored. (c.f. Table III).

The reported ^{1}H nmr spectrum[69] of $[B_{12}H_{12}]^{2-}$ exhibits no sharp lines but rather a broad plateau about 400 Hz wide, i.e., covering an area equivalent to the expected quartet since the ^{11}B-^{1}H coupling constant is ∿130 Hz. Upon irradiation with the ^{11}B resonance frequency, this multiplet collapses to a sharp line at -2.0 ppm relative to tetramethylsilane (TMS).

ii. ^{11}B nmr spectra

Spin-spin coupling of the ^{11}B and ^{1}H nuclei affords two possible orientations ($m_s=\frac{1}{2},-\frac{1}{2}$). Thus, a ^{11}B resonance should split into a doublet. The ^{11}B nmr spectra of the dodecahydrododecaborate ion does exhibit a single doublet[69], thus confirming the equivalence of the 12 boron atoms of the cage (Fig. 8). Moreover, this equivalence could only occur in an icosahedron or a cube-octahedron. The nmr technique does not distinguish between the two structures.

Muetterties et al.[69] have improved the nmr spectral data reported earlier[62] for the $[B_{12}H_{12}]^{2-}$ ion. They

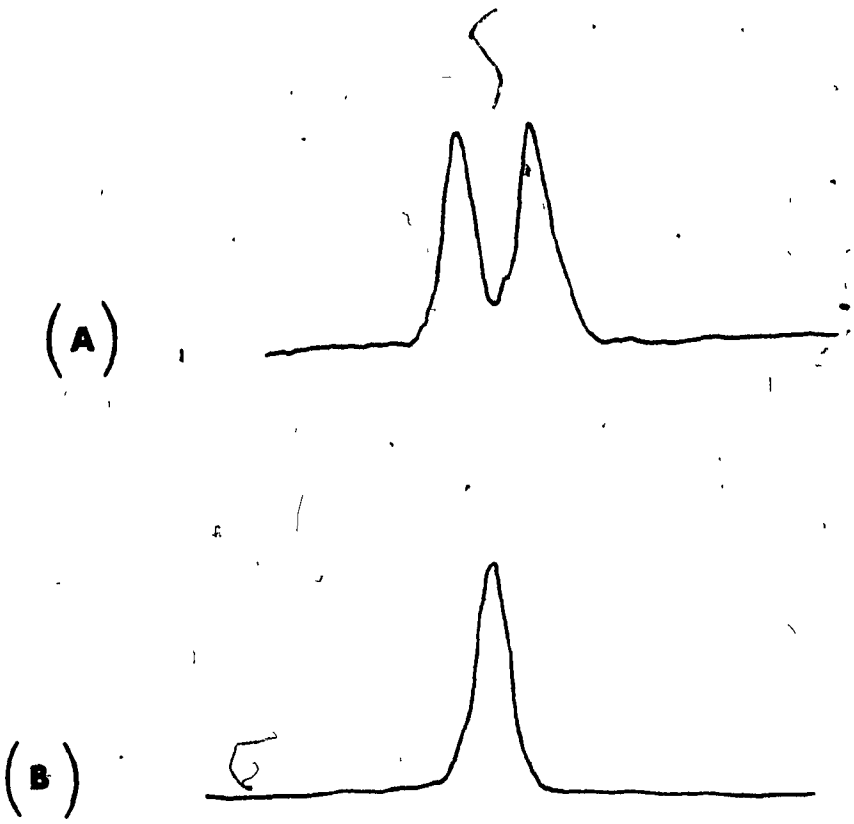

FIGURE 8: ^{11}B nmr spectrum of $K_2B_{12}H_{12}$ (in H_2O) before (A) and after (B) irradiation with proton resonance frequency.

TABLE III: Splitting due to B-H spin coupling

Isotope	Natural abundance	Nuclear spin (I)	Orientations (m)	Number of lines	Relative intensity (H=1)
^{1}H	99.98%	½	½, -½	2	1
^{10}B	18.83%	3	3, 2, 1, 0, -1, -2, -3	7	0.020
^{11}B	81.17%	3/2	3/2, ½, -½, -3/2	4	0.165

indicated the chemical shift as + 35 ppm and the ^{11}B-^{1}H coupling constant as 130 Hz; methyl borate (TMB) was used as a reference. The ^{11}B-^{11}B spin interaction is weak and can be ignored. The same can be said about the ^{10}B-^{1}H spin-spin coupling. The doublet obtained in the spectra of $[B_{12}H_{12}]^{2-}$ can be reduced to a singlet upon irradiation at 60 M Hz to decouple the protons. The ^{11}B nmr spectra of the perhalogen derivatives consist of one, relatively sharp line[81]. Table IV lists the chemical shifts for these anions.

TABLE IV: NMR absorptions for $[B_{12}X_{12}]^{2-}$ (X=H, Cl, Br, I)

Anion	Solvent	Chemical shift, ppm	Reference	Remarks
$[B_{12}H_{12}]^{2-}$	H_2O	35.0	TMS	Doublet
$[B_{12}Cl_{12}]^{2-}$	MeCN	31.0	TMB	Singlet
$[B_{12}Br_{12}]^{2-}$	MeCN	30.7	TMB	Singlet
$[B_{12}I_{12}]^{2-}$	MeCN	34.4	TMB	Singlet

c. Vibrational spectra

Vibrations of a discrete $[B_{12}H_{12}]^{2-}$ ion of I_h symmetry span the irreducible representations given below (Eq. 12) ;

the spectroscopic activities are shown in parentheses.

$$\Big[\Big]^{I_h}_{gen} = 2\underline{a}_g \text{ (Raman)} + 4\underline{h}_g \text{ (Raman)} + 3\underline{t}_{iu} \text{ (ir)} \qquad (12)$$

Muetterties et al.[79] have studied the vibrational spectra of the dodecaborate ions, $[B_{12}H_{12}]^{2-}$ and $[B_{12}D_{12}]^{2-}$, and have made tentative assignments on the basis of the Teller-Redlich product rule. The infrared spectra consist of only three bands, giving additional support for the icosahedral structure. Also, the Raman spectra of the aqueous solutions contain two strongly polarized and four depolarized bands. Surprisingly, however, the Raman spectra of the perhalogen derivatives exhibit only one band, and this has been attributed to accidental polarizability cancellations[79].

Since the main purpose of this thesis is the study of the vibrational spectra of the dodecahydrododecaborate(2-) ion and its derivatives, nothing more will be said here about these earlier results.

C. CHEMICAL REACTIONS AND DERIVATIVES

Despite the abnormal kinetic stability of the $[B_{12}H_{12}]^{2-}$ ion, it still undergoes a number of chemical reactions. Many of these reactions reflect the aromatic character of the ion. The important reactions can be classified according to their type as follows:

1. Electrophilic Substitution Reactions

a. Halogenation

The dodecaborate(2-) ion is readily halogenated[81] upon reaction with F_2, Cl_2, Br_2 and I_2 or the corresponding halogen acids HF, HCl, etc., (Eqs. 13-15):

$$[B_{12}H_{12}]^{2-} + H^+ \rightleftharpoons [B_{12}H_{13}]^- \quad (13)$$

$$[B_{12}H_{13}]^- + F^- \longrightarrow [B_{12}H_{13}F]^{2-} \longrightarrow [B_{12}H_{11}F]^{2-} + H_2 \quad (14)$$

$$[B_{12}H_{12}]^{2-} + 6Cl_2 \longrightarrow [B_{12}Cl_{12}]^{2-} + 6H_2 \quad (15)$$

The perhalogen derivatives have similar physical properties to $[B_{12}H_{12}]^{2-}$[81].

b. Diazotization

The action of nitrous acid on $[B_{12}H_{12}]^{2-}$ produces a diazonium salt (Eq. 16) which is formulated as a charge-compensated inner salt[82].

$$[B_{12}H_{12}]^{2-} + 4HNO_2 \xrightarrow{H_2O} B_{12}H_{10}(N{=}N)_2 + 3H_2O + 5_2O \,. \quad (16)$$

c. Carbonyl derivatives

Carbon monoxide reacts directly with $H_2[B_{12}H_{12}]$ under acidic conditions (130°/1000 atm.) to yield the mono- and dicarbonyl derivatives, $[B_{12}H_{11}CO]^-$ and $B_{12}H_{10}(CO)_2$, respectively[83]. The same compounds are formed when $[B_{12}H_{12}]^{2-}$ is treated with oxalyl chloride $(COCl)_2$ or when the (N=N) groups in the diazonium salts are replaced by CO under high pressure[84]. These carbonyl derivatives are further examples of charge-compensated salts.

d. Benzoylation

Benzoyl chloride reacts with $[B_{12}H_{12}]^{2-}$ to give products having B-O bonds such as $[B_{12}H_{10}(OH)_2]^{2-}$ and $[B_{12}H_{11}(OCH_2\cdot ph)]^{2-}$ (Eq. 17)[85].

$$[B_{12}H_{12}]^{2-} + ph\cdot CO\cdot Cl \xrightarrow{H^+} \longrightarrow [B_{12}H_{11}OCO\cdot ph]^{2-} + \quad + [B_{12}H_{10}(OH)_2]^{2-} \qquad (17)$$

e. Amination

Using hydroxy-O-sulphonic acid in aqueous solutions, the mono- and diamino- derivatives are obtained (Eq. 18)[86].

$$[B_{12}H_{12}]^{2-} + [NH_2\text{-}O\text{-}SO_3]^- \xrightarrow{H_2O} B_{12}H_{11}(NH_3) + \\ + B_{12}H_{10}(NH_3)_2 \qquad (18)$$

Use of Vilsmeier reagent $[CHCl{=}NMe_2Cl]$ affords first the monoderivative $B_{12}H_{11}[NMe_2\text{-}CH_2Cl^-]$, and then the diderivative $B_{12}H_{10}[NMe_2\text{-}CH_2Cl]_2$[87].

f) Tropylium ion derivatives

The reaction between tropylium bromide and $[B_{12}H_{12}]^{2-}$ yields the yellow $[C_7H_6]$ $[B_{12}H_{11}]^-$ ion, the colour probably being due to an internal charge-transfer transition[88].

2. Nucleophilic Substitution Reactions

These reactions are acid-catalyzed and occur between different Lewis bases (L) and the dodecaborate ion resulting in products such as $[B_{12}H_{11}L]^-$ or $[B_{12}H_{10}L_2]$. Examples of the Lewis bases used are N,N-dimethyl formamide, Me_2CO, H_2S, Me_2S_2, Me_2S, MeCN, olefins, carboxylic acids, certain alcohols and certain ethers (Eqs. 19-21)[85,89].

$$[B_{12}H_{12}]^{2-} + H_2S \xrightarrow{H^+} [B_{12}H_{11}SH]^{2-} \qquad (19)$$

$$[B_{12}H_{12}]^{2-} + Me_2S(\text{or } Me_2S_2) \xrightarrow{H^+} [B_{12}H_{11}SMe]^{2-} + \\ + [B_{12}H_{10}SMe_2]^{2-} + [B_{12}H_9SMe_3]^{2-} \qquad (20)$$

$$(H_3O)_2[B_{12}H_{12}] + \underset{\text{styrene}}{\text{ph-CH=CH}_2} \xrightarrow{H^+} [B_{12}H_{10}(C_8H_9)_2]^{2-} \qquad (21)$$

Halogenation of the dodecahydrododecaborate anion with halogen acids can also be explained as nucleophilic reactions, especially in non-aqueous media (Eqs. 22,23)[81].

$$[B_{12}H_{12}]^{2-} \xrightleftharpoons{H^+} [HB_{12}H_{12}]^{-} \xrightleftharpoons{H^+} H_2B_{12}H_{12} \qquad (22)$$

$$[HB_{12}H_{12}]^{-} + Cl^{-} \longrightarrow \longrightarrow [B_{12}H_{11}Cl]^{-2} + H_2 \qquad (23)$$

3. Oxidation Coupling

Polarographic studies show that the electrochemical oxidation of the dodecaborate ion, in MeCN at +1.45 V (vs. sce), yields the coupled product $[B_{24}H_{23}]^{2-}$[42]. On the other hand, $KMnO_4$ (80°) oxidizes $[B_{12}H_{12}]^{2-}$ ion to boric acid through intermediates such as $[B_{12}H_{11}OH]^{2-}$ and $[B_{12}H_{10}(OH)_2]^{2-}$ etc. The $[B_{12}H_{12}]^{2-}$ ion also reduces $[Cr_2O_7]^{2-}$ to $Cr(OH)_2$ in neutral solutions without evidence of oxidative coupling[70].

4. Perhalogen Derivatives

In this section, some of the chemistry of the perhalogen derivatives will also be described.

The boron hydride ion $[B_{12}H_{12}]^{2-}$ reacts with elemental halogen or other halogenating agents to produce halogen

substituted derivatives (Eqs. 24-28)[81]. The perhalogen ions are usually prepared by the exhaustive halogenation of $[B_{12}H_{12}]^{2-}$ with elemental halogens with the exception of F_2 which does not afford the perhalo species. In the case of the periodo anion, the reaction proceeds only after the addition of excess iodine monochloride.

$$[B_{12}H_{12}]^{2} + HF \xrightarrow{\Delta,\ H_2O} [B_{12}H_6F_6]^{2-} \qquad (24)$$

$$+ F_2 \xrightarrow{0°,\ H_2O} [B_{12}F_{11}(OH)]^{2-} \qquad (25)$$

$$+ Cl_2 \xrightarrow{R.T.,\ H_2O} [B_{12}Cl_{12}]^{2-} \qquad (26)$$

$$+ Br_2 \xrightarrow{5\text{-}15°,\ MeOH/H_2O} [B_{12}Br_{12}]^{2-} \qquad (27)$$

$$+ I_2 + ICl \xrightarrow[\text{Reflux, 43 hr}]{C_2H_2Cl_4 \text{ or } CCl_4} [B_{12}I_{12}]^{2-} \qquad (28)$$

These are electrophilic substitution reactions which increase in rate in the order Cl > Br > I.

The extraordinary stability of the perhalo species is comparable to that of the dosododecahydroborate ion $[B_{12}H_{12}]^{2-}$. The introduction of halogens into the cage structure increases the oxidative stability of these ions; for instance, the action

of hot $KMnO_4$ (80°) on the halo ions is very slow, while 20% aqueous NaOH at 85° does not seem to affect $[B_{12}I_{12}]^{2-}$. This high kinetic stability is also manifested by the very acidic (stronger than H_2SO_4) hydroxonium salts $(H_3O)_2[B_{12}X_{12}]$ obtained upon passing the solutions of these halo derivatives through an acidic ion exchange resin[81]. Their thermal stability is demonstrated by the fact that heating $Cs_2B_{12}Cl_{12}$ to 700° causes no noticeable degradation; however, at 900°, there is 50% decomposition. Refluxing $Ag_2B_{12}Cl_{12}$ in water does not result in the formation of insoluble AgCl, showing the high strength of the B-X bonds[81].

The perhalogen species absorb energy in the UV region and therefore undergo many photochemical reactions, particularly nucleophilic substitution reactions (Eqs. 29-32)[90,91].

$$[B_{12}Cl_{12}]^{2-} + [CN]^- \xrightarrow[H_2O]{h\nu} [B_{12}Cl_5(CN)_7]^{2-} \qquad (29)$$

$$[B_{12}Br_{12}]^{2-} + [CN]^- \xrightarrow[\text{6-7 days, water}]{h\nu} [B_{12}Br_3(CN)_9]^{2-} \longrightarrow$$

$$[B_{12}Br_2(CN)_9H]^{2-} \longrightarrow [B_{12}Br(CN)_9H_2]^{2-} \qquad (30)$$

$$[B_{12}Br_{12}]^{2-} + \text{KCNO} \xrightarrow[\text{1.5 hr, } H_2O]{h\nu} [B_{12}Br_{11}(OCN)]^{2-} + [B_{12}Br_{10}(OCN)_2]^{2-} \longrightarrow [B_{12}Br_{10}(OH)_2]^{2-} \quad (31)$$

$$[B_{12}Br_{12}]^{2-} + NaN_3 \xrightarrow[H_2O]{h\nu} [B_{12}Br_{11}N_3]^{2-} \longrightarrow [B_{12}Br_{10}(N_3)_2]^{2-} \quad (32)$$

These reactions are believed to proceed <u>via</u> S_N1 heterolytic cleavage of the B-X bonds (Eqs. 33,34). Binuclear nucleophilic displacement mechanisms (S_N2) are ruled out in view of the bulk of the icosahedral cage[71].

$$[B_{12}X_{12}]^{2-} \xrightarrow[\text{bond cleavage}]{h\nu} [B_{12}X_{12}^*]^{2-} \longrightarrow [B_{12}X_{11}]^- + X^- \quad (33)$$

$$[B_{12}X_{11}]^- + Y^- \longrightarrow [B_{12}X_{11}Y]^{2-} \quad (34)$$

D. <u>USES</u>

The dodecaborate ion has various important industrial uses. It is beneficial as a sequestering agent for metals in

an aqueous medium[38]. Diazonium salts have a potential use as explosion initiators. The addition of $Li_2[B_{12}H_{12}]$ to hydrocarbon fuels modifies their combustion properties[2]. The silver salt, $Ag_2[B_{12}H_{12}]$, is used as a film-emulsion stabilizer and sensitizer in photography[92]. The thermal stability of the $[B_{12}H_{12}]^{2-}$ ions has led to their use in high temperature polymers[93].

An important medical application for the dodecaborate ion is in cancer chemotherapy, especially in the treatment of brain tumors. Aqueous solutions of the ^{10}B-enriched $[B_{12}H_{12}]^{2}$ are injected intravenously and the tumor area is irradiated by a small neutron source[94]. The ^{10}B atom has a great capacity to absorb thermal neutrons since it has a larger capture cross-section (3850 barns) than that for ^{11}B (0.05 barns).

$$^{10}B + {}^{1}_{0}n \longrightarrow {}^{11}B \longrightarrow {}^{7}_{3}Li + {}^{4}_{2}He + 2.4\ MeV \qquad (35)$$

The considerable energy liberated at the molecular level (Eq. 35) is sufficient to destroy the cancerous cells. The low toxicity[95] and the abnormal hydrolytic stability of the dodecaborate anion render it very suitable for this type of tumor therapy. The $[B_{12}H_{11}SH]^{2-}$ derivative is about 10-15 times as toxic as $Na_2B_{12}H_{12}$ but it is absorbed by tumor tissue much more readily than by blood or normal tissue. For this reason, the $[B_{12}H_{11}SH]^{2-}$ salt is used as well as $[B_{12}H_{12}]^{2-}$ in brain-tumor chemotherapy[96].

CHAPTER II EXPERIMENTAL SECTION

A. INSTRUMENTATION

The ir spectra were recorded on a Perkin Elmer model 521 double beam grating spectrophotometer (range 4000-300 cm^{-1}). The spectra were calibrated against water vapour bands (1576.2, 1616.7 and 1653.3 cm^{-1}) and the 667.3 cm^{-1} band of atmospheric CO_2[97]. The precision of the frequencies is ±2 cm^{-1} in the 4000-2000 cm^{-1} region and ±1 cm^{-1} in the 2000-300 cm^{-1} region.

Raman spectra were obtained on a Jarrell-Ash model 25-300 Raman spectrophotometer equipped with Coherant Radiation model 52 Ar^+ and Kr^+ lasers. The excitation wavelengths used were 514.5 (Ar^+) and 647.1 nm (Kr^+). The incident light was perpendicular to the plane of the slit. The spectra were calibrated against the emission lines (162.3, 218.9, 830.6 and 1031.5 cm^{-1}) of a standard neon lamp. The frequencies are considered to be accurate to ±1-2 cm^{-1}. The powdered samples were placed in sealed Pyrex capillary tubes. Low-temperature measurements (73±0.5 K) were achieved by the use of a cold-temperature controller, composed of regulator EA 2337, digital display EC 2367 and three-term controller EA 2349, Oxford Instruments, England. The low-temperature sample cell was a model CF-100 cryostat (Oxford Instruments Co., England) cooled with liquid nitrogen.

Melting points were taken on a Gallenkamp melting

point apparatus using sealed capillaries and are uncorrected.

B. MATERIALS

1. Sources

The materials used were obtained from the sources indicated below:

Decaborane-14 ($B_{10}H_{14}$): Alfa Inorganics.

Triethylamine-borane ($Et_3N \cdot BH_3$): Aldrich Chemicals Co. Inc.

Trimethylamine-borane ($Me_3N \cdot BH_3$): Matheson, Coleman and Bell.

Triethylamine hydrochloride ($Et_3NH{:}HCl$): Eastman Organic Chemicals.

Tetradecane ($C_{14}H_{30}$): Philips Petroleum.

Diethylene glycol dimethyl ether, diglyme [$(Me\text{-}O\text{-}CH_2\text{-}CH_2)_2O$]: :Aldrich Chemicals Co. Inc.

Rexyn (101)-H, ion-exchange resin: Fisher Scientific Co.

Rexyn (102)-H, ion-exchange resin: Fisher Scientific Co.

Molecular sieves (Sinde 3A): Fisher Scientific Co.

1,2-dimethoxy ethane [$(MeO \cdot CH_2)_2$]: Aldrich Chemicals Co.,

$NaBH_4$, CsF, CsCl, KOH : Alfa Inorganics

MeCN: Fisher Scientific Co.

$Cs_2B_{12}H_{12}$, $Cs_2B_{12}Cl_{12} \cdot H_2O$, $Cs_2B_{12}Br_{12} \cdot H_2O$, $[Me_4N]_2B_{12}I_{12}$: Dr. W.H. Knoth, E.L. du Pont de Nemours and Co. Inc., Walmington, Delaware.

Me_2CO: Anachemia Chemicals Ltd.

D_2O, DCl 38% } Merck, Sharp and Dohme Ltd.

Et_2O: Mallinckrodt Ltd.

n-hexane: Fisher Scientific Co.

Some of the materials were purified further before use, as follows:

2. Decaborane-14

Decaborane is an extremely toxic substance. The maximum allowable concentration (M.A.C.) is 0.05 ppm, while the maximum detectable concentration (M.D.C.) is 0.7 ppm[98]. This means that in the presence of the odour a serious health hazard exists. This chemical has an unpleasant pungent odour somewhat reminiscent of chocolate. The lethal dose for rats is 0.022 g/Kg body weight. Inhalation or skin contact with the chemical will produce toxic symptoms of fatigue, dizziness, headache, tremors, nervousness, cramps, etc.[98]. The chemical appears to cause liver and kidney damage and to affect ther nervous system. Decaborane has a vapour pressure of 1.4 torr at 65° and 19 torr at 100°. It is practically insoluble in water, 35-40 mg/l. Methyl alcohol, ammoniacal and alkaline solutions react readily with decaborane and therefore can be used as decontaminating agents. Administration of oxygen can help relieve the discomfort due to inhaling

vapours. Halogenated solvents form shock-sensitive mixtures with decaborane and must never be used for crystallization or as an extinguishing agent[99]. Soda-lime, silica gel and triethanol-amine (absorbed on unglazed china) absorb decaborane vapours and they could be used in gas-mask canisters or in storage areas[98].

The decaborane received was wet-looking, very slightly yellowish crystals. Two methods of purification were used in the laboratory. First, recrystallization from n-hexane (or heptane) produces colourless needles, and second, sublimation under vacuum [80° (oil-bath)/10^{-3} torr] onto an ice-cold finger, yields a white waxy compact material. Sublimation afforded less personal exposure to the material and gave a compound of high purity when it was repeated twice (mp 100-100.5°, lit.[98] 99.5°). The temperature of the oil-bath was carefully controlled since decaborane can become unstable near 100° and can explode on contact with air at this temperature (flash point 80°, ignition point 149°). Therefore, the sublimation apparatus was cooled to room temperature before opening to air. The bands observed in the ir spectrum of decaborane in Nujol are 620 m, 727 s, 765 m, 815 m, 858 m, 902 m, 938 m, 970 m, 1008 s, 1037 w, 1105 w, 1515 s, 1560 w, 1875 w, 1930 w, 2570 vs cm^{-1}. The band at 2570 cm^{-1} was split presumably due to a lattice interaction with Nujol. These values compare favorably with those reported in the literature[100].

3. Triethylamine-borane Complex

This air-sensitive colourless liquid was purified, just before use, by two successive distillations under dry nitrogen (90-92°/8-10 torr). The pure product melts at -4° (lit.[101] -4°). It was always stored under nitrogen. The chemical is highly toxic, comparable to the boranes. Therefore, similar precautions to those applied in handling decaborane were also undertaken in this case. The ir frequencies for $Et_3N{:}BH_3$ were 771 s, 792 m, 805 m, 855 m, 865 m, 966 w, 1020 s, 1035 s, 1050 s, 1100 m, 1115 m, 1130 w, 1180 vs, 1311 m, 1420 s, 1480 s, 2060 w, 2160 m, 2300 vs, 2350 vs, 2400 vs, 3020-2910 vs, br. cm^{-1}.

4. Trimethylamine-borane Complex

This borazane was received as waxy white needle-like crystals (mp. 92°). It was purified by sublimation [70-80° (oil-bath), 4 cm Hg]. The pure product melts at 94-95° (lit.[102] 93°). The compound is hygrascopic and is easily hydrolyzed[103]; consequently it was stored in a very dry environment under nitrogen. A Nujol mull of $Me_3N{\cdot}BH_3$ exhibits the following bands in the ir: 440 m, 847 s, 915 m, 1005 s, 1120 m, 1170 vs, 1260 s, 1320 m, 1403 m, 2066 m, 2270 s, 2310 m, 2370 s, 3040 s cm^{-1}. Again, because of toxicity problems, this was handled in a similar manner to $Et_3N{:}BH_3$.

5. Tetradecane

The hydrocarbon was first dried over P_2O_5 and then distilled over P_2O_5 (110°/5 torr). The ir spectrum is very similar to that of Nujol, i.e. no peaks characteristic of unsaturation being observed.

6. Bis-(2-methoxyethyl)ether, diglyme

The liquid was purified by distillation (bp 161-162°) from sodium benzophenone ketyl under nitrogen. For every 100 ml of crude ether, 3 g of benzophenone and 4 g of pure sodium were added. The material was stored under nitrogen.

C. SYNTHESIS OF THE DODECAHYDRODODECABORATE(2-) SALTS

1. $[Et_3NH]_2B_{12}H_{12}$

The salt was prepared according to the method of Miller and Muetterties[104] with slight modification (Eq. 36).

$$B_{10}H_{14} + 2Et_3N{:}BH_3 \xrightarrow[200°]{C_{14}H_{30}} [Et_3NH]_2B_{12}H_{12} + 3H_2 \qquad (36)$$

The reaction apparatus consisted of a 150 ml round-bottom, 3-neck flask. The central neck was fitted with a side-arm dropping funnel. On one of the side necks, a condenser whose outlet was connected to a mercury bubbler was mounted. The third neck carried a thermometer and a nitrogen inlet.

The flask was equipped with a magnetic stirrer. The apparatus was flushed with dry nitrogen (dried over KOH pellets). Then, a small flame was used to dry the apparatus while it was swept by a stream of dry nitrogen. The tetradecane solvent (60 ml) was added and the flask was immersed in a high-boiling, paraffin-oil bath. With the nitrogen stream flowing continuously, the bath was heated up to 200-210°. Triethylamine-borane (19 ml, 15.5 g, 0.135 M) and decaborane (7.2 g, 0.059 M) were mixed thoroughly in a 100 ml beaker in a glove bag under a nitrogen atmosphere. (Caution: the mixture is extremely sensitive to moisture and oxygen). To hasten the solubility of decaborane, the mixture was gently heated on a small hot plate previously introduced into the glove bag. Some insoluble material appeared which was removed by filtration under nitrogen. The resulting yellowish, clear solution of decaborane-14 in triethylamine-borane was transferred to the dropping funnel and was added dropwise to the hot tetradecane (200°) over a period of 30 min. The falling drops reacted immediately on reaching the solvent, as indicated by the resulting turbidity. No drops were allowed to run down the wall of the flask. At all times, a slow stream of nitrogen was kept flowing through the system. The mercury bubbler was used to check the nitrogen flow rate and, more importantly, to prevent air from being drawn into the reaction flask since decaborane reacts explosively with air at high temperatures. After the addition was complete, the reaction was allowed

to proceed at the same temperature for another 20 min. The heating was then stopped and the reaction flask was cooled to room temperature before opening it to the atmosphere. The resulting solid was collected on a sinter-glass funnel and was washed with diethyl ether (200 ml) to remove the tetradecane. After drying, the product weighed 16.8 g (84% yield). This crude product was boiled in 300 ml water for about 10 min and gradually dissolved with some hydrogen evolution. 8N HCl (2 ml) was added to the hot solution which was then filtered while hot to remove some insoluble gummy material. The filtrate was chilled in an ice-bath and the desired $[Et_3NH]_2B_{12}H_{12}$ product crystallized out (yield, 6.5 g). Concentration of the filtrate gave another 3.2 g of the pure product.

The gummy material which separated out from the boiling water was collected. Treatment with acetone and n-hexane, followed by recrystallization (at 0°) from warm MeCN (300 ml), resulted in additional pure $[Et_3NH]_2B_{12}H_{12}$ (2.5 g). The overall yield of the pure crystalline product was 12.2 g, 0.035 M (yield, 62%; decomp. ~300°, lit.[69] 298-300°). In the ir spectrum (KBr disc), the following bands were observed: 445 w, 468 m, 717 m, 744 w, 794 m, 843 m, 1030 vs, 1064 vs, 1077 m, sh, 1159 m, 1276 m, 1363 m, 1391 s, sp, 1404 vs, sp, 1447 vs, sp, 1450 vs, sp, 1457 s, 1470 s, 1636 w, br, 1866 w, 2006 w, 2040 w, 2480 vvs, br, 2740 m, 2770 m, 2882 m, 2942 m cm^{-1}. The reported[104] ir frequencies for a

Nujol mull of $[Et_3NH]_2B_{12}H_{12}$ are 720 m, 745 w, 797 w, 847 m, 1030 s, 1065 s, 1160 m, 1275 w, 1640 w, 1850 w, 2020 w, 2040 w, 2500 s, 3150 m cm^{-1}.

2. $[Me_3NH]_2B_{12}H_{12}$

This compound was prepared by a method similar to that of Miller and Muetterties (Eq. 37)[104]:

$$B_{10}H_{14} + 2Me_3N{:}BH_3 \xrightarrow[180^\circ, N_2]{C_{14}H_{30}} [Me_3NH]_2B_{12}H_{12} + 3H_2 \qquad (37)$$

A dry 50 ml, 3-neck flask was equipped with a condenser, nitrogen gas-inlet, thermometer and a dropping funnel in the same way as described in the $[Et_3NH]_2B_{12}H_{12}$ synthesis, except that the dropping funnel was wrapped with heating tape (Fisher Scientific Co.). After starting nitrogen flow, tetradecane (20 ml) was placed in the reaction flask which was subsequently heated to 180-190° in an oil-bath. Mixing of the reactants, $Me_3N{:}BH_3$ (3.2 g, 0.044 M) and decaborane (2.4 g, 0.020 M), was achieved by heating (~80°) and stirring under nitrogen in a glove bag. The resulting liquid was then transferred quickly to the dropping funnel (heated by the electric tape). The dropwise addition (30 min) of this mixture to the hot tetradecane (180-190°) was followed by extra reaction time of 20 min before the apparatus was allowed to cool to room temperature. The resulting whitish

solid was filtered out of the tetradecane and washed on a sinter-glass funnel with small portions of diethyl ether. After air drying the crude product weighed 3.6 g (71% yield). This material was boiled in water (50 ml) for about 10 min in order to hydrolyze any unreacted decaborane. The solution was then acidified with 0.2N HCl (2 ml) and filtered while hot to separate the gummy material that was formed during the hydrolysis. The filtrate was chilled in an ice bath to produce 3.1 g (61% yield) of a white solid. The ir spectrum showed that the desired $[B_{12}H_{12}]^{2-}$ ion was mixed with several other ions such as $[B_{12}H_{11}(NMe_3)]^-$ (ir bands: 2500, 1055, 955, 890, 725 cm^{-1})[67]; $[H_2B(NMe_3)_2]^+$ (ir bands: 2500, 1100-1200, 720-900 cm^{-1})[105] and $[B_{11}H_{14}]^-$ (ir bands: 2510, 1250, 1110, 868, 720 cm^{-1})[37]. Successive treatment of this mixed product with n-hexane, acetone, methanol, 2-methoxy ethane, and diglyme followed by recrystallization from water produced pure $[Me_3NH]_2B_{12}H_{12}$ (2.1 g, 41% yield, decomp. ~310°), as judged by its ir spectrum in Nujol: ~3600 m, br, 3130 s, 3020 m, 2485 vs, 1250 w, 1063 s 975 m, 720 m cm^{-1}).

3. $K_2B_{12}H_{12}$

Two methods are available to obtain $K_2B_{12}H_{12}$ from the alkylammonium analogues. The first method is the neutralization procedure (Eq. 38)[62].

$$[Et_3NH]_2B_{12}H_{12} + 2KOH \longrightarrow K_2B_{12}H_{12} + Et_3N + 2H_2O \qquad (38)$$

The KOH used was previously standardized against potassium hydrogen phthalate and was free from carbonates. To a suspension of the triethylammonium salt in water (0.85 g/10 ml H_2O) was added the exact amount of potassium hydroxide (0.26 g, 4.64 ml of 1N-KOH) necessary to convert the salt to its K^+ analogue. The mixture was then boiled gently until there was no longer an amine odour (∿15 min). After cooling, the solution was evaporated on a rotary evaporator to give white $K_2B_{12}H_{12}$ crystals (0.5 g, 92% yield).

The second procedure made use of ion-exchange resins. A solution of $[Et_3NH]_2B_{12}H_{12}$ (0.8 g/10 ml H_2O) was made alkaline (pH∿10), boiled to expell amine gases, cooled to room temperature and then passed through a strongly acidic ion-exchange resin [Rexyn-101 (H)] (15.0x1.0 cm). The acidic effluent ($H_2B_{12}H_{12}$) was concentrated on a rotary evaporator at room temperature. This acidic solution could either be titrated against a standard KOH solution or passed through another column (25.0x1.0 cm) of acidic cation-exchange resin in the K^+ form, to yield $K_2B_{12}H_{12}$ (Eq. 39. When the two methods were tried starting from 0.8 g of $[Et_3NH]_2B_{12}H_{12}$, they gave identical products with nearly quantitative yields (∿92%, 0.47 g). The synthesis of $K_2B_{12}H_{12}$ <u>via</u> the cation-exchange technique has not been reported previously.

It is worth mentioning here that when an alkaline solution of $[Et_3NH]_2B_{12}H_{12}$ (0.7 g/10 ml H_2O) was passed through a weakly acidic cation-exchange resin (20.0x1.0 cm) [Rexyn 102(H)],

the effluent was strongly acidic $(H_3O)^+$. However, this type of resin is not recommended[106] for complete conversion to $(H_3O)_2B_{12}H_{12}$ since the equilibrium in Eq. 40 is shifted to the left (compare with Eq. 39 for strongly acidic resins).

$$RSO_3H + Na_2B_{12}H_{12} \rightleftharpoons H_2B_{12}H_{12} + RSO_3Na + H_2O \qquad (39)$$

$$RCOOH + Na_2B_{12}H_{12} \rightleftharpoons H_2B_{12}H_{12} + RCOONa + H_2O \qquad (40)$$

4. $K_2B_{12}D_{12}$

Deuteration of $K_2B_{12}H_{12}$ was carried out according to Muetterties et al's[69] method. $K_2B_{12}H_{12}$ (1.1 g, 5.0 mM) was dissolved in D_2O (8 ml) and the solution was acidified with 2-3 drops of DCl (38% in D_2O). After standing for one week, the solution was evaporated to dryness using a rotary evaporator. The residue was redissolved in D_2O (6 ml) and one drop of DCl solution was added. The solution was then left standing for another week before it was evaporated to dryness under reduced pressure. After this process of dissolution and evaporation had been repeated five times, the solution was finally refluxed for 1 hr. Evaporation to dryness was followed by drying over P_2O_5 under vacuum (40°/10^{-4} torr) for 3 hr. This yielded 1.1 g of the ~90% D-enriched product as judged by ir analysis. The Nujol mull of $K_2B_{12}D_{12}$ showed strong ir bands at 1875, 930 and 598 cm^{-1}.

5. $Cs_2B_{12}H_{12}$

This borane salt was prepared according to the method described by Muetterties et al.[69]. The triethylammonium salt (1.3 g, 5.0 mM) was dissolved in 1N-KOH solution (∿10 ml) and then boiled gently for 15 min in order to expell the liberated amine (Eq. 41). The solution was then cooled and neutralized by the slow addition of 2N-H_2SO_4 (∿2 ml).

$$[Et_3NH]_2B_{12}H_{12} + 2KOH \longrightarrow K_2B_{12}H_{12} + 2Et_3N + 2H_2O \qquad (41)$$

$$K_2B_{12}H_{12} + 2CsF \longrightarrow Cs_2B_{12}H_{12} + KF \qquad (42)$$

A CsF solution (50%) was next added in drops until no further precipitation occurred (∿3 ml). The precipitate was digested for 10 min and then the flask was immersed in an ice-bath for 1 hr before filtering off the while product. The solid was washed three times with ice-cold water (5-6 ml) and recrystallized at 0° from boiling water. After drying in vacuo for 2 hr (50°/10^{-4} torr), the pure crystalline product weighed 1.75 g (87% yield). The ir spectrum resembled that of the potassium analogue.

6. $Cs_2B_{12}H_{12}\cdot CsCl$

This double salt separates in the above synthesis instead of $Cs_2B_{12}H_{12}$ when the reaction medium contains an

excess of chloride ion[69].

A solution of 1NKOH (20 ml) was added to a stirred suspension of $[Et_3NH]_2B_{12}H_{12}$ (1.3 g, 5.0 mM) in H_2O (10 ml). The solution was boiled until no further amine odour was detected (15-20 min). After cooling, 4N-HCl (60 ml) was added and the solution was filtered. A concentrated solution of CsCl (5 ml) was added dropwise while stirring and the copious precipitate which appeared was digested for 30 min. The flask was chilled in ice for 1 hr and the white product was washed on the filter with small portions of ice-cold water. The solid was recrystallized at ice temperature from 80 ml of boiling water. The pure product weighed 2.5 g (87% yield) after drying in vacuo over P_2O_5 for 1 hr ($40°/10^{-4}$ torr).

7. $Na_2B_{12}H_{12}$

This salt was synthesized following the method described by Adams et al.[68] (Eq. 43).

$$B_{10}H_{14} + 2NaBH_4 \xrightarrow[160°,\ N_2]{\text{diglyme,}} Na_2B_{12}H_{12} + 5H_2 \qquad (43)$$

The reaction apparatus consisted of a dry 2-neck 100 ml round-bottom flask equipped with a reflux condenser, a nitrogen inlet and a magnetic stirrer. The nitrogen outlet at the top of the condenser was connected to a mercury bubbler in order to

prevent air from contacting the hot reaction mixture and to assure a constant flowrate of nitrogen (dried over KOH pellet). After starting the nitrogen flow diglyme (30 ml), then decaborane-14 (1.2 g, 1.0 mM) and finally sodium borohydride (0.8 g, 2.1 mM) were added. The reaction mixture was stirred and heated at reflux (160°, oil-bath) under a continuous flow of dry nitrogen. The mixture assumed a deeper yellow colour as the reaction proceeded. After 7 hr, the reaction flask was cooled and chilled in an ice salt bath (∿-10°). The whitish solid that had separated ($Na_2B_{12}H_{12}$·diglyme) was then filtered out and dried for 2 hr under vacuum. In order to remove the diglyme ether of crystallization, the solid was thrice dissolved in H_2O (5 ml) and evaporated to dryness. Finally, the salt was dried over P_2O_5 (110°/10^{-4} torr) for 10 hr. The white powder obtained weighed 1.0 g (54% yield). Apart from the $[B_{12}H_{12}]^{2-}$ bands at 720, 1070 and 2470 cm^{-1}, the ir spectrum (Nujol) showed strong water absorptions (at ∿3500, ∿1600 and ∿1000 cm^{-1}) indicating that the salt was hydrated. The water of crystallization was found to be very strongly bounded in the crystal lattice of $Na_2B_{12}H_{12}$. In the analogous K^+ salt, dehydration was much more easily achieved.

D. PERHALOGEN DERIVATIVES

1. $Cs_2B_{12}I_{12}$

This salt was obtained from the donated $[Me_4N]^+$

analogue. A solution of $(Me_4N)_2[B_{12}I_{12}]$ (0.4 g, 0.25 mM) in warm MeCN/H_2O (10 ml, 50% solution) was passed through a strongly acidic ion-exchange column [Rexyn-101(H), 20.0x1.0 cm]. The highly acidic solution which was eluted was then evaporated to dryness on a rotary evaporator in order to remove gaseous HI. The evolution of HI seemed to indicate the presence of the double salt $(Me_4N)_2[B_{12}I_{12}]NMe_4I$ as an impurity. The resulting solid, $(H_3O)_2[B_{12}I_{12}]\cdot xH_2O$, was redissolved in water (10 ml) and the desired Cs^+ periodo salt was precipitated by the addition of a concentrated CsF solution.

$$H_2B_{12}I_{12} + 2CsF \longrightarrow Cs_2B_{12}I_{12} + HF \qquad (44)$$

The solid which formed was recrystallized at ice temperature from boiling water and dried over P_2O_5 for 4 hr (40°/10^{-4} torr) to give 0.41 g (85% yield) of pure $Cs_2B_{12}I_{12}$. The most important bands in the ir spectrum (Nujol) appeared at 939 vs, 926 vs, 905 s, sh and 478 m cm^{-1}.

2. $Cs_2B_{12}Cl_{12}$ and $Cs_2B_{12}Br_{12}$

These salts were received as monohydrates and were dried over P_2O_5 (40°/10^{-4} torr), the perchloro derivative for ~4 hr and the perbromo derivative for 12 hr. The ir spectra were free of H_2O absorptions and showed a strong band at 1032 cm^{-1} for the chloro salt and a doublet 1000, 986 cm^{-1} for the bromo derivative.

CHAPTER III RESULTS AND DISCUSSION

A. VIBRATIONAL SPECTRA OF THE $[B_{12}H_{12}]^{2-}$ ANION

1. Calculation of Normal Modes

Group theoretical calculations are often used to obtain the vibrational modes of a molecule of known symmetry[1]. The usual procedure starts by determining the number of unshifted atoms after each symmetry operation. Then, this number is multiplied by the matrix contribution of the particular symmetry operation for these unshifted atoms. This procedure generates the reducible representation spanning the vibrational modes. In order to arrive at the number of times any given irreducible representation occurs in the reducible representation, the following reduction equation, commonly known as the "magic formula", is used[107]:

$$n^{\gamma} = \frac{1}{g} \sum_{j} g_j \chi_j \chi_j^{\gamma} \qquad (45)$$

where n^{γ} is the number of times that the γth irreducible representation appears in a reducible representation; g_j is the number of symmetry operations in the jth class; χ_j is the character of the reducible representation; and χ_j^{γ} are the elements of the character table for this point group.

Jahn and Teller[108] employed group theory to obtain the vibrational modes of all the common symmetry groups.

including the icosahedron. In the case of $[B_{12}H_{12}]^{2-}$, the 24 atoms of the icosahedron will produce $3 \times 24 = 72$ degrees of freedom or vibrational modes. The resulting reducible representation spans the species shown in Eq. 46 (see also Appendix I).

$$\Big\lceil^{I_h}_{\text{total}} = 2\underline{a}_g + 2\underline{t}_{1g} + 4\underline{t}_{1u} + 2\underline{t}_{2u} + 2\underline{g}_g + 2\underline{g}_u + 4\underline{h}_g + 2\underline{h}_u \qquad (46)$$

After subtracting the non-genuine rotational and translational modes ($\underline{t}_{1g}$ and $\underline{t}_{1u}$), we obtain the following genuine vibrations:

$$\Big\lceil^{I_h}_{\text{total}} = 2\underline{a}_g + \underline{t}_{1g} + 3\underline{t}_{1u} + 2\underline{t}_{2u} + 2\underline{g}_g + 2\underline{g}_u + 4\underline{h}_g + 2\underline{h}_u \qquad (47)$$

Owing to the very high symmetry of the $[B_{12}H_{12}]^{2-}$ ion, most of these vibrations are optically-inactive. The only active fundamentals are given in Eq. 48, where the spectroscopic activity is shown in parentheses.

$$\Big\lceil^{I_h}_{\text{gen. (opt. active)}} = 2\underline{a}_g(\text{Raman}) + 4\underline{h}_g(\text{Raman}) + 3\underline{t}_{1u}(\text{ir}) \qquad (48)$$

The ir and Raman modes belong to different symmetry species because the $[B_{12}H_{12}]^{2-}$ ion has a centre of symmetry and so the rule of mutual exclusion applies.

The next step in the group theoretical treatment of the vibrational problem is to carry out an analysis based on the different types of internal coordinates. The five internal coordinates of the $[B_{12}H_{12}]^{2-}$ icosahedron consist of changes in the two bond lengths, B-H and B-B, and changes in the three interbond angles, $\hat{BBH}$, $\hat{BBB}$ (acute) and $\hat{BBB}$ (obtuse). The reducible representations derived for these internal coordinates are shown in Table V (see also Appendix I).

TABLE V: Internal coordinates for the $[B_{12}H_{12}]^{2-}$ icosahedron

I_h	E	$15C_2$	$20C_3$	$12C_5$	$12C_5^2$	i	15σ	$20S_6$	$12S_{10}$	$12S_{10}^3$
B-H	12	0	0	2	2	0	4	0	0	0
B-B	30	2	0	0	0	0	4	0	0	0
$\hat{BBH}$	60	0	0	0	0	0	4	0	0	0
$\hat{BBB}_{ac.}$	60	0	0	0	0	0	4	0	0	0
$\hat{BBB}_{ob.}$	60	0	0	0	0	0	4	0	0	0

Reduction of these representations using the magic formula leads to the following irreducible representations:

$$\Big\lceil^{I_h}_{B\text{-}H} = \underline{a}_g + \underline{t}_{1u} + \underline{t}_{2u} + \underline{h}_g \qquad (49)$$

$$\Big\lceil^{I_h}_{B\text{-}B} = \underline{a}_g + \underline{g}_g + 2\underline{h}_g + \underline{t}_{1u} + \underline{t}_{2u} + \underline{g}_u + \underline{h}_u \qquad (50)$$

$$\Big\lceil^{I_h}_{BBH} = \underline{a}_g + \underline{t}_{1g} + \underline{t}_{2g} + 2\underline{g}_g + 3\underline{h}_g + 2\underline{t}_{1u} + 2\underline{t}_{2u} + 2\underline{g}_u + 2\underline{h}_u \qquad (51)$$

The B-$\hat{\text{B}}$-B angles [acute (60°) and obtuse (108°)] reduce in the same way as the B-$\hat{\text{B}}$-H angle above.

The total number of modes obtained from combining representations of the internal coordinates is much higher than the total number of modes obtained from treating the structure as a composite of vibrating atoms.

$$\Big\lceil_{\text{B-H}} = \underline{a}_g + \underline{h}_g + \underline{t}_{1u} + \underline{t}_{2u} \qquad (52)$$

$$\Big\lceil_{\text{B-B}} = \underline{a}_g + \underline{g}_g + 2\underline{h}_g + \underline{t}_{1u} + \underline{t}_{2u} + \underline{g}_u + \underline{h}_u \qquad (53)$$

$$\Big\lceil_{\text{(3) angles}} = 3\underline{a}_g + 3\underline{t}_{1g} + 3\underline{t}_{2g} + 6\underline{g}_g + 9\underline{h}_g + 6\underline{t}_{1u} + 6\underline{t}_{2u} + 6\underline{g}_u + 6\underline{h}_u \qquad (54)$$

$$\Big\lceil^{\text{int.}}_{\text{total}} = 5\underline{a}_g + 3\underline{t}_{1g} + 3\underline{t}_{2g} + 7\underline{g}_g + 12\underline{h}_g + 8\underline{t}_{1u} + 8\underline{t}_{2u} + 7\underline{g}_u + 7\underline{h}_u \qquad (55)$$

$$\Big\lceil^{I_h}_{\text{total}} = 2\underline{a}_g + 2\underline{t}_{1g} + 2\underline{g}_g + 4\underline{h}_g + 4\underline{t}_{1u} + 2\underline{t}_{2u} + 2\underline{g}_u + 2\underline{h}_u \qquad (56)$$

$$\text{difference} = 3\underline{a}_g + \underline{t}_{1g} + 3\underline{t}_{2g} + 5\underline{g}_g + 8\underline{h}_g + 4\underline{t}_{1u} + 6\underline{t}_{2u} + 5\underline{g}_u + 5\underline{h}_u$$

The difference (Eq. 57) represents the redundant species in the internal coordinate calculations. These redundancies result from the interdependence of the internal coordinates, especially the inter-bond angles. For example, it is physically impossible to alter all the angles of a given type in the same manner at the same time. Since the B-H orbitals are nearly independent from the B-B skeletal system[75,79], it can be safely assumed that the redundancies belong to the representations of the different inter-bond angles. This large number of redundant modes is a consequence of the high symmetry of the structure.

After omitting the optically-inactive species, the representations reduce as follows:

$$\Gamma_{\text{B-H}} = \underline{a}_g + \underline{h}_g + \underline{t}_{1u} \tag{58}$$

$$\Gamma_{\text{B-B}} = \underline{a}_g + 2\underline{h}_g + \underline{t}_{1u} \tag{59}$$

$$\Gamma_{\text{(3) angles}} = \underline{h}_g + \underline{t}_{1u} \tag{60}$$

$$\Gamma^{I_h}_{\text{gen. (opt. active)}} = 2\underline{a}_g(R) + 4\underline{h}_g(R) + 3\underline{t}_{1u}(ir) \tag{61}$$

The above representations (Eqs. 58-60) can also be expressed in terms of hydrogen or boron atom movements. For example, the vibrational species which are due to hydrogen atom movements will be composed of B-H stretching and B-B-H bending modes. In the same way, the vibrations due to boron atom movements will include the B-B stretching species and the B-B-B bending species. Since the high symmetry of the $[B_{12}H_{12}]^{2-}$ ion has resulted in the equivalence of the representations of the three inter-bond angles, it is impossible to assign specific modes to the different angle coordinates.

2. Application of the Product Rule

Isotopic substitution studies afford additional aids in the assignment of the internal modes. Calculations using the vibrational frequencies of isotopic molecules provide valuable information about the nature of the motions involved in each vibration. For example, we make use of the fact that atoms which move with considerable amplitudes in a particular normal mode produce larger isotopic shifts than those atoms having minimal displacements in the same mode[109]. Another important theorem which is applied in the study of isotope effects is the Teller-Redlich product rule which states that the product of the harmonic $(\frac{\omega_i}{\omega})$ values for all vibrations of a given symmetry type is independent of the potential constants and depends only on the symmetry of the molecule and the masses of the atoms involved in the vibra-

tion. The general equation and the detailed application of this rule to $[B_{12}H_{12}]^{2-}$ and $[B_{12}D_{12}]^{2-}$ are shown in Appendix II.

To apply the product rule, a molecule is divided into sets of equivalent atoms, i.e., atoms that are transformed into one another by the symmetry operations[109]. In the case of $[B_{12}H_{12}]^{2-}$, there are two such sets, the (B_{12}) and the (H_{12}) sets. On applying the usual group theoretical approach to these sets, the characters χ_j are produced.

TABLE VI: Characters of sets of equivalent atoms in the $[B_{12}H_{12}]^{2-}$ ion

	E	$15C_2$	$20C_3$	$12C_5$	$12C_5^2$	i	15σ	$20S_6$	$12S_{10}$	$12S_{10}^3$
χ_j (B_{12})	36	0	0	2	2	0	4	0	0	2
χ_j (H_{12})	36	0	0	2	2	0	4	0	0	2

Reduction of these representations give the symmetry species

attributed to the movements of atoms of each set (Eq. 62).

$$\Gamma_{B_{12}} = \Gamma_{H_{12}}$$

$$= \underline{a}_g + \underline{t}_{1g} + \underline{g}_g + 2\underline{h}_g + 2\underline{t}_{1u} + \underline{t}_{2u} + \underline{g}_u + \underline{h}_u \qquad (62)$$

When only optically active species are considered, we obtain:

$$\Gamma_{(B_{12})} = \underline{a}_g + 2\underline{h}_g + 2\underline{t}_{1u} \qquad (63)$$

$$\Gamma_{(H_{12})} = \underline{a}_g + 2\underline{h}_g - 2\underline{t}_{1u} \qquad (64)$$

$$\Gamma_{B_{12}H_{12}} = 2\underline{a}_g + 4\underline{h}_g + 4\underline{t}_{1u} \qquad (65)$$

These results are complicated by the fact that a non-genuine translational mode ($\underline{t}_{1u}$) has to be subtracted from only one of these equations and we do not know from which one. Another complicating factor is the feasibility of mixing the hydrogen

and the boron vibrations in this highly symmetrical ion. For these reasons, this approach fails to furnish any useful information.

Studying the vibrational isotopic effect for the two isotopic molecules $[B_{12}H_{12}]^{2-}$ and $[B_{12}D_{12}]^{2-}$ provides a clearer indication about the type of atoms involved in a given vibration. A useful formula for this purpose is $\frac{\nu^i}{\nu} \simeq \sqrt{\frac{m}{m_i}}$, where ν is the observed frequency of the vibration, m is the mass of the representative atom in a vibrating set; and the superscript (i) denotes the heavier isotope[109]. When the $(\frac{\nu^i}{\nu})$ value is near unity, this indicates that the vibration considered is due to movements of boron atoms. On the other hand, if the isotopic ratio $(\frac{\nu^i}{\nu})$ is close to $\sqrt{\frac{m_H}{m_D}} = \sqrt{0.5}$, the corresponding vibration is regarded as a result of H(D) atom movements. When the $(\frac{\nu^i}{\nu})$ values are intermediate between 1 and $\sqrt{0.5}$, the vibrations involve both the hydrogen and the boron atoms[79].

The Teller-Redlich theorem is based on a harmonic oscillator approximation and thus holds strictly only for the zero-order frequencies ω_i. However, the observed fundamentals (ν_i) are the ones normally used in these calculations, and since $\omega_i^i - \nu_i^i$ is smaller than $\omega_i - \nu_i$, the $\frac{\nu^i}{\nu}$ ratio is smaller than $\frac{\omega^i}{\omega}$. Consequently, the product $\frac{\nu_1^i}{\nu_1}.\frac{\nu_2^i}{\nu_2}...$ is always larger than $\frac{\omega_1^i}{\omega_1}.\frac{\omega_2^i}{\omega_2}...$[109]. Also, for vibrations involving hydrogen atom movements, the value of $(\frac{\nu^i}{\nu})^2$ is around 0.57 instead of

the theoretical value, $\frac{m_H}{m_D} = 0.50$. Application of the product rule to the vibrational fundamentals of $[B_{12}H_{12}]^{2-}$ and $[B_{12}D_{12}]^{2-}$ helps in the assignment of the various normal modes of these icosahedral ions (see Appendix II).

This type of approach was carried out initially by Muetterties et al.[79]. However, owing to the greater accuracy of the measurements in the present case, the procedure will be repeated here using the data observed in this study.

The group theoretical predictions for the $[B_{12}H_{12}]^{2-}$ ion [and also the $[B_{12}X_{12}]^{2-}$ (X=Cl, Br, I) ions] are that there should be three ir-active bands ($3\underline{t}_{1u}$ and six Raman-active ones ($2\underline{a}_g + 4\underline{h}_g$). Moreover, there should be three B-H stretching modes ($\underline{a}_g + \underline{t}_{1u} + \underline{h}_g$), four B-B stretching modes ($\underline{a}_g + \underline{t}_{1u} + 2\underline{h}_g$), one B-B-H bending mode ($\underline{t}_{1u}$) and one B-B-B bending mode ($\underline{h}_g$).

These predictions apply to the "free ion" in solution. Muetterties et al.[79] recorded the ir and Raman spectra of $Na_2[B_{12}H_{12}]$ and $Na_2[B_{12}D_{12}]$ (~90% D-enriched) in aqueous solutions. In the present study, the aqueous ir spectra were not re-investigated; however, in view of the superior Raman instrumentation now available, these spectra were re-examined. Muetterties et al.[79] used a Rank and Wiegand Raman spectrophotometer[110] with Hg-arc excitation (435.8 nm line). Using modern Raman spectrometers and laser excitation, much higher resolution and higher quality spectra are obtainable.

TABLE VII: Vibrational spectra (cm^{-1}) of aqueous $[B_{12}H_{12}]^{2-}$ and $[B_{12}D_{12}]^{2-}$

$[B_{12}H_{12}]^{2-}$ ir Ref.79	$[B_{12}H_{12}]^{2-}$ Raman Ref.79	$[B_{12}H_{12}]^{2-}$ This work	$[B_{12}D_{12}]^{2-}$ ir Ref.79	$[B_{12}D_{12}]^{2-}$ Raman Ref.79	$[B_{12}D_{12}]^{2-}$ This work	Isotopic ratio square (ν^i/ν^2) (from this work)	Sym.	Vib. no.	Proposed assignment
	2518	2517[a] vs		1912	1910[f] vs	0.58 (H)	a_g	ν_1	B-H(D) out-of-phase-breath
2480			1882			0.57 (H)	t_{1u}	ν_3	B-H(D) str.
	2475	2472[b] vs		1867	1864[g] vs	0.57 (H)	h_h	ν_6	B-H(D) str.
1070			932			0.76 (B+H)	t_{1u}	ν_4	B-B str. and B-H def. (cage vibration)
	949	954 m		888	896 m	0.88 (B)	h_g	ν_7	B-B str.
	770	774[c] m		736	622[h] m	0.65 (B+H)	h_g	ν_8	B-B str. and B.H def.
	743	746[d] s		716	718[i] s	0.93 (B)	a_g	ν_2	in-phase cage breath. (B-B str.)
720			596			0.68 (B+H)	t_{1u}	ν_5	B-B-H bend.
	584	582[e] m		620	542 w	0.87 (B)	h_g	ν_9	B-B-B bend.

Satellite ^{10}B bands (cm^{-1}):

[a] 2530 [c] 780 [e] 590 [g] 1872 [i] 738

[b] 2480 [d] 755 [f] 1938 [h] 648

[j] The B and H in parentheses indicate which atoms are moving in a particular vibration.

3. Band Assignments

The observed vibrational spectra of the $[B_{12}H_{12}]^{2-}$ and $[B_{12}D_{12}]^{2-}$ ions in aqueous solutions are given in Table VII. Typical spectra are shown in Fig. 12. The assignments are best discussed in terms of the following group vibrations: B-H stretching, boron cage skeletal modes and B-B-H bending modes.

a. B-H stretching modes

The strongest absorption in the aqueous ir spectrum of the $[B_{12}H_{12}]^{2-}$ ion is at 2480 cm^{-1}. Deuterium substitution shifts this band to 1882 cm^{-1} and the isotopic ratio square (0.57) shows that the vibration is due to movements of the hydrogen atoms of the cage. Thus, these bands are readily assigned to the B-H(D) stretching vibrations (ν_1). The B-H absorption is at higher energy than is usually found for B-H stretching in ions, e.g., 2270-2240 cm^{-1} for $[BH_4]^-$.[76] This frequency shift is perhaps due to the super-aromaticity of the icosahedral cage[77].

In the Raman spectra of both $[B_{12}H_{12}]^{2-}$ and $[B_{12}D_{12}]^{2-}$, there are two strong bands which can be attributed to B-H(D) stretching. The isotopic product rule data indicate that these bands are due to the movements of the hydrogen atoms of the molecules. For $[B_{12}H_{12}]^{2-}$, the band at 2472 cm^{-1} is depolarized and is thus considered to belong to the h_g species

(ν_6). The other band at 2517 cm^{-1} is the strongest in the Raman spectrum and is strongly polarized ($\rho \approx 0.1$). Thus, this band is attributed to the totally symmetric $\underline{a}_g$ mode (ν_1). The corresponding assignements for $[B_{12}D_{12}]^{2-}$ are 1910 ($\underline{a}_g$, ν_1) 1864 cm^{-1} ($\underline{h}_g$, ν_6). All the B-H(D) stretching bands are extremely intense in both the ir and Raman and there are significantly weaker, higher energy, satellite bands attributable to ^{10}B substituted molecules (see footnotes to Table VII).

b. The cage or skeletal vibrations

i. B-B stretching modes

One of the main features of the ir spectrum of $[B_{12}H_{12}]^{2-}$ is the strong absorption at 1070 cm^{-1} which is shifted to 932 cm^{-1} in the spectrum of the D-enriched isotopic species. This is a characteristic vibration of polyhedral boranes and is usually called the cage absorption[69]. The mode is attributed mainly to B-B stretching, but it is apparently strongly mixed with other vibrations because of its high frequency and high intensity. This is confirmed by Teller-Redlich isotopic calculations which indicate that movements of both H(D) and boron atoms contribute to these fundamentals. Therefore, these normal modes also include B-B-H(D) bending motions. It is evident that these bands are of $\underline{t}_{1u}$ symmetry (ν_4), since this is the only species having ir activity in the icosahedral point group.

In the Raman spectra of $[B_{12}H_{12}]^{2-}$, the intense absorption at 746 cm^{-1} is strongly polarized ($\rho \approx 0.1$) and consequently belongs to the totally symmetric $\underline{a}_g$ mode (ν_2). Deuterium substitution shifts this band to 718 cm^{-1} and $(\frac{\nu_2^1}{\nu_2})$ calculations prove that this fundamental derives from movements of boron atoms only. On this basis, the 746 cm^{-1} (H) and 718 cm^{-1} (D) bands are assigned to the B-B stretching of the in-phase breathing vibration of the icosahedral cage.

Two medium intensity Raman lines are observed in the solution spectra of $[B_{12}H_{12}]^{2-}$ at 954 and 774 cm^{-1}, with the corresponding bands for $[B_{12}D_{12}]^{2-}$ appearing at 896 and 622 cm^{-1}, respectively. The product rule calculations indicate that these bands also originate mainly from boron atom movements. These peaks are depolarized and therefore belong to the $\underline{h}_g$ species, ν_7 and ν_8. The broadness of these bands could be a result of accidental coincidences with either combination, overtone or ^{10}B isotope bands. The low intensities of the ν_7 and ν_8 B-B stretching vibrations is presumably indicative of weak intra-icosahedral forces.

ii. <u>The skeletal bending vibrations</u>

The medium intensity Raman band at 582 cm^{-1} for $[B_{12}H_{12}]^{2-}$ has an energy suggestive of a bending mode. Isotopic data show that this fundamental is a consequence of boron atom movements. Therefore, the band has been assigned to the B-B-B skeletal bending mode. Since the 582 cm^{-1} band is de-

polarized, it is due to the $\underline{h}_g$ symmetry species (ν_9). In $[B_{12}D_{12}]^{2-}$ this band appears at 542 cm^{-1}, but with very low intensity. Presumably this is why this band was not reported by Muetterties et al.[79] in their study of the dodecaborate ions. Instead they assigned the much stronger peak at $\sim$ 620 cm^{-1} to ν_9. That this frequency is 40 cm^{-1} higher than that of the (H) isotope led Weber and Thorpe[111] to suggest that the 620 cm^{-1} is not due to ν_9 and that the true location of this mode was $\sim$ 570 cm^{-1}. Our experimental value of 542 cm^{-1} provides additional support for Weber and Thorpe's[111] theoretical calculations.

c. Hydrogen bending modes

The ir bands at 720 and 596 cm^{-1} in the spectra of $[B_{12}H_{12}]^{2-}$ and $[B_{12}D_{12}]^{2-}$, respectively, are sharp and of medium-to-strong intensity. They are assigned to B-B-H(D) bending vibrations on the basis of isotope shift calculations which confirm that both boron and hydrogen atoms are involved in producing these modes. In common with the rest of the ir fundamentals, these bands (ν_5) have $\underline{t}_{1u}$ symmetry. Since the absorption for $[B_{12}H_{12}]^{2-}$ falls in the B-B stretching group frequency range[112], the isotopic study was of great value in making the assignment.

The proposed vibrational assignments for $[B_{12}H_{12}]^{2-}$ and $[B_{12}D_{12}]^{2-}$ are summarized in Table VII. It is worth emphasizing that unlike in many vibrational studies all the pre-

dicted fundamentals were observed.

B. VIBRATIONAL SPECTRA OF THE SOLID DODECABORATES

1. Introduction

The spectra of crystals usually show more bands than those of liquids or gases.

Inter-molecular interactions are much stronger in crystalline structures and this results in lowering of the symmetries of the free ions in crystals. This lowering of symmetry may remove the degeneracy of certain modes and may activate others which were inactive in the free species.

In solids, apart from the normal internal modes, there are also characteristic low-frequency bands usually called external or lattice modes[107]. These modes arise from the motions of the complete molecules relative to one another. The lattice bands are optically-active and usually appear in 0-50 cm^{-1} range, although some above 200 cm^{-1} have been reported[109,113]. These vibrations can be further subdivided into translatory and rotatory modes according to the origin of their motions. There are also three optically-inactive modes characteristic of the solid state, viz., the acoustic modes, which are responsible for propagating sound waves throughout crystals. These three modes result from the translational motions of the molecule as a whole within the crystal.

2. Factor Group Analysis

Because of the repetition patterns within crystal structures, the vibrational modes of solids can be considered as the resultants of identical in-phase movements within each primitive unit cell. On this basis, the different fundamental modes of a crystal can be obtained in a similar manner to those of discrete molecules, except that the entire primitive unit cell is considered. Thus, in factor group analyses, the entire unit cell of a crystalline lattice is treated as a vibrating unit subject to symmetry restrictions arising only from the geometry of the entire primitive unit cell. Rather than the molecular point group, as in the case for the free molecule, we use the factor group, i.e., the point group which is isomorphous with the space group of the unit cell of the crystal[113]. To obtain the point group isomorphous with a factor group, we drop the superscript of the Schoenflies symbol of the factor group. The group theoretical equations used are as follows:

i. Total number of modes

$$\chi_j = m_j(P)\ [\pm(1 + 2\cos\theta_j)] \qquad (66)$$

ii. Lattice modes

- Translational modes

$$[\chi_j(T')] = [m_j(S-1)]\ (\pm 1 + 2\cos\theta_j) \qquad (67)$$

- Rotational modes

$$[\chi_j(R')] = [m_j(S-V)]\ (1 + 2\cos\theta_j) \qquad (68)$$

iii. Acoustical modes

$$[\chi_j(T)] = 2\cos\theta_j \pm 1 \qquad (69)$$

where V is the number of monoatomic ions in the molecule; S is the total number of ions or groups of atoms in the unit cell; (S-V) is the number of polyatomic or complex ions; $m_j(P)$ is the number of atoms which remain invariant under an operation of class j; θ_j is the angle of rotation of an operation of class j; $m_j(S)$ is the number of ions or groups of atoms which transfer into themselves or their equivalents or whose centre of symmetry remain invariant under an operation of the class j; and $m_j(S-V)$ is the number of non-linear polyatomic groups which are invariant under an operation of class j[107].

In each case, the representations obtained from the above equations are reduced by the use of the "magic formula" to yield the corresponding number of modes (n).

iv. Internal modes

These intra-molecular vibrations [n(i)] are obtained by subtraction of acoustic and lattice modes from the total

number of modes. This can be achieved either by using the general equation (Eq. 70) or more simply Eq. 71.

$$\chi_j(i) = [m_j(P)-m_j(S)](2\cos\theta_j \pm 1)-m_j(S-V)(\pm 1 \pm 2\cos\theta_j) \qquad (70)$$

or

$$n(i) = [n(N)-n(T)-n(T')-n(R')] \qquad (71)$$

In order to apply successfully the factor group equations, it is important to recognize those invariant atoms or groups under the various symmetry operations of the factor (space) group. The atoms that are related by one or a succession of primitive translations are considered the same or identical atoms. The non-primitive translations are those included in the screw axes or glide planes. Furthermore, a point is regarded as invariant under the operation that transforms it either into itself or into an identical site in an adjacent unit cell. On the other hand, a site is not called invariant if the operation considered carries it into an identical or equivalent point in the same unit cell or into an equivalent point in another adjacent unit cell. (Equivalent points are those having different coordinates but originating from the same symmetry operation).

3. Vibrational Spectra of $K_2B_{12}H_{12}$ and $K_2B_{12}D_{12}$

a. Application of factor group analysis

These salts crystallize in the space group $Fm3(T_h^3)$ of the cubic system with four molecules in the crystallographic unit cell[72]. The primitive Bravais cell, however, has only one molecule (Fig. 9). Since this Bravais cell does not possess cubic symmetry, it cannot be utilized in the spectroscopic analysis. The Wigner-Seitz or primitive-symmetric cell possessing the symmetry of the space group, in our case cubic, is the spectroscopic cell used in the factor group analysis (Fig. 10). This cell is a dodecahedron formed by both the K^+ ions and the $[B_{12}H_{12}]^{2-}$ icosahedral units. In this dodecahedron, the K^+ ions occupy the triedged intersections (C_3 axes), while the $[B_{12}H_{12}]^{2-}$ icosahedral units are located at the quadri-edged intersections (C_4 axes) or at the centre of the Wigner-Seitz cell (Fig. 11)[107].

Using the symmetry of the Wigner-Seitz cell (Fig. 11) and applying the procedures of the factor group analysis outlined earlier, the different modes of vibrations for $K_2B_{12}H_{12}$ (or its isostructural analogues) can be obtained. The results of this analysis are summarized in Table VIII.

From the factor group calculations, we arrive at the number of modes for each type of motion in the crystal. From Table VIII, the [redacted]rational representation for the $K_2B_{12}H_{12}$ crystal reduces as shown in Eq. 72; the optical

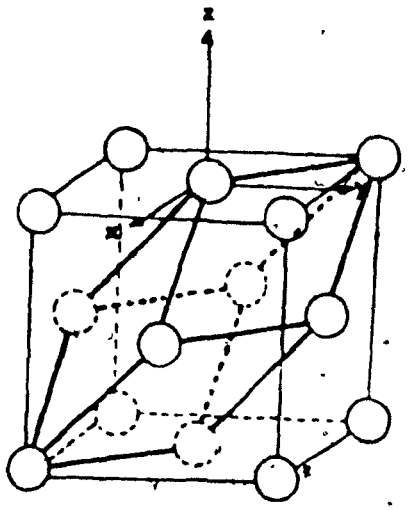

FIGURE 9:

The primitive cell superimposed on the Bravais lattice of $K_2B_{12}H_{12}$.

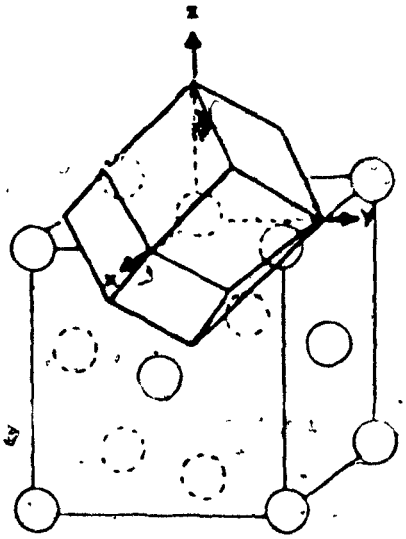

FIGURE 10:

The Wigner-Seitz cell superimposed on the Bravais lattice of $K_2B_{12}H_{12}$.

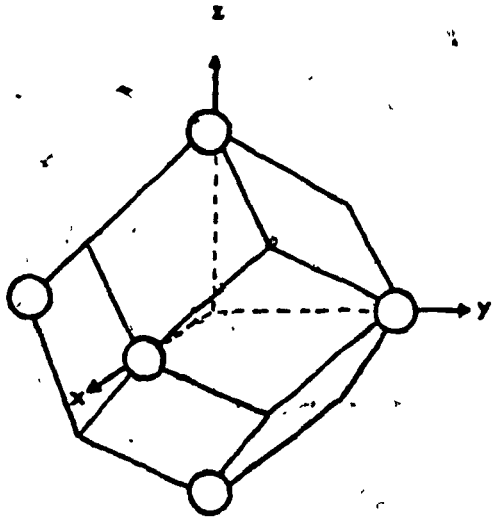

FIGURE 11: Wigner-Seitz cell for $K_2B_{12}H_{12}$.

TABLE VIII: Factor group analysis for $K_2B_{12}H_{12}$ and its isostructural analogues[a]

T_h^3	E	$3C_2$	$8C_3$	i	3σ	$8S_6$	N	T	T'	R'	n_i	Activity
A_g	1	1	1	1	1	1	4	0	0	0	4	Raman
E_g	2	2	-1	2	2	-1	4	0	0	0	4	Raman
$F_g=T_g$	3	-1	0	3	-1	0	9	0	1	1	7	Raman
A_u	1	1	1	-1	-1	-1	2	0	0	0	2	
E_u	2	2	-1	-2	-2	1	2	0	0	0	2	
$F_u=T_u$	3	-1	0	-3	1	0	11	1	1	0	9	ir
$m_j(P)$	26	2	2	0	8	0						
$m_j(S)$	3	3	3	1	1	0						
$m_j(S-V)$	1	1	1	1	1	1						
$\pm1+2\cos\theta_j$	3	-1	0	-3	1	0						
$1\pm2\cos\theta_j$	3	-1	0	3	-1	0						
$[\chi_j(N)]$	78	-2	0	0	8	0						
$[\chi_j(T)]$	3	-1	0	-3	1	0						
$[\chi_j(T')]$	6	-2	0	0	0	0						
$[\chi_j(R')]$	3	-1	0	3	-1	0						
$[\chi_j(n_i)]$	66	2	0	0	8	0						

[a] $m_j(P)$ is the number of atoms which remain invariant under an operation of class j.

$m_j(S)$ is the number of ions or groups whose centre of symmetry remain invariant under the operation considered.

$m_j(S-V)$ is the number of polyatomic groups or ions among $m_j(S)$ which remain invariant under an operation of class j.

$[\chi_j(N)]$ is the representation for total number of modes.

$[\chi_j(T)]$ is the representation for acoustic or pure translational modes.

$[\chi_j(T')]$ is the representation for translational lattice modes.

$[\chi_j(R')]$ is the representation for rotational lattice modes.

$[\chi_j(n_i)]$ is the representation for internal vibrational modes.

activity of each individual species is indicated in parentheses.

$$\Big\lceil^{T_h}_{\text{cryst., total}} = 4\underline{a}_g(R) + 4\underline{e}_g(R) + 9\underline{t}_g(R) + 2\underline{a}_u(\text{inact.}) + 2\underline{e}_u(\text{inact.}) + 11\underline{t}_u(\text{ir}) \quad (72)$$

The representations for the internal and external modes are given in Eqs. 73 and 74, respectively.

$$\Big\lceil^{T_h}_{\text{cryst., int.}} = 4\underline{a}_g(R) + 4\underline{e}_g(R) + 7\underline{t}_g(R) + 2\underline{a}_u(\text{inact.}) + 2\underline{e}_u(\text{inact.}) + 9\underline{t}_u(\text{ir}) \quad (73)$$

$$\Big\lceil^{T_h}_{\text{cryst., ext.}} = \underline{t}_g(R) + \underline{t}_u(\text{ir}) \quad (74)$$

These equations represent all the possible modes obtainable under the T_h symmetry model. However, since most of the normal modes of the free $[B_{12}H_{12}]^{2-}$ anion are optically inactive and T_h symmetry is still a high symmetry group, many of the solid state modes will also be inactive. These inactive

TABLE IX: Correlation diagram for the free $[B_{12}H_{12}]^{2-}$ ion under I_h and T_h symmetries

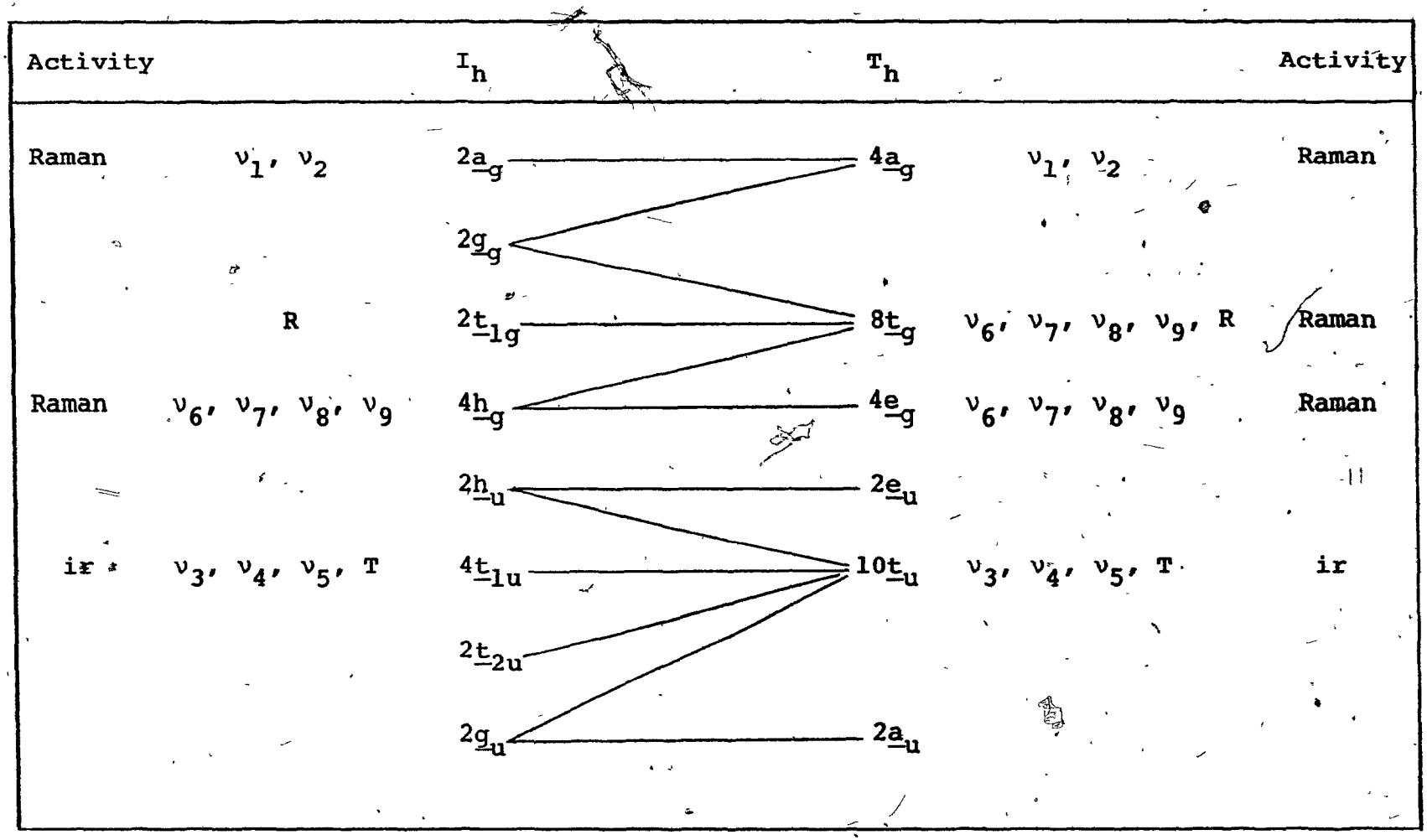

TABLE X: Complete correlation diagram for solid $K_2B_{12}H_{12}$ or its isostructural analogues

	Free ion symmetry I_h	Site symmetry T_h	Crystal symmetry T_h^3		Activity
ν_1, ν_2	$2\underline{a}_g$	$4\underline{a}_g$	$4\underline{a}_g$	ν_1, ν_2	Raman
	$2\underline{g}_g$				
T, R	$3\underline{t}_{1g}$	$9\underline{t}_g$	$9\underline{t}_g$	T, R, ν_6, ν_7, ν_8, ν_9	Raman
ν_6, ν_7, ν_8, ν_9	$4\underline{h}_g$	$4\underline{e}_g$	$4\underline{e}_g$	ν_6, ν_7, ν_8, ν_9	Raman
	$2\underline{h}_u$	$2\underline{e}_u$	$2\underline{e}_u$		
ν_3, ν_4, ν_5, T	$5\underline{t}_{1u}$	$11\underline{t}_u$	$11\underline{t}_u$	T, ν_3, ν_4, ν_5	ir
	$2\underline{t}_{2u}$				
	$2\underline{g}_u$	$2\underline{a}_u$	$2\underline{a}_u$		

TABLE XI: Correlation diagram for the optically-active modes of $K_2B_{12}H_{12}$ or its analogues

	Free ion symmetry I_h	Site symmetry T_h	Crystal symmetry T_h^3		Activity
ν_1, ν_2	$\underline{a}_g$	$\underline{a}_g$	$\underline{a}_g$	ν_1, ν_2	Raman
T, R	$\underline{t}_{1g}$	$\underline{t}_g$	$\underline{t}_g$	ν_6, ν_7, ν_8, ν_9, T, R	Raman
ν_6, ν_7, ν_8, ν_9	$\underline{h}_g$	$\underline{e}_g$	$\underline{e}_g$	ν_6, ν_7, ν_8, ν_9,	Raman
ν_3, ν_4, ν_5, T	$\underline{t}_{1u}$	$\underline{t}_u$	$\underline{t}_u$	ν_3, ν_4, ν_5, T	ir

modes are eliminated by correlating the free-ion modes with those of the crystalline solid. The three point groups needed to establish the correlation diagram are those of the free molecule (I_h), the factor group (T_h^3) and the site that the molecule occupies in the unit cell of the crystal. The site group is usually a subgroup of both the molecular and the factor groups[107] (rarely it is the same as either one but it is, of course, never of higher symmetry).

The multiplicity of the site occupied by the icosahedra should be equal to the number of molecules per unit cell (Z). In the case of $K_2B_{12}H_{12}$, Z=4. In the representation of the T_h^3 space group (Halford's tables), there is only one site having multiplicity of (4)[107]. Therefore, the site group for the icosahedra is easily established as having a T_h symmetry. Since, for $K_2B_{12}H_{12}$, the site group is isomorphous with the space group, there is no further splitting in going from the site symmetry to the factor group.

In order to equalize the number of modes on both sides of the correlation diagram, extra translatory species have to be added to the representation of the free ion. There are 2 x 3 = 6 translatory modes resulting from the movements of the two K^+ cations. These species are obtained from the character table of the tetrahedral point group (T) which is the site group of the K^+ ions in the crystal lattice of $K_2B_{12}H_{12}$. The two translational modes ($2\underline{t}$) of the T point group are split into two species ($\underline{t}_{1g} + \underline{t}_{1u}$) under icosahedral

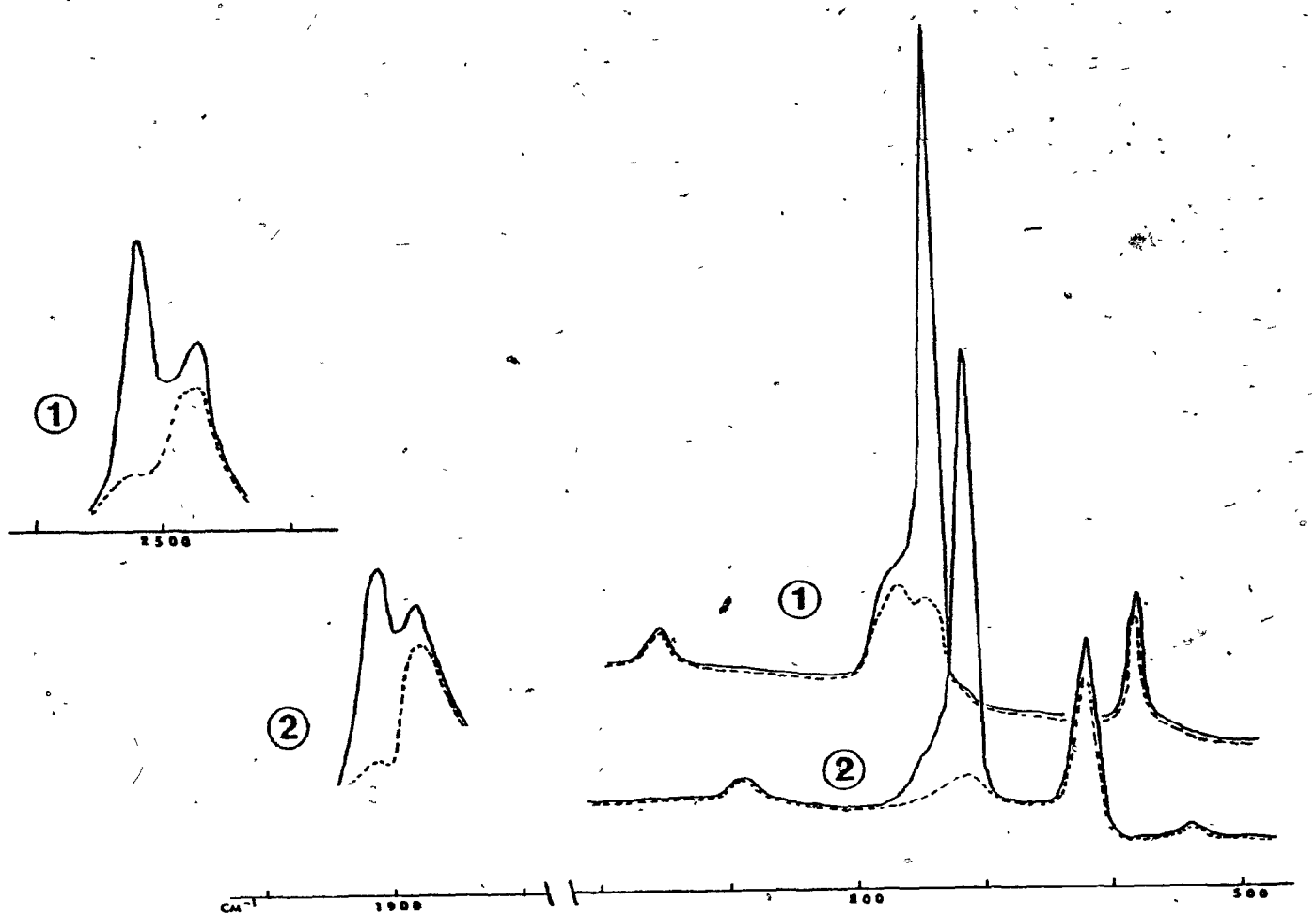

FIGURE 12: Raman spectra of aqueous solutions of (1) $K_2B_{12}H_2$ and $K_2B_{12}D_{12}$ (——— and ----- for ∥ and ⊥ spectra respectively).

symmetry. Using the correlation diagram (Table XI), the optically-inactive species can be eliminated. Equation 75 represents the optically-active modes of the $K_2B_{12}H_{12}$ salt.

$$\Big\lceil^{T_h}_{\text{cryst., opt. act.}} = 2\underline{a}_g(R) + 5\underline{t}_g(R) + 4\underline{e}_g(R) + 4\underline{t}_u(ir) \qquad (75)$$

The internal and external modes are shown in Eqs. 76 and 77.

$$\Big\lceil^{T_h}_{\text{cryst., int.}} = 2\underline{a}_g(R) + 4\underline{e}_g(R) + 4\underline{t}_g(R) + 3\underline{t}_u(ir) \qquad (76)$$

$$\Big\lceil^{T_h}_{\text{cryst., ext.}} = \underline{t}_g \text{ (trans. or rotn., R)} + \underline{t}_u \text{ (trans., ir)} \qquad (77)$$

The normal vibrations of $K_2B_{12}H_{12}$ (or $K_2B_{12}D_{12}$) can also be classified in terms of internal coordinates, as in Eqs. 78-81.

$$\Big\lceil^{T_h}_{\text{B-H(D)}} = \underline{a}_g(R) + \underline{e}_g(R) + \underline{t}_g(R) + \underline{t}_u(ir) \qquad (78)$$

$$\Big\lceil^{T_h}_{B\text{-}B} = \underline{a}_g(R) + 2\underline{e}_g(R) + 2\underline{t}_g(R) + \underline{t}_u(ir) \qquad (79)$$

$$\Big\lceil^{T_h}_{B\text{-}B\text{-}B} = \underline{e}_g(R) + \underline{t}_g(R) \qquad (80)$$

$$\Big\lceil^{T_h}_{B\text{-}B\text{-}H(D)} = \underline{t}_u(ir) \qquad (81)$$

The correlation analysis clearly indicates that all the ir bands of the free ion will appear in the spectra of the crystalline solid without further splitting. There is also an ir-active lattice band expected in the far-ir region. The Raman spectrum of the solid should include the two $\underline{a}_g$ modes of the icosahedral ion and four doublets ($\underline{e}_g + \underline{t}_g$), as well as a low-frequency lattice band.

b. Band assignments

In order to discuss the vibrational spectra of $K_2B_{12}H_{12}$ and its deuterated analogue, the following vibrational classes will be considered: B-H stretching ($\underline{a}_g$, $\underline{e}_g$ +

TABLE XII: Calculation of the isotopic ratio squares for solid $K_2B_{12}H_{12}$ and $K_2B_{12}D_{12}$

$K_2B_{12}H_{12}$ ir	$K_2B_{12}H_{12}$ Raman[b]	$K_2B_{12}D_{12}$ ir	$K_2B_{12}D_{12}$ Raman[b]	Isotopic ratio square $(\nu i/\nu)^2$[a]		Normal mode	Proposed assignments.
	2521 vs		1905 vs	0.57	(H)	ν_1 ($\underline{a}_g$)	B-H(D) cage breath.
2471 vs		1876 vs		0.58	(H)	ν_3 ($\underline{t}_{1u}$)	B-H(D) str.
	2495 vs		1878 vs	0.57	(H)	ν_6 ($\underline{h}_g$)	B-H(D) str.
1074 s		928 s		0.74	(B+H)	ν_4 ($\underline{t}_{1u}$)	B-B str. and B-H bend. (cage vibration)
	960 m		892 m	0.87	(B)	ν_7 ($\underline{h}_g$)	B-B str.
	766 m		621 m	0.65	(B+H)	ν_8 ($\underline{h}_g$)	B-B str. and B-H def.
	757 m		721 m	0.90	(B)	ν_2 ($\underline{a}_g$)	B-B str. (in-phase cage breath.)
715 m		597 m		0.70	(B+H)	ν_5 ($\underline{t}_{1u}$)	B-B-H bend.
	585 m		547 w	0.87	(B)	ν_9 ($\underline{h}_g$)	B-B-B bend.

[a]The B and H in parentheses indicate which atoms are moving in a particular vibration.
[b]When an $\underline{h}_g$ mode splits, the average of the doublet is used.

$\underline{t}_g$, $\underline{t}_u$), B-B stretching ($\underline{a}_g$, $2(\underline{e}_g + \underline{t}_g)$, $\underline{t}_u$), B-B-B bending ($\underline{e}_g + \underline{t}_g$), B-B-H bending ($\underline{t}_u$), lattice bands ($\underline{t}_g$, $\underline{t}_u$), together with the combination and overtones and the ^{10}B isotope satellite bands.

i. B-H stretching modes

The strongest absorptions in the ir spectra are the B-H stretching modes at 2471 (Nujol) and 2485 cm^{-1} (KBr) with the deuterated salt absorbing in the 1880-1872 cm^{-1} range in Nujol. The isotopic effect calculations indicate that these bands are of H(D) origin. In the Nujol mull ir spectrum, the B-H stretching fundamental of $K_2B_{12}H_{12}$ at 2471 cm^{-1} shows some fine structure on the high energy side of the band. This structure is attributed to solid-Nujol lattice-lattice interactions. The bands of solid $K_2B_{12}H_{12}$ and $K_2B_{12}D_{12}$ are only slightly shifted from the 2480 and 1882 cm^{-1} values for the free $[B_{12}H_{12}]^{2-}$ and $[B_{12}D_{12}]^{2-}$ ions, respectively. The bands are all assigned to the $\nu_3(\underline{t}_u)$ modes.

In the Raman spectrum of solid $K_2B_{12}H_{12}$, the B-H stretching region displays three strong peaks at 2521 (ν_1, $\underline{a}_g$) and 2497 and 2492 cm^{-1} (ν_6, $\underline{e}_g + \underline{t}_g$). Again, the assignments are made by analogy with those for the free ion. On deuteration, these bands shift to 1905 cm^{-1} (ν_1, $\underline{a}_g$) and 1886 and 1868 cm^{-1} (ν_6, $\underline{e}_g + \underline{t}_g$). Application of the isotopic product rule to these frequencies gives the ratio square $(\frac{\nu_i}{\nu})^2 \simeq 0.57$

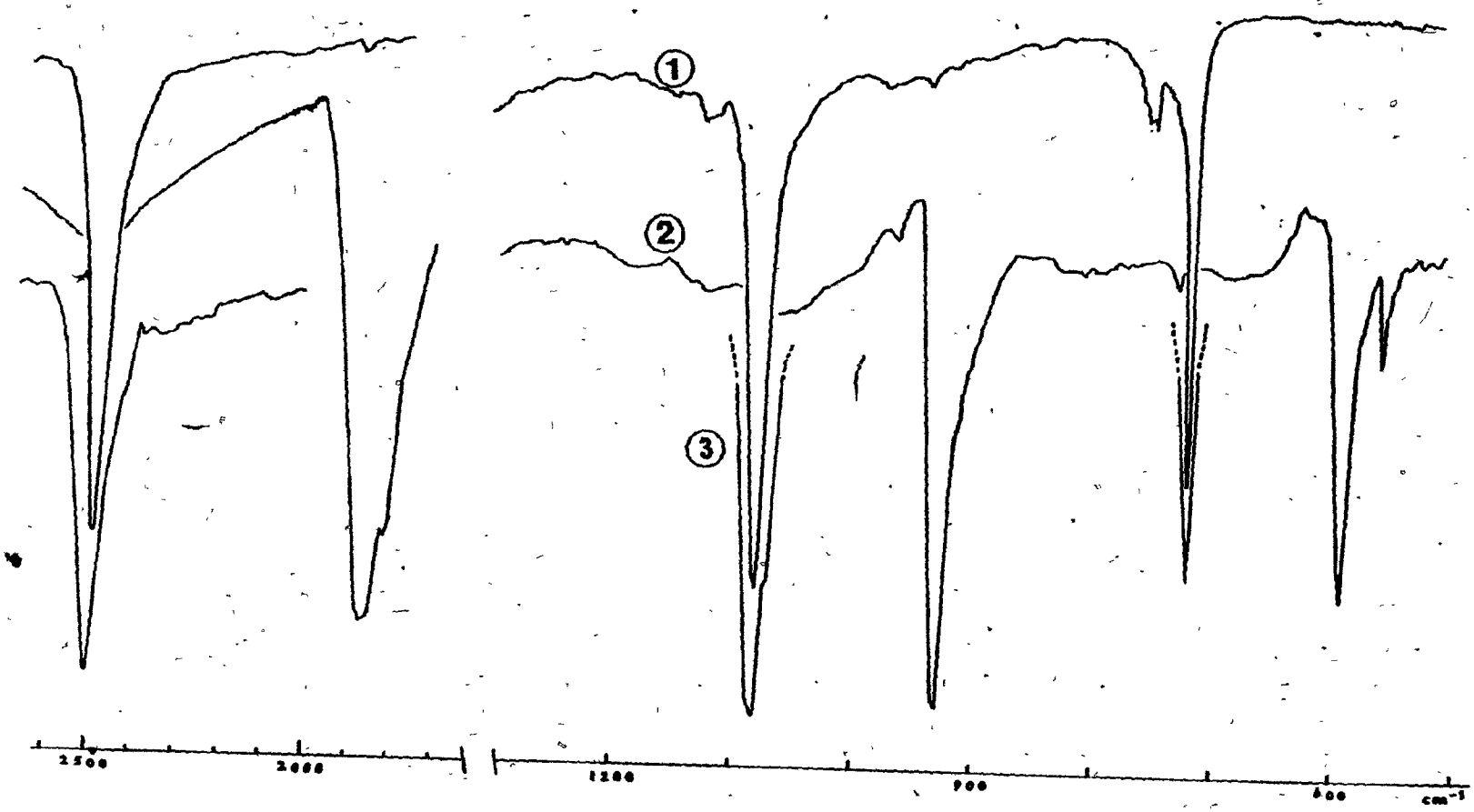

FIGURE 13: Infrared spectra (Nujol mull) of (1) $K_2B_{12}H_{12}$ (2) $K_2B_{12}D_{12}$ (3) $Cs_2B_{12}H_{12}$.

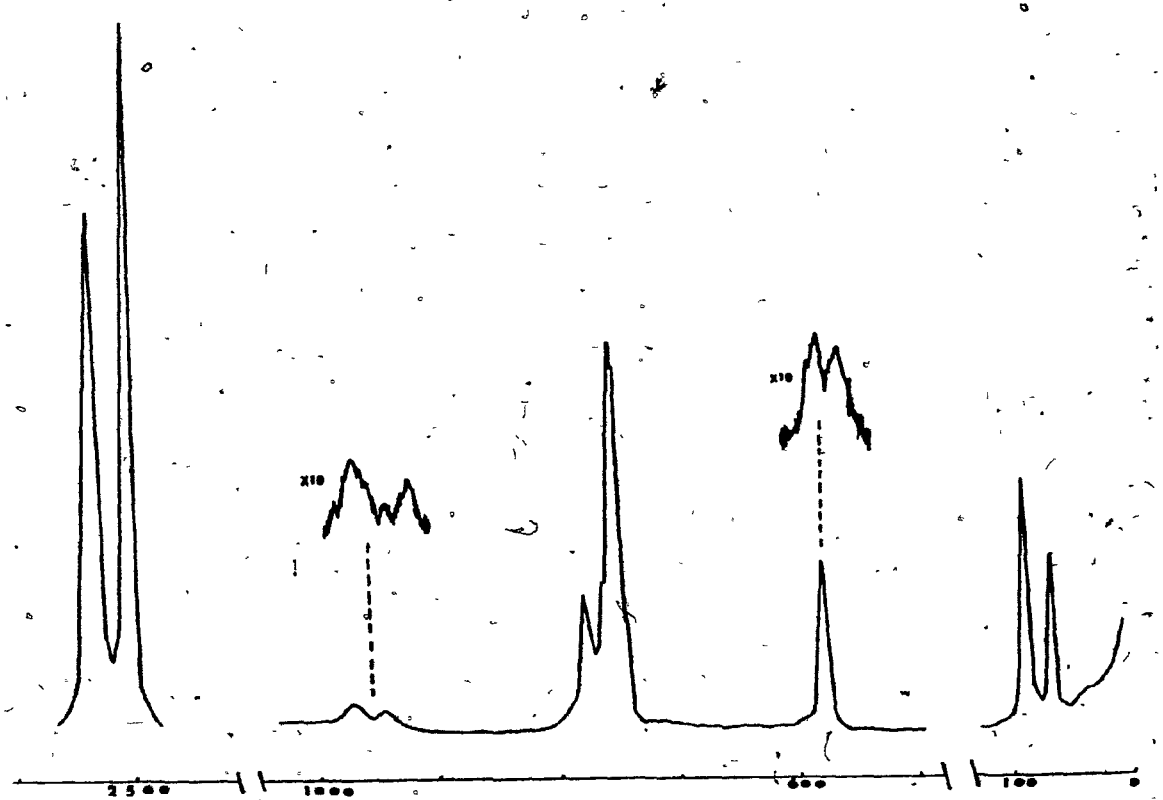

FIGURE 14: Raman spectrum of solid $K_2B_{12}H_{12}$ [Ar^+ excitation, 514 nm (∿400 mW)]. Conditions for survey spectrum: slit widths, 3 cm^{-1}; time constant, 1 sec; scan speed, 100 cm^{-1} min^{-1}.

FIGURE 15: Raman spectrum of solid $K_2B_{12}D_{12}$ [Ar^+ excitation, 514.5 nm (~300 mW)]. Conditions for survey spectrum: slit widths, 2 cm^{-1}; time constant, 1 sec; scan speed, 20 cm^{-1} min^{-1}.

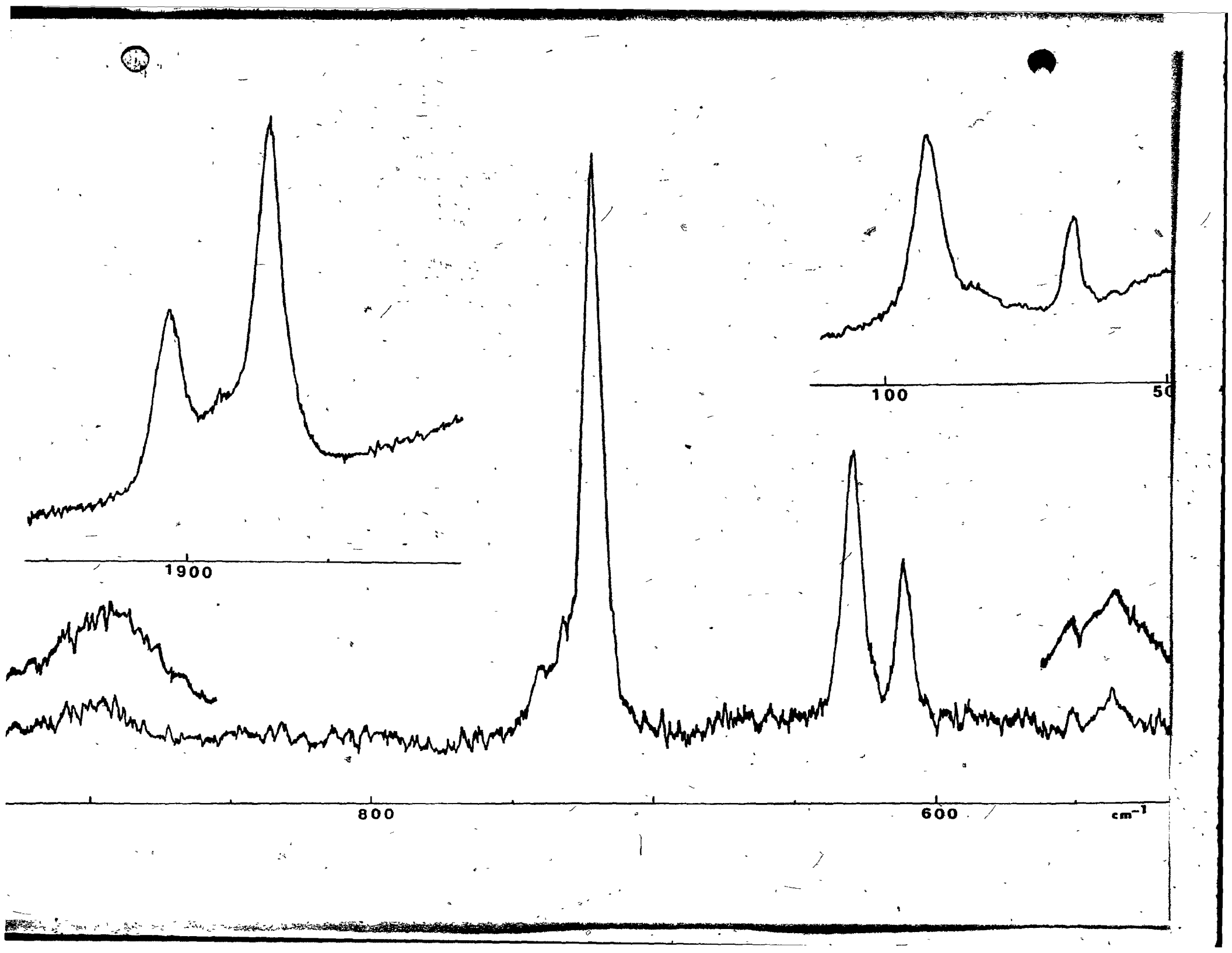
1900
100
800
600
cm⁻¹

confirming that these absorptions are due to movements of hydrogen atoms.

ii. Skeletal or cage absorptions

1) B-B stretching modes

The ir spectrum of solid $K_2B_{12}H_{12}$ shows the strong cage absorption characteristic of polyhedral boranes at 1074 cm^{-1} (ν_4, $\underline{t}_u$). This absorption drops to 928 cm^{-1} upon deuteration. The Teller-Redlich rule shows that both hydrogen and boron motions contribute to these fundamentals [$(\nu^i/\nu)^2 \approx 0.76$].

In the Raman spectrum, the strong lines at 757 and 721 cm^{-1} for $K_2B_{12}H_{12}$ and $K_2B_{12}D_{12}$, respectively, are shown by the product rule to be a result of boron atom movements [$(\nu^i/\nu)^2 \approx 0.90$]. Since the corresponding bands in the solution spectra are polarized, these bands are assigned to $\underline{a}_g$ modes (ν_2).

Two weak-to-medium intensity doublets appear in the Raman spectrum of solid $K_2B_{12}H_{12}$ at 973, 947 (ν_7, $\underline{e}_g + \underline{t}_g$) and 781, 751 cm^{-1} (ν_8, $\underline{e}_g + \underline{t}_g$). The analogous bands in the D-enriched salt are located at 894, 891 (ν_7, $\underline{e}_g + \underline{t}_g$) and 629, 612 cm^{-1} (ν_8, $\underline{e}_g + \underline{t}_g$), respectively. From the isotopic substitution data, these fundamentals are apparently due to boron atom movements; however, in ν_8, there are also hydrogen atom vibrations [compare $(\nu^i/\nu)^2 \approx 0.87$ and 0.65 for ν_7 and ν_8,

respectively]. As expected, the corresponding ν_7 and ν_8 solution bands are depolarized and have frequencies that are approximately the average of the associated doublets. This strongly supports the notion that the doublets are a result of the predicted solid-state splittings.

2) B-B-B bending modes

This skeletal vibration appears as a relatively strong doublet at 588 and 583 cm^{-1} in the Raman spectrum of solid $K_2B_{12}H_{12}$. This doublet is presumably due to crystal-field splitting of the 582 cm^{-1} (ν_9, $\underline{h}_g$) solution band and is therefore assigned as ν_9, $\underline{e}_g + \underline{t}_g$. Isotopic (D) substitution shifts these bands to 547 and 538 cm^{-1}, respectively.. The isotopic ratio square $(\frac{\nu^i}{\nu})^2$ is near unity confirming that the vibrations of boron atoms are the origin of these fundamentals.

iii. B-B-H bending modes

The hydrogen bending mode appears in the ir spectrum at 715 cm^{-1} for solid $K_2B_{12}H_{12}$ and at 598 cm^{-1} for the D-enriched salt. The product rule calculations confirm that the vibrations originate from the movements of both the boron and the hydrogen atoms [$(\nu^i/\nu)^2 \simeq 0.70$]. This ν_5, $\underline{t}_u$ peak is of medium intensity and is characteristic of boron hydrides of similar structure. According to Weber and Thorpe[111], the

hydrogen atoms contributing to this vibration move in a direction perpendicular to the B-H bond.

iv. Lattice modes

There are two peaks at 91(s) and 67(m) cm^{-1} in the Raman spectrum of solid $K_2B_{12}H_{12}$. These two bands appear at nearly the same frequencies in the Raman spectrum of $K_2B_{12}D_{12}$ [91(s) and 65(m) cm^{-1}, respectively]. Since lattice modes are not greatly affected by isotopic substitution, these bands are easily distinguished from the internal modes of the molecule. The 91 cm^{-1} bands, being of higher intensity, are assigned to the rotational $\underline{t}_g$ mode because rotational modes are generally more intense than translational ones[114].

According to the factor group analysis, there should be only one Raman-active lattice mode. This could be either the rotatory or the translatory vibration since both belong to the Raman-active $\underline{t}_g$ species. Consequently, the peaks at $\sim$ 66 cm^{-1} for the two salts can be considered to be the translational lattice fundamentals. Laser radiation interaction with the lattice frequencies may be partly responsible for the intensity of these translational bands[107].

On the basis of the weak combination bands listed below, it is quite probable that the ir-active translational lattice mode occurs at $\sim$ 240 cm^{-1}: 2755 $\approx$ 240 + 2521; 2720 $\approx$ 240 + 2492; 1220 $\approx$ 240 + 973; 1025 $\approx$ 240 + 781 and

$1003 \simeq 240 + 757\ cm^{-1}$.

v. Combinations and overtones

Binary combinations and overtones of the ir fundamentals will not be ir-active since the resulting species will have "gerade" (g) symmetry. These fundamentals, however, will be Raman-active. On the other hand, the binary combinations and overtones of the Raman bands will have Raman activity. Combination bands resulting from ir and Raman fundamentals are allowed in the ir spectrum. Ternary combinations and overtones of ir fundamentals are ir-active and those of Raman fundamentals are Raman active. Mixed ternary combinations such as (2 ir + 1 Raman) fundamentals are only Raman active, while summations (or differences) of (1 ir + 2 Raman) frequencies give rise to bands active in the ir spectrum. These selection rules are summarized in Eqs. 82-87 considering an icosahedral model.

$$\underline{t}_{1g}^2 = \underline{t}_{1u}^2 = \underline{t}_{2g}^2 = \underline{t}_{2u}^2 = A_g + H_g \quad (R) \tag{82}$$

$$\underline{h}_u^2 = \underline{h}_g^2 = A_g + G_g + H_g \quad (R) \tag{83}$$

$$\underline{a}_g + \underline{t}_{1u} = F_{1u} \quad (ir) \tag{84}$$

TABLE XIII: Expected and observed binary combinations and overtones of $K_2B_{12}H_{12}$ (cm^{-1})[a]

	ν_1 2493 a_g (R)	ν_2 757 a_g (R)	ν_3 2471 t_u (ir)	ν_4 1074 t_u (ir)	ν_5 715 t_u (ir)	ν_6 2521 a_g+t_g 2492 (R)	ν_7 973 a_g+t_g 947 (R)	ν_8 782 a_g+t_g 751 (R)	ν_9 588 a_g+t_g 583 (R)
ν_1 (R) 2493 a_g	(R) 4986	(R) (3250)	(ir) (4964)	(ir) (3567)	(ir) (3208)	(R) 5014 4985	(R) 3466 3430	(R) 3275 3244	(R) 3081 3076
ν_2 (R) 757 a_g		(R) (1514)	(ir) (3228)	(ir) (1831)	(ir) (1472)	(R) 3278 3249	(R) (1730) 1704	(R) (1539) 1508	(R) 1345 1340
ν_3 (ir) 2471 t_u			(R) 4942	(R) (2545)	(R) 3186	(ir) (4992) (4963)	(ir) (3444) (3418)	(ir) (3253) (3222)	(ir) (3059) (3054)
ν_4 (ir) 1074 t_u				(R) (2148)	(R) 1789	(ir) (3585) (3566)	(ir) (2057) (2021)	(ir) (1856) (1825)	(ir) (1662) (1657)
ν_5 (ir) 715 t_u					(R) 1430	(ir) (3236) (3207)	(ir) (1698) (1662)	(ir) (1497) (1466)	(ir) (1303) (1298)
ν_6 (R) 2521 2492 a_g+t_g						(R) 5042 5013 4984	R 3504 3468 3475 3439	R 3303 3274 3272 3243	R 3109 3104 3080 3075
ν_7 (R) 973 947 a_g+t_g							R 1946 (1920) (1894)	R 1755 1729 1724 1698	R 1597 1592 1561 1556
ν_8 (R) 782 751 a_g+t_g								R 1564 1533 1502	R 1370 1365 1339 1334
ν_9 (R) 588 583 a_g+t_g									R 1176 1166

Sym. about diagonal

[a]Observed frequencies are in parentheses.

$$\underline{a}_g + \underline{t}_{1g} = F_{1g} \qquad (R) \qquad (85)$$

$$\underline{t}_{1u} + \underline{h}_g = T_{1u} + T_{2u} + G_u + H_u \qquad (ir) \qquad (86)$$

$$\underline{t}_{1u} + \underline{h}_u = T_{1g} + T_{2g} + G_g + H_g \qquad (R) \qquad (87)$$

From the above equations, we can see that some inactive vibrations, e.g., $\underline{h}_u$ or $\underline{t}_{1g}$ can become active when combined with other fundamentals or overtones. Combination and overtones can be predicted through group theoretical calculations and examples are given in Appendix I.

Table XIII lists the expected frequencies for the $K_2B_{12}H_{12}$ combination and overtone bands with their optical activity indicated in parentheses. All the predicted ir-active binary combination bands were observed in the actual spectra. However, few Raman-active combinations or overtones were detected. Also, there are some combination bands involving the low-frequency lattice modes. The observed combinations and overtones are arranged together with the rest of $K_2B_{12}H_{12}$ frequencies in Table XIV.

vi. Satellite bands

The ^{10}B isotope has a relative abundance of 18.8%

and therefore isotopic bands are expected to appear in vibrational spectra especially for fundamentals of high intensity. In the ir spectrum of $K_2B_{12}H_{12}$, the three ir fundamentals show very weak ^{10}B satellite bands at higher energies in the correct proportion to that of the parent bands. Examples of the ir isotopic bands together with the associated parent symmetry species are as follows: 2510 s (ν_3, $\underline{t}_u$), 1118 w (ν_4, $\underline{t}_u$) and 748 w cm^{-1} (ν_5, $\underline{t}_u$).

In Raman scattering, isotopic bands also appear for the different fundamentals. In the Raman spectrum of $K_2B_{12}D_{12}$, the 738 cm^{-1} peak, which Muetterties et al.[79] had assigned to the (ν_8, $\underline{h}_g$) mode, is in fact more likely to be a ^{10}B satellite of the strong 721 cm^{-1} (ν_2, $\underline{a}_g$) band. The important Raman satellite bands are assigned in Table XIV. The isotopic frequency shift is found to be within 3% of the parent band frequency. Confirmation of the satellite band assignments must await complete normal coordinate calculations on the $[B_{12}H_{12}]^{2-}$ and the various isotopically substituted species.

vii. Low-temperature spectra

Raman spectra were also recorded for solid $K_2B_{12}H_{12}$ and $K_2B_{12}D_{12}$ at 73 ± 0.5 K primarily to determine whether or not any phase changes take place at low temperature. The spectra are essentially the same as those recorded at room temperature and no new splittings of the bands were detected,

TABLE XIV: Vibrational frequencies of $K_2B_{12}H_{12}$, $K_2B_{12}D_{12}$ and $Cs_2B_{12}H_{12}$ (pages 98, 99 and 100)

TABLE XIV: Vibrational frequencies of $K_2B_{12}H_{12}$, $K_2B_{12}D_{12}$ and $Cs_2B_{12}H_{12}$ (cm^{-1})

$K_2B_{12}H_{12}$					$K_2B_{12}D_{12}$					$Cs_2B_{12}H_{12}$		PROPOSED ASSIGNMENT	
IR		RAMAN			IR		RAMAN			IR	RAMAN		
Solution[b] (H_2O)	Solid[c]	Solution (H_2O)	Solid (room temp.)	Solid (73K)	Solution[b] (D_2O)	Solid[c]	Solution (D_2O)	Solid (room temp.)	Solid (73K)	Solid[c]	Solid (room temp.)	SYMMETRY[d]	VIBRATION
	3558 w											T_u	$\nu_1 + \nu_4$ or $\nu_4 + \nu_6$
	3460 w												
	3450 w									~3450 m		T_u	$\nu_3 + \nu_7$
	3440 w											T_u	$\nu_3 + \nu_7$?
	~3255 w											T_u	$\nu_3 + \nu_8$
	~3195 w				2480 w							T_u	$\nu_1 + \nu_5$ or $\nu_5 + \nu_6$
	~3080 w				2420 w								$\nu_3 + \nu_9$
	2960 w												
	2945 w												
	2840 w												
	2755 w												
	2720 w									2750 w		T_u	$\nu_1 + 240$ (or 220)[e]
										2675 w		T_u	$\nu_6 + 240$ (or 220)[e]
		2517 vs	2531 m 2521 vs	2532 m 2520 vs			1909 w 1905 vs	1907 w 1904 vs			2506 vs	A_g	ν_1, ^{10}B effect
			2501 m	2500 m			1897 w	1896 w				A_g	ν_1, B-H(D) str. (cage breath.)
		2472 vs	2497 vs 2492 vs	2497 vs 2491 vs		1864 vs	1886 m 1868 vs	1884 m 1869 vs			2475 s,sh 2471 s	$E_g + E_g$	ν_6, ^{10}B shift ν_6, B-H(D) str.
2480 vs	2510 s 2471 vs				1882 vs	1882 s 1876 vs							ν_3, ^{10}B satellite
	2430 w									2488 vs		T_u	ν_3
				2125 w									?
												E_g	$2\nu_4$
	2055 w					1835 w				2020 w		T_u	$\nu_4 + \nu_7$ or $\nu_4 + 2\nu_9$
	2020 w					1820 w						T_u	$\nu_4 + \nu_7$
	1980 w					1700 w				1970 w		T_u	$\nu_5 + 2\nu_9$

TABLE XIV: continued

	1878 w			1570 w			τ_u	$\nu_4 + \nu_8$	
	1820 w			1640 w			τ_u	$\nu_2 + \nu_4$	
	1710 w			1530 w			1770 w	τ_u	$\nu_5 + \nu_7$	
	1635 w							τ_u	$\nu_4 + \nu_9$ or $\nu_5 + \nu_7$	
	1620 w						1620 w		H_2O vapour ?	
	1600 m,br									
	1500 w,br							τ_u	$\nu_5 + \nu_8$ or $\nu_2 + \nu_5$	
	1420 w							τ_u	$\nu_5 + \nu_8$	
	1400 w							τ_u	$\nu_2 + 2\nu_4$	
	1380 w								?	
	1350 w								?	
1310	1310 w			1010 w				τ_u	$\nu_5 + \nu_9$	
	1260 w							τ_u	$2\nu_4 - \nu_7$	
	1220 w							τ_u	$\nu_7 + 240$	
	1118 w			964 w			1120 w	ξ_u	ν_4, ^{10}B effect	
1070 s	1074 vs		932 s	928 vs			1075 vs	ξ_u	ν_4, cage absorption	
	1025 w						1035 w	τ_u	$\nu_8 + 240$ (or 220)*	
	1003 w							τ_u	$\nu_2 + 240$	
		971 vw			900 w	898 w			ν_7, satellite	
		973 m	975 m		894 w	895 m	973 m	$a_g + t_g$	ν_7, B-B str. and a 'weak' satellite	
	954 m	955 w		896 m						
		947 m	948 m		891 m	892 m	938 m			
	938 vw								?	
	918 w								?	
	828 vw							τ_u	$2\nu_5 + \nu_9$ or 716 + 91	
		787 m	786 w		629 s	629 s	787 m			
	774 m	781 m	782 m	622 s				$a_g + t_g$	ν_8, B-B str. and B-H def.	
		751 s	752 s		612 m	612 m	772 m			
		771 m	772 m		738 m	737 m	763 m	a_g	ν_2, cage breath (B-B) & ^{10}B shift	
	746 vs	757 vs	758 vs	718 vs	721 vs	721 vs	747 vs			

TABLE XIV: continued

	752 w										T_u	$\nu_5 + 65$
	748 w				620 w					750 w	t_u	ν_5, satellite
720 m	715 m,sp			596 m,sp	597 s					715 m	t_u	ν_5, B-B-H bend.
		684 w										
		681 w						560 w			H_g	$\nu_9 + 91$
								550 w			H_g	$\nu_8 - 90$
		592 w								591 w		ν_9, satellite
		588 m	588					547 m	547 m	586 m	$a_g + t_g$	ν_9, B-B-B def.
	582 m	583 m	583			542 m		538 m	537 m	581 m		
		91 s	95 s,sp					91 s,sp	96 s,sp	57 vvs,sp		rotn. lattice
		67 m	68 m					65 m	67 m	43 m		trans. lattice

[a] The intensities given are relative to the most intense peak within each spectrum. Throughout this thesis, abbreviations used in the description of peaks are, v = very, s = strong, m = medium, w = weak, sh = shoulder, sp = sharp, br = broad.

[b] Taken from ref. 79.

[c] As a Nujol mull.

[d] Throughout this thesis, lower-case letters are used for fundamental modes while upper-case letters are assigned to combinations and overtones.

[e] In case of $Cs_2B_{12}H_{12}$.

although many of the peaks were sharper at the lower temperature. These results indicate the absence of any phase change in the solids over the temperature range investigated. The spectral data are compared in Table XIV.

The T_h site symmetry for $[B_{12}H_{12}]^{2-}$ icosahedra in the crystal lattices of $K_2B_{12}H_{12}$ and $K_2B_{12}D_{12}$ is confirmed by both the room and low temperature measurements. The results also indicate that the two salts are isostructural.

Combinations and overtones usually decrease in intensity with decreasing temperature[109]. Consequently, they are more easily distinguished from the fundamentals by comparing the room temperature spectra with those taken at low temperature.

The Raman-active lattice modes were shifted to higher frequencies on decreasing the temperature. On cooling, the unit cells of the crystals shrink thus bringing the potassium cations closer to the icosahedral $[B_{12}H_{12}]^{2-}$ or $[B_{12}D_{12}]^{2-}$ units. This will cause an increase in the force constants of these interactions and so, the energies of these modes will increase[113]. The 91 cm^{-1} lattice bands in the Raman spectra of $K_2B_{12}H_{12}$ and its deuterated analogue are shifted to 95 and 96 cm^{-1}, respectively, in the low temperature spectra (73° K).

4. Vibrational Spectra of $Cs_2B_{12}H_{12}$

a. Factor group analysis

In 1973, Uspenskaya et al.[73] reported that this

TABLE XV: Factor group analysis for $Cs_2B_{12}H_{12}$

O_h^5	E	$8C_3$	$3C_2$	$6C_4$	$6C_2'$	i	$8S_6$	$3\sigma_h$	$6S_4$	$6\sigma_d$	N	T	T'	R'	n_i	Activity
A_{1g}	1	1	1	1	1	1	1	1	1	1	2	0	0	0	2	Raman
A_{2g}	1	1	1	-1	-1	1	1	1	-1	-1	2	0	0	0	2	
E_g	2	-1	2	0	0	2	-1	2	0	0	4	0	0	0	4	Raman
$F_{1g}=T_{1g}$	3	0	-1	1	-1	3	0	-1	1	-1	4	0	0	1	3	
$F_{2g}=T_{2g}$	3	0	-1	-1	1	3	0	-1	-1	1	5	0	1	0	4	Raman
A_{1u}	1	1	1	1	1	-1	-1	-1	-1	-1	0	0	0	0	0	
A_{2u}	1	1	1	-1	-1	-1	-1	-1	1	1	2	0	0	0	2	
E_u	2	-1	2	0	0	-2	1	-2	0	0	2	0	0	0	2	
$F_{1u}=T_{1u}$	3	0	-1	1	-1	-3	0	1	-1	1	7	1	1	0	5	ir
$F_{2u}=T_{2u}$	3	0	-1	-1	1	-3	0	1	1	-1	4	0	0	0	4	
$m_j(P)$*	26	0	2	0	4	0	0	8	2	6						
$m_j(S)$	3	1	3	1	1	1	1	1	3	3						
$m_j(S-V)$	1	1	1	1	1	1	1	1	1	1						
$\pm 1+2\cos\theta_j$	3	0	-1	1	-1	-3	0	1	-1	1						
$1\pm 2\cos\theta_j$	3	0	-1	1	-1	3	0	-1	1	-1						
$[\chi_j(N)]$	78	0	-2	0	-4	0	0	8	-2	6						
$[\chi_j(T)]$	3	0	-1	1	-1	-3	0	1	-1	1						
$[\chi_j(T')]$	6	0	-2	0	0	0	0	0	-2	2						
$[\chi_j(R')]$	3	0	-1	1	-1	3	0	-1	1	-1						
$[\chi_j(n_i)]$	66	0	2	-2	-2	0	0	8	0	4						

*For explanation of symbols, see the footnotes in Table VIII

salt crystallizes in the $Fm3m(O_h^5)$ space group of the cubic system (vide supra, p. 18, footnote). The crystallographic unit cell contains four molecular formulae, but the Wigner-Seitz primitive cell contains only one molecule. This primitive symmetric cell is a dodecahedron possessing the O_h symmetry and is formed by both the Cs^+ atoms and the $[B_{12}H_{12}]^{2-}$ icosahedral units and is analogous to the dodecahedral Wigner-Seitz cell of solid $K_2B_{12}H_{12}$[107].

Using the symmetry of the spectroscopic Wigner-Seitz cell (Fig. 11) and applying the procedures of the factor group analysis outlined earlier, we can arrive at the different vibrational modes for solid $Cs_2B_{12}H_{12}$. This analysis is summarized in Table XV. The molecular representation for the total number of vibrations is shown in Eq. 88.

$$\Big[\Big]^{O_h}_{\text{crys., tot.}} = 2\underline{a}_{1g}(R) + 2\underline{a}_{2g}(\text{inact.}) + 2\underline{a}_{2u}(\text{inact.}) + 4\underline{e}_g(R) + 2\underline{e}_u(\text{inact.}) + 5\underline{t}_{2g}(\text{inact.}) + 4\underline{t}_{1g}(R) + 7\underline{t}_{1u}(\text{ir}) + 4\underline{t}_{2u}(\text{inact.}) \qquad (88)$$

Eq. 88 represents the total number of modes possible for this symmetry, but since many modes are inactive in the free-ion to start with, the corresponding modes in the solid state

TABLE XVI: Correlation diagram for the free $[B_{12}H_{12}]^{2-}$ ion under I_h and O_h symmetries

Activity		I_h	O_h		Activity
Raman	ν_1, ν_2	$2\underline{a}_g$	$2\underline{a}_{1g}$	ν_1, ν_2	Raman
	R	$2\underline{t}_{1g}$	$4\underline{t}_{1g}$		
		$2\underline{g}_g$	$2\underline{a}_{2g}$		
Raman	ν_6, ν_7, ν_8, ν_9	$4\underline{h}_g$	$4\underline{e}_g$	ν_6, ν_7, ν_8, ν_9	Raman
			$4\underline{t}_{2g}$	ν_6, ν_7, ν_8, ν_9	Raman
ir	ν_3, ν_4, ν_5, T	$4\underline{t}_{1u}$	$6\underline{t}_{1u}$	ν_3, ν_4, ν_5, T	ir
		$2\underline{g}_u$	$2\underline{a}_{2u}$		
		$2\underline{h}_u$	$2\underline{e}_u$		
		$2\underline{t}_{2u}$	$4\underline{t}_{2u}$		

TABLE XVII: Complete correlation diagram for solid $Cs_2B_{12}H_{12}$

	Free ion symmetry I_h	Site symmetry O_h	Crystal symmetry O_h^5		Activity
ν_1, ν_2	$2\underline{a}_g$	$\underline{a}_{1g}$	$2\underline{a}_{1g}$	ν_1, ν_2	Raman
R	$2\underline{t}_{1g}$	$\underline{t}_{1g}$	$4\underline{t}_{1g}$	R	
	$2\underline{g}_g$	$\underline{a}_{2g}$	$2\underline{a}_{2g}$		
ν_6, ν_7, ν_8, ν_9	$4\underline{h}_g$	$\underline{e}_g$	$4\underline{e}_g$	ν_6, ν_7, ν_8, ν_9	Raman
$2T^*$	$2\underline{t}_2^*$	$\underline{t}_{2g}$	$5\underline{t}_{2g}$	ν_6, ν_7, ν_8, ν_9, T	Raman
ν_3, ν_4, ν_5, T	$4\underline{t}_{1u}$	$\underline{t}_{1u}$	$7\underline{t}_{1u}$	ν_3, ν_4, ν_5, T	ir
	$2\underline{g}_u$	$\underline{a}_{2u}$	$2\underline{a}_{2u}$		
	$2\underline{h}_u$	$\underline{e}_u$	$2\underline{e}_u$		
	$2\underline{t}_{2u}$	$\underline{t}_{2u}$	$4\underline{t}_{2u}$		

*These are the translational modes of the two Cs^+ cations which occupy T_d sites; therefore, the translations belong to the $\underline{t}_2$ species of the T_d point group.

TABLE XVIII: Correlation diagram for the optically-active modes of $Cs_2B_{12}H_{12}$ or its isostructural analogues

	Free ion symmetry I_h	Site symmetry O_h	Crystal symmetry O_h^5		Activity
ν_1, ν_2	$\underline{a}_g$	$\underline{a}_g$	$\underline{a}_g$	ν_1, ν_2	Raman
R	$\underline{t}_{1g}$	$\underline{t}_{1g}$	$\underline{t}_{1g}$	R	Inactive
ν_6, ν_7, ν_8, ν_9	$\underline{h}_g$	$\underline{e}_g$	$\underline{e}_g$	ν_6, ν_7, ν_8, ν_9	Raman
T[a]		$\underline{t}_2^*$	$\underline{t}_{2g}$	$\underline{t}_{2g}$	ν_6, ν_7, ν_8, ν_9, T	Raman
ν_3, ν_4, ν_5, T	$\underline{t}_{1u}$	$\underline{t}_{1u}$	$\underline{t}_{1u}$	ν_3, ν_4, ν_5, T	ir

[a]Translational modes of the Cs^+ ions which occupy T_d symmetry sites. Translations under the T_d point group belong to the $\underline{t}_2$ species.

will also be optically inactive. We can eliminate these modes by drawing the correlation diagram (Table XVIII) between the point groups of the free-ion, the site in the crystallographic lattice and the factor group. The site group is easily established as the O_h, since it is the only group in the Fm3m representation having multiplicity of (4). The correlation reduces the number of active modes to Eq. 89 with the external modes expressed by Eq. 90.

$$\left\lceil\right.^{O_h}_{\text{cryst., active, tot.}} = 2\underline{a}_{1g}(R) + 4\underline{e}_g(R) + 5\underline{t}_{2g}(R) + 4\underline{t}_{1u}(ir) \qquad (89)$$

$$\left\lceil\right.^{O_h}_{\text{cryst., ext.}} = \underline{t}_{2g}(R) + t_{1u}(ir) \qquad (90)$$

Obviously, these equations correspond to Eqs. 75 and 77 of the K^+ salt (T_h^3). One minor difference is that the rotational lattice mode is Raman-active under T_h symmetry, while it is inactive for the O_h group.

b. Band assignments

The proposed assignments are given in Table XIV and will be discussed in terms of the same categories as those for the free $[B_{12}H_{12}]^{2-}$ ion: B-H stretching ($\underline{a}_{1g}$, $\underline{e}_g + \underline{t}_{2g}$, $\underline{t}_{1u}$) B-B stretching ($\underline{a}_{1g}$, $2(\underline{e}_g + \underline{t}_{2g})$, $\underline{t}_{1u}$), B-B-B bending ($\underline{e}_g + \underline{t}_{2g}$), B-B-H bending ($\underline{t}_{1u}$) and the solid lattice modes ($\underline{t}_{2g}$, $\underline{t}_{1u}$).

i. B-H stretching modes

The most intense line in the ir spectrum of solid $Cs_2B_{12}H_{12}$ is the B-H stretching at 2488 cm^{-1}. The solid-Nujol lattice-lattice interactions cause the appearance of fine structure on the high energy side of the band. This fundamental is only very slightly shifted from the 2480 cm^{-1} position of the free $[B_{12}H_{12}]^{2-}$ ion. Therefore, this band is assigned to the $\underline{t}_{1u}$ mode (ν_3).

There is a strong peak at 2506 cm^{-1} in the Raman spectrum of the solid which we attribute to the $\underline{a}_{1g}$ B-H stretching mode (ν_1), the out-of-phase breathing of the hydrogen atom icosahedron. There is a second strong Raman peak in the B-H stretching range at 2471 cm^{-1} with a fairly strong shoulder at 2475 cm^{-1}. These two bands can be assigned to the ν_6, $\underline{e}_g + \underline{t}_{2g}$ mode. This fundamental corresponds to the 2472 cm^{-1} absorption (ν_6, $\underline{h}_g$) of the free $[B_{12}H_{12}]^{2-}$ which undergoes correlation field splitting in the crystalline

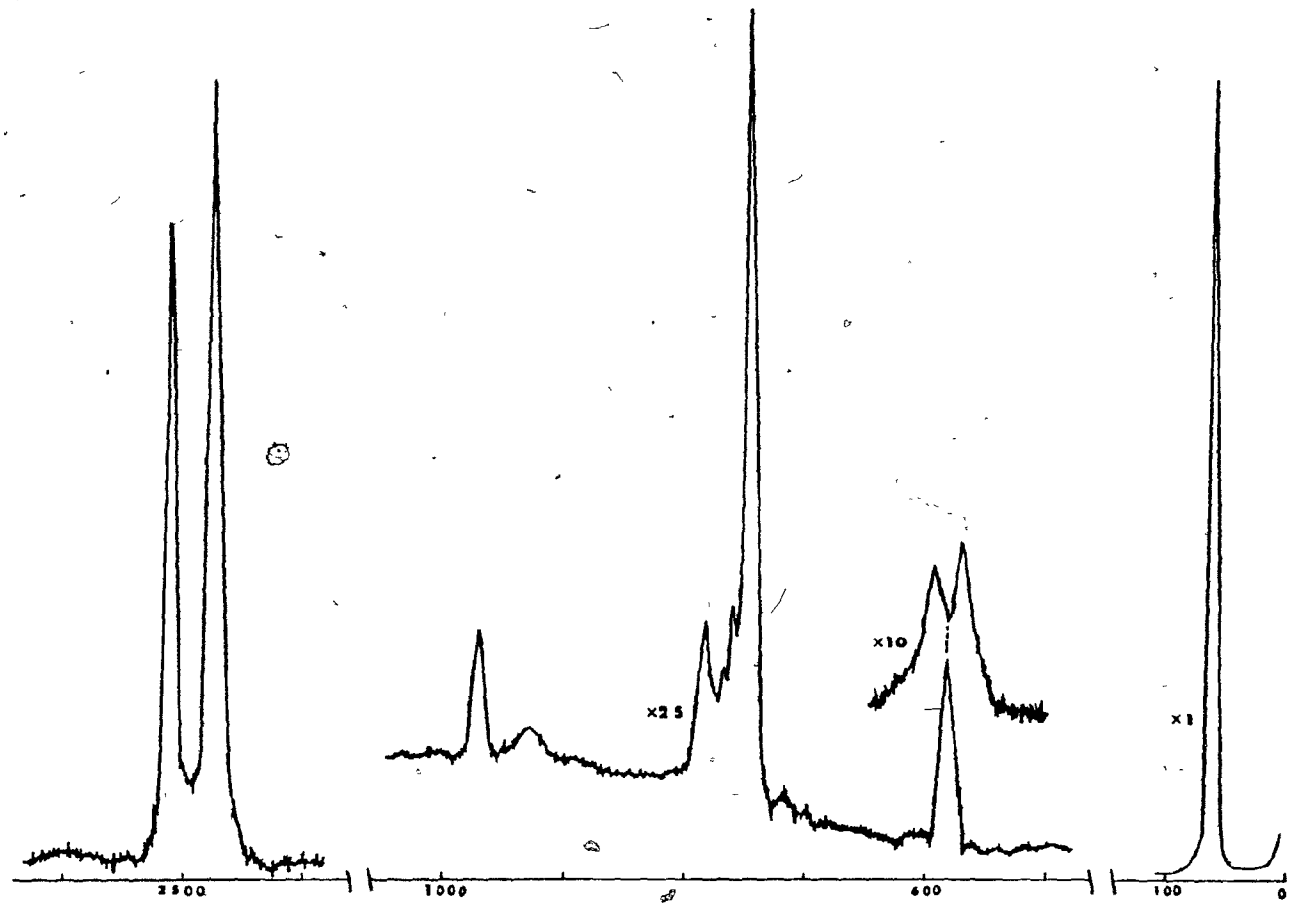

FIGURE 16: Raman spectrum of solid $Cs_2B_{12}H_{12}$ [Ar^+ excitation, 488 nm (∿400 mW)]. Conditions for survey spectrum: slit widths, 3.5 cm^{-1}; time constant, 1 sec; scan speed, 100 cm^{-1} min^{-1}.

state.

ii. Skeletal or cage absorptions

1) B-B stretching modes

The characteristic cage absorption of solid $Cs_2B_{12}H_{12}$ appears in the ir spectrum at 1075 cm^{-1} (ν_4, $\underline{t}_{1u}$) with a weak ^{10}B isotopic band at 1120 cm^{-1}. In the Raman, the line at 747 cm^{-1} is extremely intense and is assigned to ν_2, $\underline{a}_{1g}$ by analogy with the free ion polarized band at 746 cm^{-1}. The weak 763 cm^{-1} band is presumably a ^{10}B isotopic satellite peak derived from ν_2.

There are two medium intensity Raman doublets which are assigned to $\underline{e}_g + \underline{t}_{2g}$ symmetry because of their splitting with frequencies at 973 and 938 cm^{-1} (ν_7) and 787 and 772 cm^{-1} (ν_8). These bands correspond to the 954 (ν_7) and 774 cm^{-1} (ν_8) of the $[B_{12}H_{12}]^{2-}$ solution bands and their splittings are due to factor group effects.

2) B-B-B bending modes

The doublet appearing in the Raman spectrum of the solid at 586 and 581 cm^{-1} is considered to be due to the skeletal B-B-B bending mode. This doublet has been assigned to the ν_9, ($\underline{e}_g + t_{2g}$) by comparison with the band appearing at 582 cm^{-1} (ν_9, $\underline{h}_g$) in the solution Raman of $[B_{12}H_{12}]^{2-}$.

iii. B-B-H bending modes

The sharp medium-intensity peak at 715 cm^{-1} in the ir spectrum of solid $Cs_2B_{12}H_{12}$ is assigned to B-B-H bending. This fundamental (ν_5, t_{1u}) is a characteristic absorption in the ir spectra of the $[B_{12}H_{12}]^{2-}$ polyhedral ions and their salts.

iv. Lattice modes

The Raman band of $Cs_2B_{12}H_{12}$ at 57 cm^{-1} shifts to higher frequency on cooling (62 cm^{-1} at 223 K) and is assigned to the rotational t_{2g} lattice mode. Taking into account the difference in masses of the two alkali-metal cations, this peak may be compared with the 91 cm^{-1} peak for $K_2B_{12}H_{12}$. The translational lattice mode is much weaker and scatters at 43 cm^{-1} in the Raman. The ir translational lattice lies outside the normal ir frequency range investigated, but it is predicted at $\sim$ 220 ± 20 cm^{-1} from combination bands such as 2750 ≃ 2506 + 220, 2675 ≃ 2471 + 220, 1035 ≃ 780 + 220 cm^{-1}.

5. Vibrational Spectra of $Cs_2B_{12}H_{12}\cdot CsCl$

a. Factor group analysis

Uspenskaya et al.[73] have reported that this double salt crystallizes in the Pnma (D_{2h}^{16}) orthorhombic space group with four formula units per unit cell. The letter P in the

Hermann-Mauguin symbol indicates that the crystallographic unit cell is primitive; therefore, the cell can be used in the factor group analysis without further subdivision.

Halford's Table[115] lists the symmetries of the various sites of the Pnma space group as: $C_1(8)$, $C_s(4)$, $2C_i(4)$. If we consider that the site group of a molecule in a crystal lattice must be a subgroup of the point groups of both the free molecule and the crystal, then the C_s site is the only site having this property[116]. Therefore, we can conclude that the $[B_{12}H_{12}]^{2-}$ ions occupy a four-fold set of sites of C_s symmetry. The eight cesium cations will occupy another two sets of C_s sites. The four CsCl molecules will also be in C_s sites.

In order to apply the factor group operations, we usually require detailed X-ray maps of the unit cell. These are not yet available for the $Cs_2B_{12}H_{12}\cdot CsCl$ double salt. However, the vibrational modes can be obtained by the correlation method for factor group analysis. The four molecules of the unit cell have to be considered in the factor group calculations since the crystallographic unit cell is primitive. The vibrational modes expected for the double salt are classified in Table XIX.

The correlation diagram between the molecular (I_h) and crystal symmetries (D_{2h}^{16}) <u>via</u> the C_s site symmetry is shown in Table XX. In this table, we note that (a) the fundamentals of the free ion are multiplied by four, the number of molecules in the unit cell; (b) because the site symmetries for the

TABLE XIX: Expected vibrational modes for $Cs_2B_{12}H_{12}\cdot CsCl$

Chemical species	MODES			
	total	vib.	trans.	rotn.
4 $[B_{12}H_{12}]^{2-}$ anions	288	264	12	12
8 Cs^+ cations	24	0	24	0
4 CsCl	24	0	12	12

$[B_{12}H_{12}]^{2-}$ ions and Cs^+ ions are the same, the translational modes of these ions are combined under the t_{1u} of the I_h point group; (c) both the $[B_{12}H_{12}]^{2-}$ ions and the CsCl molecules possess internal, rotational and translational modes, while the non-structural Cs^+ ions furnish only translational modes; and (d) the CsCl molecules are not included in the correlation procedure because they do not absorb in the Raman spectrum and they have only one ir-active fundamental at 102 cm^{-1}, i.e., in the far ir-region[113]. Therefore, we can safely assume that the ir and Raman spectra of solid $Cs_2B_{12}H_{12}\cdot CsCl$ will not be complicated by bands attributable to CsCl.

After carrying out the correlation mapping, we obtain the various vibrational fundamentals on the right-hand-side of the table. The predicted number of modes for each vibrational fundamental in both the ir and Raman spectra we collected

TABLE XX: Correlation diagram for $Cs_2B_{12}H_{12}\cdot CsCl$

	Free ion symmetry I_h	Site symmetry C_s	Crystal symmetry D_{2h}		Activity
$4(\nu_1, \nu_2)$	$\underline{a}_g$ (R)		$\underline{a}_g$	$\nu_1, \nu_2, 2\nu_3, 2\nu_4, 2\nu_5, 3\nu_6, 3\nu_7, 3\nu_8, 3\nu_9$, 6T, R	R
			$\underline{b}_{1g}$	$\nu_3, \nu_4, \nu_5, 2\nu_6, 2\nu_7, 2\nu_8, 2\nu_9$, 3T, 2R	R
12T, $4(\nu_3, \nu_4, \nu_5)$	(ir) $\underline{t}_{1u}$	$\underline{a}'$	$\underline{b}_{2g}$	$\nu_1, \nu_2, 2\nu_3, 2\nu_4, 2\nu_5, 3\nu_6, 3\nu_7, 3\nu_8, 3\nu_9$, 6T, R	R
			$\underline{b}_{3g}$	$\nu_3, \nu_4, \nu_5, 2\nu_6, 2\nu_7, 2\nu_8, 2\nu_9$, 3T, 2R	R
$4(\nu_6, \nu_7, \nu_8, \nu_9)$	$\underline{h}_g$ (R)	$\underline{a}''$	$\underline{a}_u$	$\nu_3, \nu_4, \nu_5, 2\nu_6, 2\nu_7, 2\nu_8, 2\nu_9$, 3T, 2R	Inact.
			$\underline{b}_{1u}$	$\nu_1, \nu_2, 2\nu_3, 2\nu_4, 2\nu_5, 3\nu_6, 3\nu_7, 3\nu_8, 3\nu_9$, 5T, R (-T)	ir
4R	$\underline{t}_{1g}$		$\underline{b}_{2u}$	$\nu_3, \nu_4, \nu_5, 2\nu_6, 2\nu_7, 2\nu_8, 2\nu_9$, 2T, 2R (-T)	ir
			$\underline{b}_{3u}$	$\nu_1, \nu_2, 2\nu_3, 2\nu_4, 2\nu_5, 3\nu_6, 3\nu_7, 3\nu_8, 3\nu_9$, 5T, R (-T)	ir

together in Table XXI:

TABLE XXI: Expected vibrational modes for solid $Cs_2B_{12}H_{12}\cdot CsCl$

Vib. no. and symmetry (I_h model)		Number of modes expected ir	Raman	Frequency region (cm^{-1})
Raman	ν_1, $\underline{a}_g$	2	2	∿2500
	ν_2, $\underline{a}_g$	2	2	∿750
ir	ν_3, $\underline{t}_{1u}$	15	18	∿2490
	ν_4, $\underline{t}_{1u}$	15	18	∿1070
	ν_5, $\underline{t}_{1u}$	15	18	∿715
Raman	ν_6, $\underline{h}_g$	8	10	∿2470
	ν_7, $\underline{h}_g$	8	10	980-930
	ν_8, $\underline{h}_g$	8	10	790-770
	ν_9, $\underline{h}_g$	8	10	∿ 580
External modes[a]		16	24	∿50-100

[a]not including the 24 modes of CsCl

We can see that on lowering the symmetry of the free ion, modes which are either ir- or Raman-active only become active in both the ir and Raman. However, there are indications from the actual spectra that the optical activities of the free ion fundamentals are in general preserved despite the corre-

lation predictions.

b. Band assignments

The vibrational spectra of $Cs_2B_{12}H_{12}\cdot CsCl$ will be discussed in terms of the same categories as those for the $Cs_2B_{12}H_{12}$ salt: B-H stretching, B-B stretching, B-B-B bending, B-B-H bending and lattice modes. The observed frequencies are listed in Table XXII.

i. B-H stretching modes

The ν_3 B-H stretching mode appears in the ir spectrum of solid $Cs_2B_{12}H_{12}\cdot CsCl$ as a high intensity doublet absorbing at 2510 and 2480 cm^{-1} with a strong shoulder at 2520 cm^{-1}. These bands can be assigned to the $\underline{b}_{1u} + \underline{b}_{2u} + \underline{b}_{3u}$ species which correlate with the $\underline{t}_{1u}$ species of the icosahedron. The $\sim$2520 cm^{-1} shoulder is too intense to be considered a ^{10}B isotopic shift. Another possible assignment for this shoulder is the ν_1 ($\underline{b}_{1u}$ and/or $\underline{b}_{3u}$) B-H stretching mode. We should remember that ν_1 is only Raman-active in the spectrum of $Cs_2B_{12}H_{12}$ as an $\underline{a}_g$ species. A similar situation occurs for the ν_6 B-H stretching modes which may accidentally coincide with other ir fundamentals in the 2520-2480 cm^{-1} region.

In the Raman, the strong doublet at 2528 and 2508 cm^{-1} is attributed to the ($\underline{a}_g + \underline{b}_{2g}$) B-H stretching mode ($\nu_1$). The ν_6 stretching mode scatters in the Raman spectrum at $\sim$2476 and

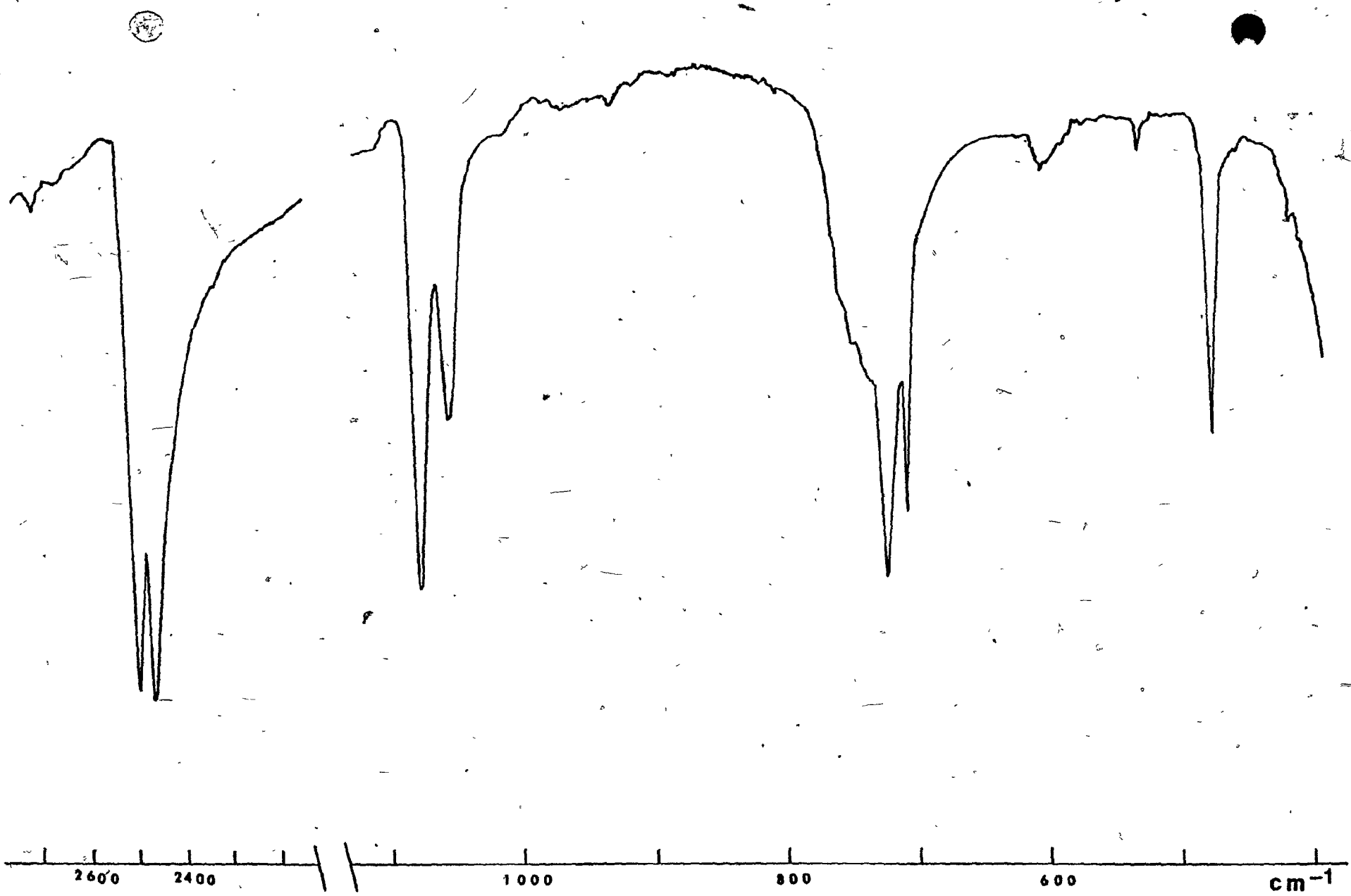

FIGURE 17: Infrared spectrum (Nujol mull) of $Cs_2B_{12}H_{12}\cdot CsCl$.

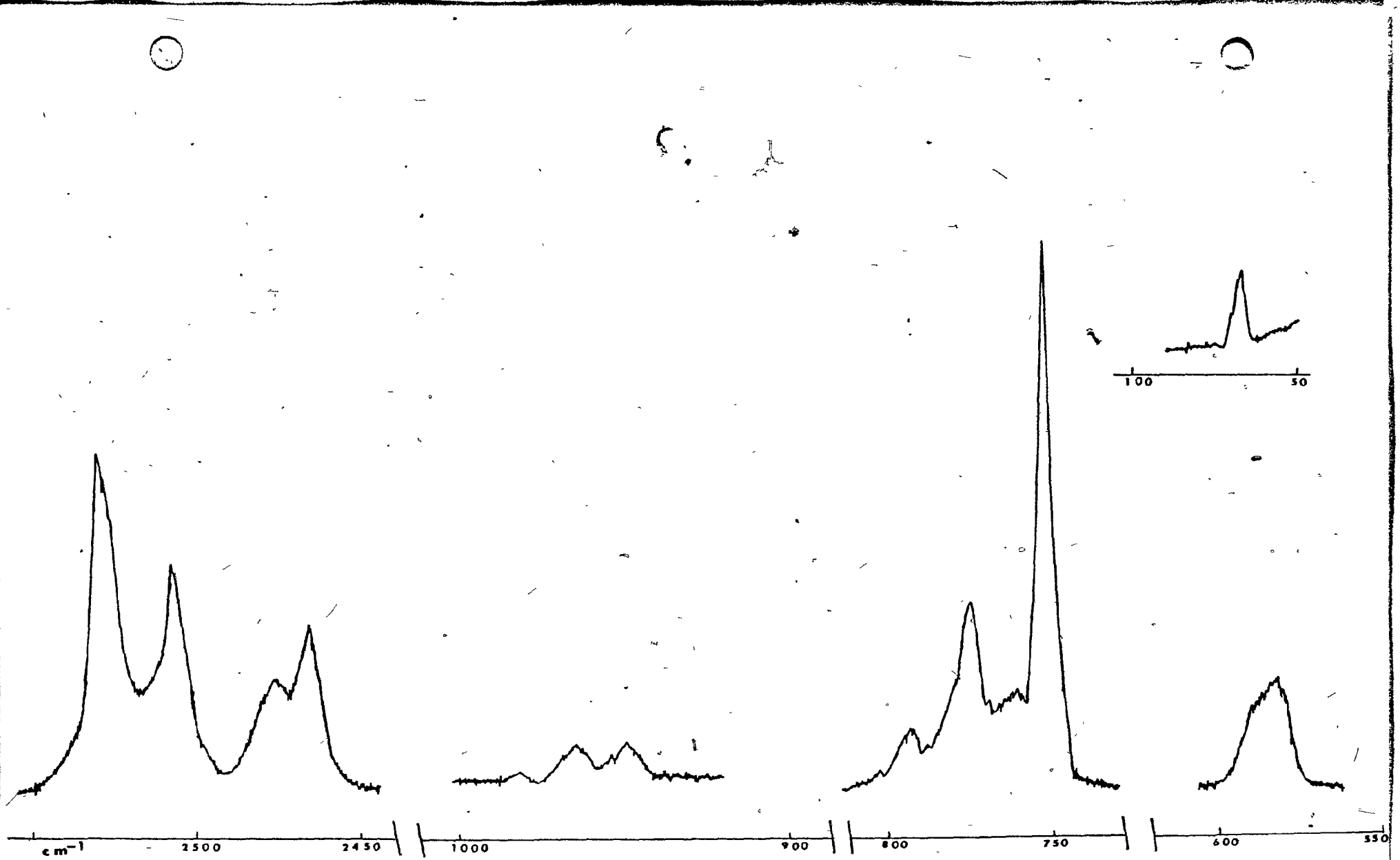

FIGURE 18: Raman spectrum of solid $Cs_2B_{12}H_{12}\cdot CsCl$ [Ar^+ excitation 514.5 nm (∿300 mW)] condition; slit widths, 2 cm^{-1}; time constant, 2 sec; scan speed, 20 cm^{-1} min^{-1}.

2466 cm^{-1} and these bands can be regarded as belonging to any two of the $\underline{a}_g$, $\underline{b}_{1g}$, $\underline{b}_{2g}$ and $\underline{b}_{3g}$ species. The ν_3 mode is also allowed in the Raman as $\underline{a}_g$, $\underline{b}_{1g}$, etc., species and may scatter in the same region as the ν_6 modes (ca. 2480-2470 cm^{-1}).

ii. B-B stretching modes

The cage vibration (ν_4) of the double salt is exhibited in the ir spectrum as a strong doublet at 1077 and 1056 cm^{-1}, i.e., in the energy range considered characteristic of the cage absorption[69]. The weak 1128 and 1116 cm^{-1} peaks can be attributed to ^{10}B isotope effects. The symmetry species for the cage doublet are most probably $\underline{b}_{1u}$ and $\underline{b}_{3u}$ since there are two modes of each species allowed in the ir, while there is only one active mode in the $\underline{b}_{2u}$ species.

In the ir, there are several weak bands which can be assigned to the now ir-allowed ν_2 ($\underline{b}_{1u} + \underline{b}_{2u}$), ν_7 and ν_8 ($3\underline{b}_{1u} + 2\underline{b}_{2u} + 3\underline{b}_{3u}$) modes. These are all B-B stretching modes (ν_8 consists partly of hydrogen bending). The frequencies for these bands are: 965, 935 (ν_7); 765 (ν_8); and 755, 742 cm^{-1} (ν_2). In the Raman, these modes scatter more strongly at 980, 965, 961, 954, 950 (ν_7); 797-790, 778-772, 770 (ν_8); and 766-760, 751, 749 cm^{-1} (ν_2). The symmetries for the ν_7 and ν_8 modes include all the Raman-active species ($\underline{a}_g$, $\underline{b}_{1g}$, $\underline{b}_{2g}$ and $\underline{b}_{3g}$). The ν_2 mode affords the two species ($\underline{a}_g + \underline{b}_{2g}$) and therefore, the much weaker, higher energy, band at 766-760 cm^{-1} cited above for

TABLE XXII: Vibrational frequencies (cm^{-1}) of $Cs_2B_{12}H_{12}\cdot CsCl$

ir[a]	Raman[b]	Assignment
2700 m,br.		
2520 s,sh.	2528 s 2508 s	ν_1, B-H breath.
2510 vs 2480 vs		ν_3, B-H str.
	2476 2466	ν_6, B-H str.
2360 m		$\nu_3-\nu_7$ or ν_6
2340 m		$\nu_3-\nu_7$ or ν_6
1128 w 1116 w		ν_4, ^{10}B-cage vib.
1077 vs 1056 vs		ν_4, B-B str. and B-H bend. (cage vib.)
	980 m	
964	965 m	ν_7, B-B str.
	961 m	
	954 m	
935	950 m	
	797-790 m	ν_8, B-B str. and B-H bend.,
765 vw	778-772 m 770 m	
755 w	766-760 m	ν_2, ^{10}B-effect
742 w	751 vs	ν_2, B-B cage breath., (a_g+b_{2g})
	749 vs	
722 m	719 vw	
710	647 vw	ν_5, B-B-H bend.
665 w	645 vw	
610 w	588-581 m	ν_9, B-B-B bend.
585 w		
532 w		
477 m		
	128 vw	Lattice modes
	66 m	

[a] In Nujol mull. [b] In solid state.

this mode is assigned to isotopic effects.

iii. B-B-B bending modes

The ν_9 B-B-B bending mode appears in the Raman spectrum as a wide composite peak at 588-581 cm^{-1}. There are ten Raman lines predicted for ν_9 ($3\underline{a}_g + 2\underline{b}_{1g} + 3\underline{b}_{2g} + 2\underline{b}_{3g}$) and this presumably accounts for the broadness of the band. The weak-intensity ir bands at 610, 585 and 532 cm^{-1} may be assigned also to the ν_9 mode. Moreover, the medium-intensity ir band at 477 cm^{-1} could also be derived from ν_9; its intensity may be due to coupling with lattice modes.

iv. B-B-H bending modes

The B-H bending mode (ν_5) appears in the ir spectrum as a doublet of medium intensity at 722 and 710 cm^{-1} and probably a very weak absorption at 665 cm^{-1} ($\underline{b}_{1u}$, $\underline{b}_{2u}$ and $\underline{b}_{3u}$). A very weak Raman peak at 719 cm^{-1} may also be attributed to the ν_5 vibration.

v. Lattice modes

The medium intensity Raman peak at 66 cm^{-1} in the spectrum of solid $Cs_2B_{12}H_{12}\cdot CsCl$ is assigned as a lattice vibration. Supposedly, 72 external modes are possible for the double salt with at least half this number being Raman-active. The

ir-active lattice modes will occur in the far-ir region and thus must await further investigation.

In the Raman, there are far fewer observed frequencies than the number of modes predicted by the selection rules. (Apart from the 66 cm^{-1} composite band, there is possibly a very weak peak at 128 cm^{-1}.) The disappearance of many modes could be explained[117] on the basis of accidental degeneracies and weak intensities. Accidental degeneracies occur quite often in the region of external modes because there are usually a large number of modes allowed in a relatively narrow energy range[117].

6. Vibrational Spectra of the Perhalogen Derivatives

a. General

The crystal structures of the perhalogen derivatives have not yet been investigated. As a starting point, however, the $M_2B_{12}X_{12}$ salts can be regarded as being isostructural with the analogous $M_2B_{12}H_{12}$ derivatives. The simplicity of the $M_2B_{12}X_{12}$ spectra suggests that minimal deviations from icosahedral geometry occur. The vibrational spectra are expected to be similar to those of the $[B_{12}H_{12}]^{2-}$ salts with the modes being shifted to lower energy in accord with the increased masses of the halogens. Consequently, the bending modes do not appear in the normal ir range and are probably located in the far-ir region. The Raman spectra display fewer bands than

expected and most of the bands appear with diminished intensity. This was explained by Muetterties et al.[79] as accidental cancellation of polarizabilities due to the oppositely charged boron and halogen atoms.

The four perhalogen salts studied were $Cs_2B_{12}Cl_{12}$, $Cs_2B_{12}Br_{12}$, $Cs_2B_{12}I_{12}$ and $(Me_4N)_2B_{12}I_{12}$. These salts were treated as being isostructural and having the same crystal structure as that most recently determined for $Cs_2B_{12}H_{12}$ [$Fm3(T_h^3)$, $Z=4$][74].

The vibrational predictions are obtained in the usual way. The optically-active internal and external modes are represented in Eqs. 91 and 92, respectively, with the optical activities being shown in parentheses.

$$\left[\begin{matrix}\text{cryst., int., act.}\end{matrix}\right]^{T_h} = 2\underline{a}_g(R) + 4\underline{e}_g(R) + 4\underline{t}_g(R) + 3\underline{t}_u(ir) \qquad (91)$$

$$\left[\begin{matrix}\text{cryst., ext., act.}\end{matrix}\right]^{T_h} = \underline{t}_g(R) + \underline{t}_u(ir) \qquad (92)$$

The vibrational fundamentals of the four perhalo salts will be analyzed in the following section and then compared with those of $Cs_2B_{12}H_{12}$.

b. Vibrational spectra of $Cs_2B_{12}Cl_{12}$

Muetterties et al.[79,81] have reported only one peak in both the ir and Raman of this salt. As will be discussed later, we feel that the assignments proposed by these authors are erroneous. In addition, we have managed to observe several new features which apparently were not detected earlier because of the inferior instrumentation then available.

The assignments for $Cs_2B_{12}Cl_{12}$ will be discussed in terms of B-Cl stretching ($\underline{a}_g$, $\underline{e}_g + \underline{t}_g$, $\underline{t}_u$), B-B stretching [$\underline{a}_g$, $2(\underline{e}_g + \underline{t}_g)$, $\underline{t}_u$], B-B-B bending modes ($\underline{e}_g + \underline{t}_g$), B-B-Cl bending ($\underline{t}_u$) and lattice modes ($\underline{t}_g$, $\underline{t}_u$). The actual vibrational data and some representative spectra are given in Table XXIII and Figs. 19, 20, respectively.

i. B-Cl stretching modes

In the ir spectrum of solid $Cs_2B_{12}Cl_{12}$, the ^{11}B-^{35}Cl stretching mode appears as a very intense absorption centered at 1032 cm^{-1} [ν_3, $\underline{t}_u$]. The strong shoulder at higher energy (1070-1060 cm^{-1}) is due to the ^{10}B-^{35}Cl stretching mode. On the other hand, the heavier chlorine ^{37}Cl isotope shifts the absorption to lower frequency and the ^{11}B-^{37}Cl mode appears as a separate band of moderate intensity at 1003 cm^{-1}.

The weak ir band at 945 cm^{-1} is believed to be a difference band [1070(ir)-134 cm^{-1}(R)].

In the Raman, no strong bands are observed in the

B-Cl stretching region (1037-579 cm^{-1})[119]. However, the two very weak bands at 1070 and 1005 cm^{-1} may be the B-Cl stretching modes (ν_1, $\underline{a}_g$) and (ν_6, $\underline{e}_g + \underline{t}_g$), respectively. The drastic decrease in intensity of these fundamentals has been attributed to accidental cancellation of polarizability[79]. The two modes are a result of the movements of boron and chlorine atoms which are oppositely charged[79].

ii. Skeletal or cage vibrations

1) B-B stretching modes

In the ir spectrum, the sharp, intense absorption at 541 cm^{-1} can be assigned to the B-B stretching cage deformation. This vibration corresponds to the ∿1070 cm^{-1} cage vibration of the $[B_{12}H_{12}]^{2-}$ closoborane ion. Both boron and halogen atom movements contribute to this fundamental. Consequently, the frequency of this vibration is expected to decrease in the order: $[B_{12}H_{12}]^{2-} > [B_{12}D_{12}]^{2-} > [B_{12}Cl_{12}]^{2-}$. In accord with this, the frequencies of the cage vibration for the above species are 1070 > 928 > 541 cm^{-1}, respectively. Muetterties et al.'s[81] assignment of the 1030 cm^{-1} line as the cage absorption in $[B_{12}Cl_{12}]^{2-}$ will perturb this order and is therefore discounted.

The most intense line in the Raman spectrum is at 301 cm^{-1}. This was reported as being polarized in an earlier study[79], and is in the B-B stretching range. Thus, it is

TABLE XXIII: Vibrational spectra (cm^{-1}) of the $[B_{12}X_{12}]^{2-}$ perhalogen derivatives

$Cs_2B_{12}Cl_{12}$		$Cs_2B_{12}Br_{12}$		$Cs_2B_{12}I_{12}$		Assignment
ir[a]	Raman[b]	ir[a]	Raman[b]	ir[a]	Raman[b]	
1400 vw						$\nu_2+\nu_3,(T_u)$
	1070 vw					ν_1?, B-X str., $\underline{a}_g$
	1005 vw					ν_6?, B-X str., $(\underline{e}_g+\underline{t}_g)$
1070 s		1010 m,sh		939 vs		ν_3, ^{10}B isotopic shift
1032 vs		1000 vs		926 vs		ν_3, B-X str., $\underline{t}_u$
1003 s		986 vs 970 m,sh		905 s,sh		ν_3, X^i shift and/or s.s.s[c]
945 w						1070-134, T_u
				745 w		905-153, T_u
625 w				478 m		ν_4?
		490 vw				ν_7? or $\nu_2+\nu_9+42$
541 s		443 s		380 s		ν_4, B-B str. and B-X def., T_u
420 w						$\nu_4-\nu_9$, T_u
	307 m 296 s		201 m 195 s		153 m 145 s	ν_8, B-B str. and B-X def., $(\underline{e}_g+\underline{t}_g)$
	301 vs		199 s		147 vs	ν_2, B-B cage breath; $\underline{a}_g$
	172 vw					ν_9+42, (E_g+T_g)
	143 m		98 m			ν_9, ^{10}B shift
	134 vs 126 s		92 s 87 m 84 s		~71 s	ν_9, B-B-B bend., $(\underline{e}_g+\underline{t}_g)$
	75 vw 48 m 42 s 39 m		67 w 59 w 42 s		42 s	Lattice modes

[a] In KBr disk. [b] In solid state. [c] Solid state splitting.

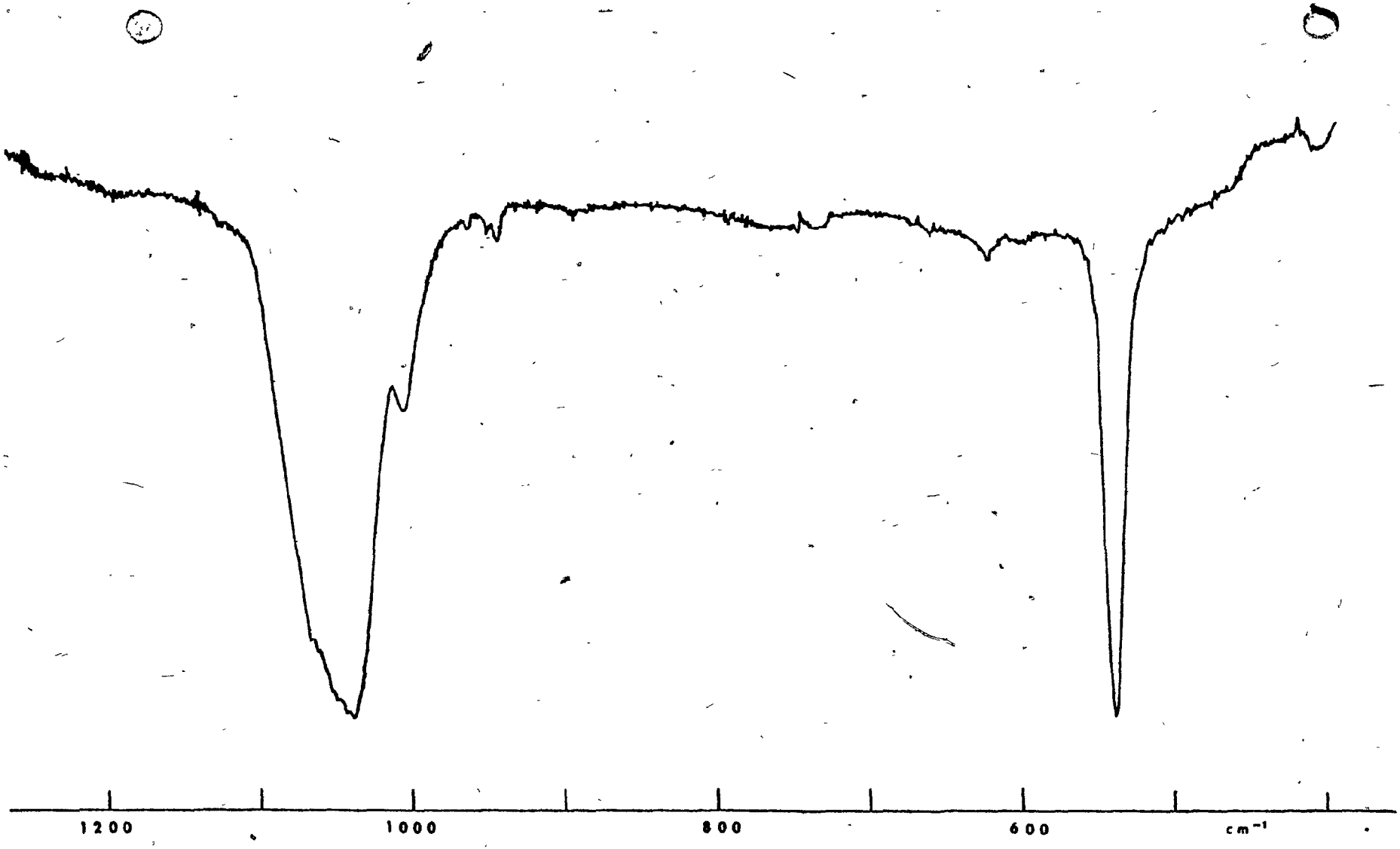

FIGURE 19: Infrared spectrum (KBr disk) of $Cs_2B_{12}Cl_{12}$.

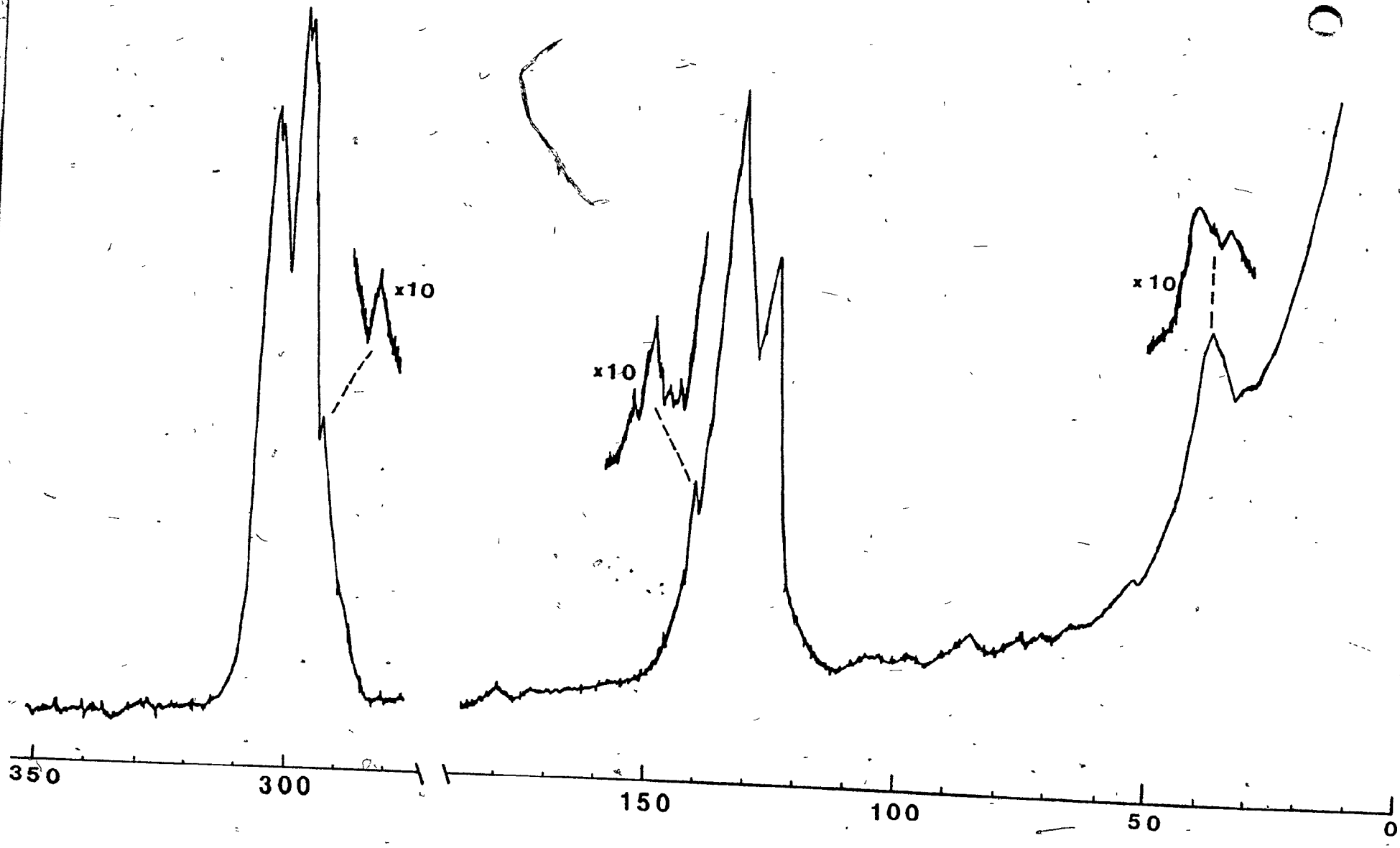

FIGURE 20: Raman spectrum of solid $Cs_2B_{12}Cl_{12}$ [Kr^+ excitation, 647.1 nm (~50 mW)]. Conditions for survey spectrum: slit widths, 2 cm^{-1}; time constant, 2 sec; scan speed, 10 cm^{-1} min^{-1}.

reasonable to assign this band to the totally symmetric breathing mode (ν_2, $\underline{a}_g$). It corresponds to the 746 cm^{-1} absorption of $Cs_2B_{12}H_{12}$ and is the result of boron atoms moving in-phase within the cage structure. Associated with this band is a doublet located at 307 and 296 cm^{-1} with the higher frequency band being the more intense. The doublet can be regarded as a B-B stretching fundamental (ν_8, $\underline{h}_g$) which is split as a result of correlation field effects ($\underline{h}_g \rightarrow \underline{e}_g + \underline{t}_g$). A much weaker, broad band at ~490 cm^{-1} could also be a B-B stretching band (ν_7, $\underline{h}_g$).

2) Skeletal bending modes

The B-B-B deformation mode appears in the 145-125 cm^{-1} Raman scattering region. Under high resolution, three bands are observed at 143 m, 134 vs and 126 s cm^{-1}. We consider two bands (134 and 126 cm^{-1}) to be derived from the B-B-B bending mode (ν_9, $\underline{h}_g$) which has been split into a doublet by effects of the crystal field ($I_h \rightarrow T_h$). The band at 143 cm^{-1} is most probably a ^{10}B-isotope satellite. Although ν_9 is mainly due to boron atom movements, the chlorine atoms seem to contribute to this mode. This explains its considerable shift from the 582 cm^{-1} for the $[B_{12}H_{12}]^{2-}$ ion to ~130 cm^{-1} in $[B_{12}Cl_{12}]^{2-}$. The contribution of chlorine atom movements to (ν_9, $\underline{h}_g$) mode has also been suggested by Weber and Thorpe[111] in their theoretical study of the $[B_{12}H_{12}]^{2-}$ ion using different force-field models. The

model that does not consider restoring forces on the hydrogen atoms gives zero frequency for the ν_9 mode since the hydrogen atoms move perpendicular to the B-H bond axis.

iii. B-B-Cl bending mode

This ν_5 (t_u) mode is expected to be ir-active. Because the fundamental is due mainly to chlorine atom movements, the frequency is expected to shift to an appreciably lower energy than the associated 720 cm^{-1} peak of $[B_{12}H_{12}]^{2-}$. Weber and Thorpe[111] have predicted a theoretical value of 166 cm^{-1} for this mode, i.e., outside the range of our available ir instrumentation.

iv. External modes

A strong lattice mode appears in the Raman spectrum of solid $Cs_2B_{12}Cl_{12}$ at 42 cm^{-1}. This is the rotational lattice mode expected from the factor group analysis. The ir-active translational lattice mode is expected in the far-ir region.

c. Vibrational spectra of $Cs_2B_{12}Br_{12}$

The ir and Raman spectra of solid $Cs_2B_{12}Br_{12}$ show great resemblance to those of $Cs_2B_{12}Cl_{12}$ with the frequency shifts in proportion to the change in masses of the two halogens. The band assignments are discussed using the same format as for

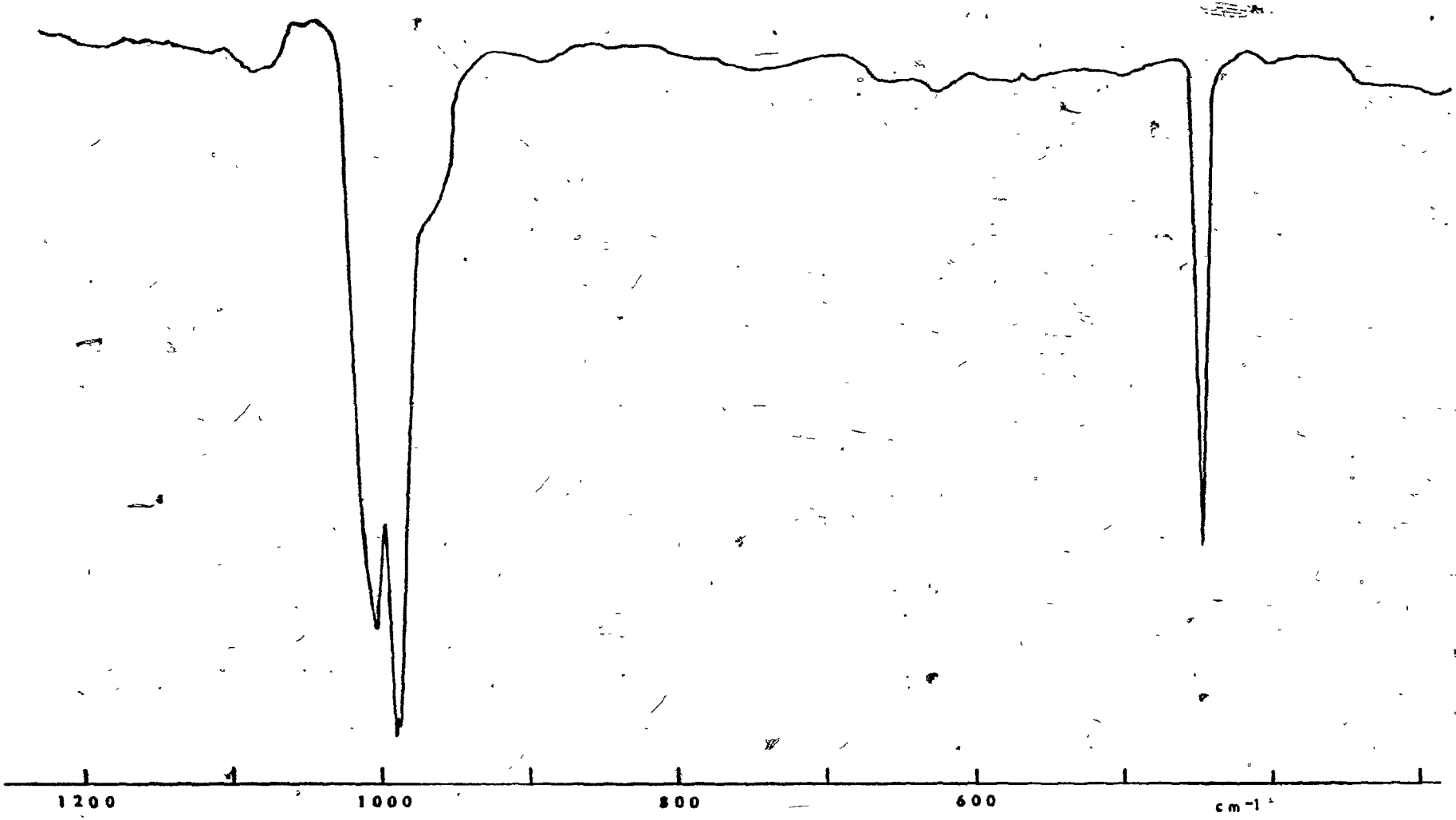

FIGURE 21: Infrared spectrum (KBr disk) of (1) $Cs_2B_{12}I_{12}$ and (2) $[Me_4N]_2B_{12}I_{12}$.

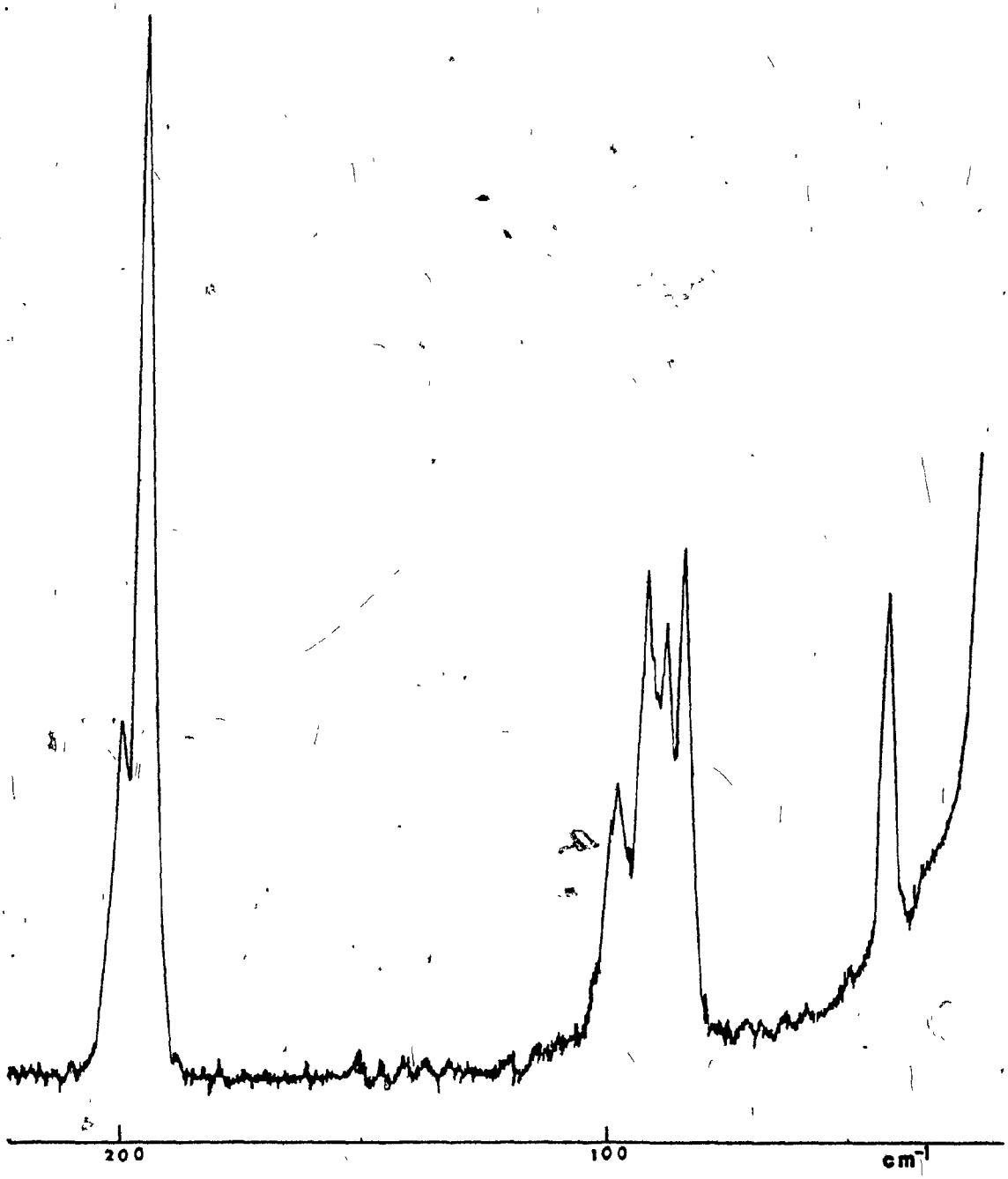

FIGURE 22: Raman spectrum of solid $Cs_2B_{12}Br_{12}$ [Ar^+ excitation, 514.5 nm (∿120 mW)]. Conditions: slit widths, 10 cm^{-1}; time constant, 2 sec; scan speed, 5 cm^{-1} min^{-1}.

the perchloro derivative: B-Br stretching ($\underline{a}_g$, $\underline{e}_g + \underline{t}_g$, $\underline{t}_u$), B-B stretching [$\underline{a}_g$, $2(\underline{e}_g + \underline{t}_g)$, $\underline{t}_u$], B-B-B bending ($\underline{e}_g + \underline{t}_g$), B-B-Br bending ($\underline{t}_u$) and lattice modes ($\underline{t}_g$, $\underline{t}_u$). The observed frequencies are also listed in Table XXIII.

i. B-Br stretching modes

The ir spectrum of solid $Cs_2B_{12}Br_{12}$ exhibits a strong doublet at 1000 and 986 cm^{-1}. Since the stable isotopes of bromine, ^{79}Br (50.5%) and ^{81}B (49.5%), occur with about the same abundance, we have assigned the first absorption to $^{11}B-^{79}Br$ stretching and the second to $^{11}B-^{81}Br$ stretching (ν_3, $\underline{t}_u$). The high frequency shoulder at 1010 cm^{-1} on this $\nu_3(\underline{t}_u)$ mode is attributed to the ^{10}B substituted species.

In the Raman spectrum, no peaks strong enough to be assigned to the B-Br stretching fundamentals (ν_1 or ν_6) could be detected.

ii. B-B stretching modes

There is an intense band in the ir spectrum of solid $Cs_2B_{12}Br_{12}$ at 443 cm^{-1} and this is assigned to the skeletal B-B stretching vibration or cage absorption (ν_4, $\underline{t}_u$) analogous to the $\sim$1070 cm^{-1} band of $[B_{12}H_{12}]^{2-}$.

A B-B stretching vibration appears as the most intense line in the Raman spectrum at 199 cm^{-1} (ν_2, $\underline{a}_g$). The two weaker bands at 201 and 195 cm^{-1} are assigned to ν_8 ($\underline{e}_g + \underline{t}_g$) which has

been split by solid-state effects. The other B-B stretching fundemental ν_7 ($\underline{e}_g + \underline{t}_g$) is absent from the Raman spectrum.

iii. B-B-B bending modes

The four intense, sharp peaks appearing in the Raman region ca. 98-84 cm^{-1} are considered to result from the B-B-B deformation mode (ν_9, $\underline{e}_g + \underline{t}_g$). This mode has been split into a doublet by the correlation field effects, and this doublet is in turn split by the ^{81}Br and ^{79}Br isotopes.

iv. B-B-Br bending modes

This ν_5 mode is supposed to appear in the ir spectrum, but is missing from the normal ir range and is presumably located in the far-ir region.

v. Lattice modes

The 42 cm^{-1} line in the Raman spectrum is probably due to the $\underline{t}_g$ rotational lattice mode of the Cs^+ cations.

d. Vibrational spectra of $Cs_2B_{12}I_{12}$

The spectra of solid $Cs_2B_{12}I_{12}$ are closely similar to those of $Cs_2B_{12}Br_{12}$ bearing in mind the change in masses of the two halogens. The band assignments will be discussed in terms of the same categories as those for the perchloro

and perbromo derivatives (vide supra, p. 123. The vibrational frequencies and the proposed assignments for solid $Cs_2B_{12}I_{12}$ are listed in Table XXIII.

i. B-I stretching modes

In the B-I stretching region of the ir, there is an intense doublet at 939 and 926 cm^{-1} with a shoulder at 905 cm^{-1}. These peaks can be assigned to the ν_3 (t_u) stretching mode. Because iodine has only one naturally occurring isotope (^{127}I), the doublet must be caused by crystal effects rather than by halogen isotopic effects, as was the case for the other perhalogen derivatives. Moreover, in this doublet, the 939 cm^{-1} peak is relatively weak and therefore may be (at least partially) due to a ^{10}B isotope shift. Consequently, it is possible that the crystal structure of $Cs_2B_{12}I_{12}$ still belongs to the T_h^3 class or to some other high symmetry class.

ii. B-B stretching modes

The strong band at 380 cm^{-1} in the ir spectrum of solid $Cs_2B_{12}I_{12}$ is assigned to the cage vibration ν_4 (t_u). The most intense Raman peak at 147 cm^{-1} is assigned to the B-B stretching vibration (ν_2, a_g). Associated with this band are two relatively weaker peaks at 153 and 145 cm^{-1} which are assigned to the $e_g + t_g$ doublet of the B-B stretching mode ν_8. The ν_7 ($e_g + t_g$) mode is too weak to be observed in the Raman

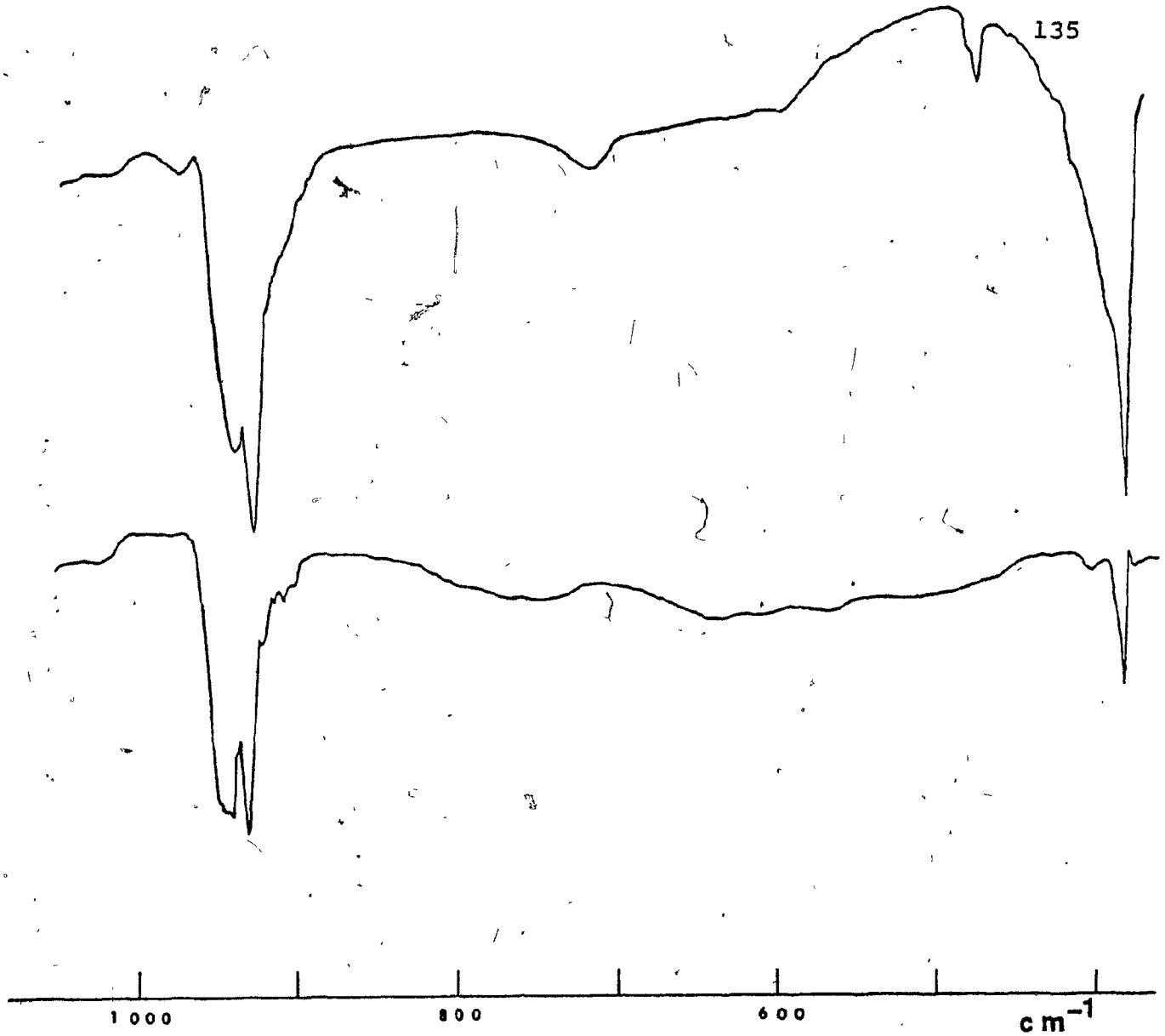

FIGURE 23: Infrared spectrum (KBr disk) of (1) $Cs_2B_{12}I_{12}$ and (2) $[Me_4N]_2B_{12}I_{12}$.

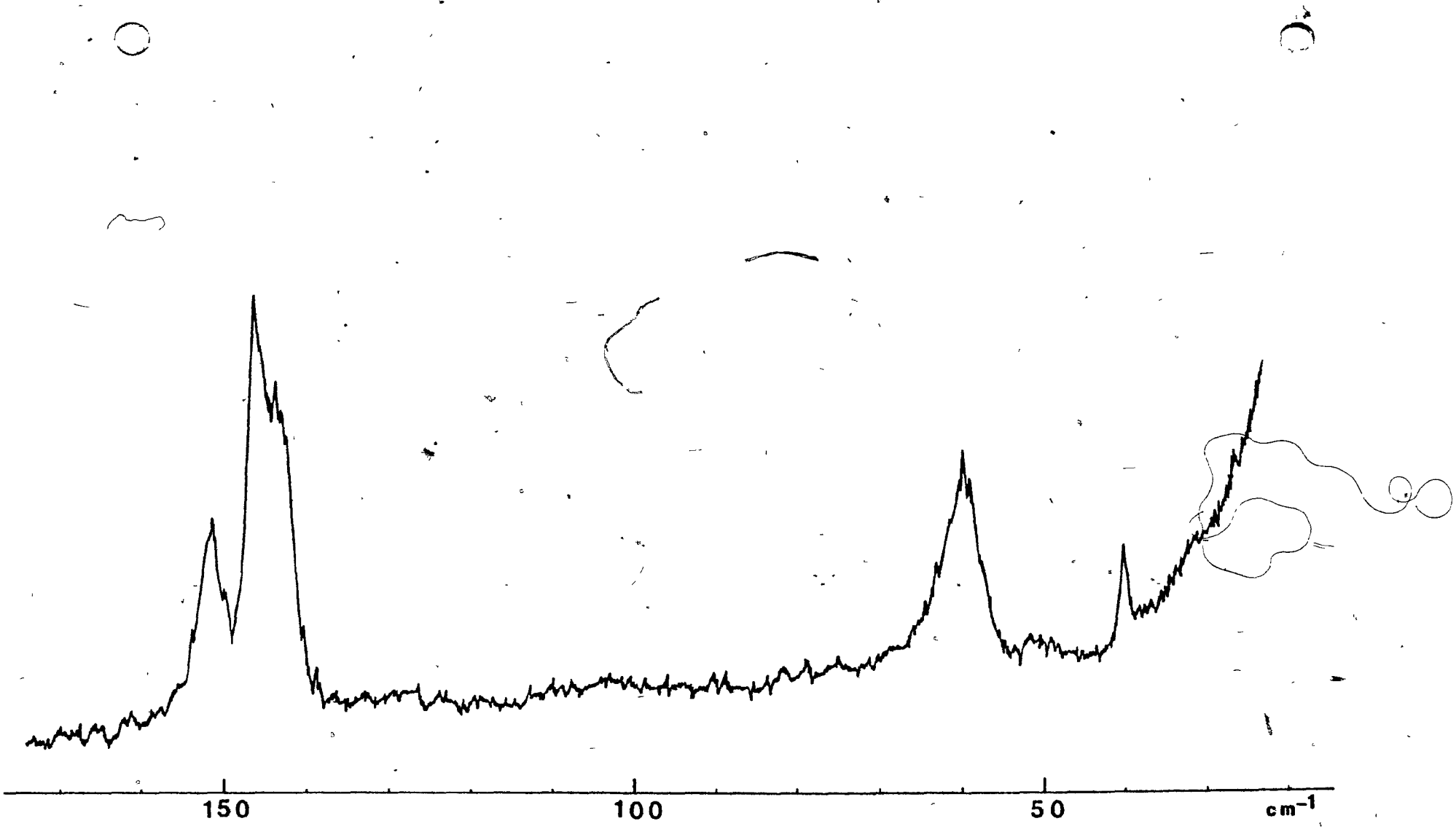

FIGURE 24: Raman spectrum of solid $Cs_2B_{12}I_{12}$ [Kr^+ excitation, 647.1 nm (∿100 mW)]. Conditions: slit widths, 1.5 cm^{-1}; time constant, 4 sec; scan speed, 5 cm^{-1} min^{-1}.

spectrum.

iii. B-B-B bending modes

The ν_9 deformation mode is displayed in the Raman as a strong line at $\sim$71 cm^{-1}. This band may be compared with the four lines in the 98-84 cm^{-1} region in the spectrum of $Cs_2B_{12}Br_{12}$. However, the solid-state splitting predicted for this fundamental was not detected. Furthermore, unlike the perchloro or perbromo salts, there are no peaks expected due to isotopic shifts.

iv. B-B-I bending modes

The ν_5 mode is probably located in the far-ir region in accord with the frequency shift due to the considerably heavier iodine atoms and so could not be observed with the instrumentation available.

v. Lattice modes

The movements of Cs^+ cations in the crystalline lattice of $Cs_2B_{12}I_{12}$ produce a Raman line at 42 cm^{-1} which can be assigned to the t_g rotational lattice mode.

e. Vibrational spectra of $[Me_4N]_2B_{12}I_{12}$

The ir spectrum of solid $[Me_4N]_2B_{12}I_{12}$ is very similar

to that of solid $Cs_2B_{12}I_{12}$, apart from bands attributable to the quaternary ammonium cations[118]. The Raman spectra of these two solids are essentially the same. Therefore, the assignments of the $[Me_4N]_2B_{12}I_{12}$ frequencies follow closely those of the Cs^+ salt. To avoid unnecessary repetition, only a summary of frequencies and their assignments will be presented here.

i. Vibrations of the $[Me_4N]^+$ cations

In the ir, the C-H antisymmetric and symmetric stretching of the methyl group appear as medium intensity bands at 3015 and 2720 cm^{-1}, respectively. The antisymmetric C-H bending vibration absorbs strongly at 1478 cm^{-1}, while the symmetric mode appears as a weak band at 1420 cm^{-1}. The C-N stretching modes absorbs weakly in the ir spectrum at 1382 and 1287 cm^{-1}. In the Raman, no bands of sufficient intensity were found which could be assigned to any of the above vibrations.

ii. B-I stretching modes

This stretching mode (ν_3, t_u) appears in the ir as a very intense doublet absorbing at 947 and 931 cm^{-1} with a weak, broad shoulder centered at 910 cm^{-1}. Unlike $Cs_2B_{12}I_{12}$, the higher energy band of the doublet is of increased intensity. This rules out the possibility of assigning this band to ^{10}B isotopic shifts. The doublet is then more likely to be a

result of the lowering of the symmetry of the crystal structure due to the interaction of both the large anions and the cations.

iii. B-B stretching modes

In the ir of solid $[Me_4N]_2B_{12}I_{12}$, a sharp line of medium-to-strong intensity appears at 384 cm^{-1}. This is assigned to the ν_2 ($\underline{t}_u$) cage absorption. The strong peak in the Raman at ~150 cm^{-1} attributable to B-B stretching is resolved into a triplet under high resolution: 146 (ν_2, $\underline{a}_g$) and 151, 143 cm^{-1} (ν_8, $\underline{e}_g + \underline{t}_g$).

iv. B-B-B bending modes

The ν_9 bending mode appears in the Raman at ~69 cm^{-1} without any apparent crystal-field splitting probably because of accidental degeneracies.

v. B-B-I bending modes

The predicted ν_5 fundamental (B-B-I bending) is presumably located in the far-ir region and so was not observed in this study.

vi. Lattice modes

The $\underline{t}_g$ rotational lattice mode scatters in the Raman at 40 cm^{-1} as a weak-to-medium intensity band.

CHAPTER IV CONCLUSIONS

Normal modes of symmetric molecules are usually obtained by using group theoretical procedures. This approach has been extensively used to assign the vibrational frequencies of small molecules such as NH_3, SO_2, etc.[107]. Moreover, the method can be extended to predict spectral data for large molecules or polymers, if they are sufficiently symmetric. Consequently, spectral predictions can be made for molecules such as polyhedral boranes, adamantane, twistane, cubane, etc., and also for sandwich compounds, especially those of the ferrocene-type and metaloboranes (vide supra, Introduction).

Molecular vibrations of the free $[B_{12}H_{12}]^{2-}$ and $[B_{12}D_{12}]^{2-}$ icosahedral ions have been predicted and studied on a group theoretical basis. The application of the Teller-Redlich product rule has helped to assign the various fundamentals. Unlike many vibrational studies, all nine modes predicted for these cage ions were observed in aqueous solutions. Molecular vibrations of the $[B_{12}H_{12}]^{2-}$ ion were studied by Weber and Thorpe[111] using different valence-force-field models. A six-parameter model based on the coupling force constants of B-B, B-H, B-B-B (60°), B-B-B (108°), and B-B-H gave values within ∿2% mean deviation of the previously reported experimental frequencies[79].

Weber and Thorpe's calculations[111] have also helped to correct the frequencies for the ν_8 and ν_9 modes of the

$[B_{12}D_{12}]^{2-}$ ion. Our experimental results have confirmed the theoretical predictions of the previous researchers. For example, the Raman-active B-B-B skeletal bending (ν_9, $\underline{h}_g$) of the $[B_{12}D_{12}]^{2-}$ ion was assigned to the 542 cm^{-1} line instead of Muetterties et al.'s[79] value of 620 cm^{-1} which is ~40 cm^{-1} higher than the corresponding frequency for $[B_{12}H_{12}]^{2-}$. This fundamental was predicted by Weber and Thorpe[111] to be at 573 cm^{-1}. We feel that our value of 542 cm^{-1} is more acceptable as a normal isotopic shift. Also, the 738 cm^{-1} peak appearing in the Raman spectrum of $[B_{12}D_{12}]^{2-}$ ion was assigned by Muetterties et al.[79] to ν_8, but it is more likely due to the ^{10}B isotope shift of the intense 718 cm^{-1} peak (ν_2, $\underline{a}_g$). Meanwhile, the Raman line at 622 cm^{-1} in the aqueous solution spectrum of $[B_{12}D_{12}]^{2-}$ was assigned by us to ν_8 rather than ν_9, as proposed by Muetterties et al.[79].

The assignment of bands in the spectra of the free ions has been of great assistance in assigning the corresponding modes of solid $K_2B_{12}H_{12}$, $Cs_2B_{12}H_{12}$, and $K_2B_{12}D_{12}$. For example, for the deuterated salt, the 629 and 622 cm^{-1} peaks were assigned to ν_8 ($\underline{e}_g + \underline{t}_g$), while the 547 and 538 cm^{-1} lines were attributed to ν_9 ($\underline{e}_g + \underline{t}_g$).

The ir spectra in Nujol of the cesium and potassium salts were essentially the same as that of the free $[B_{12}H_{12}]^{2-}$ ion in aqueous solution with minimum frequency shifts occurring indicating negligible solvent-solute interactions. As expected, there were no splittings observed for the ir fundamentals

because (a) the t_{1u} species of the free ion (I_h symmetry) and the t_u modes of the crystalline molecule (T_h symmetry) have the same degeneracy and correlate directly to one other and (b) the site symmetry is the same as that of the factor group.

For solid $Cs_2B_{12}H_{12}$, $K_2B_{12}H_{12}$ and $K_2B_{12}D_{12}$, the ir and Raman spectra were in complete accord with the factor group predictions. All the fundamentals were observed and the expected crystal field splittings were detected in the Raman spectra. The ir lattice bands (originating from the K^+ or Cs^+ ion movements within the lattices relative to the $[B_{12}H_{12}]^{2-}$ icosahedral units) were too low in energy to be observed in the normal ir range (4000-400 cm^{-1}). However, frequencies of these bands could be predicted from several combination bands in the spectra.

In crystalline $Cs_2B_{12}H_{12}\cdot CsCl$, the reduction in symmetry of the $[B_{12}H_{12}]^{2-}$ icosahedron from I_h (molecular) to C_s (site) removes all the symmetry elements except the mirror plane. This leads to a complete splitting of the bands, as illustrated in Table XXIV.

Vibrational fundamentals of $Cs_2B_{12}H_{12}\cdot CsCl$ under the D_{2h}^{16} symmetry were determined by the correlation diagram (Table XX). However, the large number of modes predicted by the factor group analysis was drastically reduced in the actual spectra. This was attributed to accidental degeneracies and/or weak intensities, especially in the lattice region where the former is often encountered. In our experimental

TABLE XXIV: Crystal field splittings for $Cs_2B_{12}H_{12}\cdot CsCl$

Molecular symmetry I_h	Site symmetry C_s	Crystal symmetry D_{2h}^{16}
$4 \times 2\ \underline{a}_g$	8a'	$2\ (\underline{a}_g + \underline{b}_{2g} + \underline{b}_{1u} + \underline{b}_{3u})$
$4 \times 3\ \underline{t}_{1u}$	12 (2a' + a")	$3\ (2\underline{a}_g + \underline{b}_{1g} + 2\underline{b}_{2g} + \underline{b}_{3g} + \underline{a}_u + 2\underline{b}_{1u} + \underline{b}_{2u} + 2\underline{b}_{3u})$
$4 \times 4\ \underline{h}_g$	16 (3a' + 2a")	$4\ (3\underline{a}_g + 2\underline{b}_{1g} + 3\underline{b}_{2g} + 2\underline{b}_{3g} + 2\underline{a}_u + 3\underline{b}_{1u} + 2\underline{b}_{2u} + 3\underline{b}_{3u})$

work, we obtained double salts of the general formula $M_2B_{12}H_{12}\cdot MX$ when an intimate mixture of a $M_2B_{12}H_{12}$ compound and an alkali halide was pressed under high pressure (10 tons/in^2) during the preparation of ir discs. The spectra of the resulting salts were very similar to those of the authentic $Cs_2B_{12}H_{12}\cdot CsCl$ double salt.

In the Raman spectra of perhalogen derivatives, we have managed to observe several new features because of the superior instrumentation now available. For example, we found ν_9, B-B deformation mode to be at 135-125, 98-84 and $\sim$71 cm^{-1}

for the perchloro, perbromo and periodo species, respectively. The Raman singlets appearing at ∿300 and ∿200 cm^{-1} for the perchloro and perbromo ions, respectively, were incorrectly assigned by Muetterties et al.[79] to the symmetric boron-halogen stretching modes (ν_1, a_g). We consider the 300 cm^{-1} frequency to be too far removed from the 1037-579 cm^{-1} frequency range accepted for B-Cl stretching modes[119]. The same comment applies to the ∿200 cm^{-1} peak of the perbromo species and the ∿145 cm^{-1} band of the periodo salt. In addition, the polarization ratios for these lines (ρ=0.38) are too large for such high symmetry molecules (I_h) considering that the polarization ratios for the totally symmetric modes of the $[B_{12}H_{12}]^{2-}$ and $[B_{12}D_{12}]^{2-}$ ions are all less than 0.1. Consequently, depolarized bands were suspected to be included with the a_g modes. This was experimentally confirmed by splitting the ∿300, ∿200 and ∿145 cm^{-1} peaks of the perchloro, perbromo and periodo salts, respectively, into several lines under high resolution. These lines were assigned to the ν_2 (a_g) and ν_8 (e_g + t_g) B-B stretching modes.

The absence of strong boron-halogen absorptions in the Raman spectra of the solid perhalogen derivatives was attributed to accidental cancellation of polarizabilities. Since this phenomenon occurred in the spectra of the three perhalo derivatives studied, it seemed to be a general result of the electronic properties of these compounds. The fundamentals that were missing or observed with very weak intensity

were those involving vibrations of the oppositely charged halogen and boron atoms.

Through theoretical calculations, Weber and Thorpe[111] have predicted the missing frequencies for the ν_1, ν_4-ν_9 modes of the $[B_{12}Cl_{12}]^{2-}$ species. We were able to locate the ν_4, ν_8 and ν_9 fundamentals in the spectra of all the perhalo derivatives studied. The ν_1, ν_6 and ν_7 modes were too weak to be experimentally detected and only in the spectra of the perchloro species were they possibly present as very weak bands. The ν_5 bending modes lay outside the range of our available ir instrumentation and therefore were not investigated.

The low number of bands observed in the ir and Raman spectra of solid dodecaborates compared to the larger number of modes predicted from the factor group analyses, led us to three conclusions. First, the geometry of the icosahedron was preserved to a great extent in the lattices of the solids. This was confirmed by the X-ray analysis of $K_2B_{12}H_{12}$ which showed minimal distortion of the icosahedron by the potassium ions[72]. The second conclusion was that there must be minimal coupling between the four icosahedra of the unit cells. Such coupling could have caused band splitting due to the in-phase and out-of-phase interactions of each vibration. The third conclusion was that the perhalogen derivatives were probably isostructural with the corresponding dodecahydroborates. The spectra of the perhalo derivatives were even simpler than those of the $[B_{12}H_{12}]^{2-}$ salts and since they

cannot possess higher symmetry, then they are more likely to be of the same or comparable high symmetry. In other words, the introduction of the twelve large halogen atoms did not seem to decrease either the icosahedral symmetry of the $[B_{12}H_{12}]^{2-}$ ion or the T_h symmetry of the lattice of the crystalline solid. This is evident from the fact that the twelve halogen atoms constitute an outer icosahedral shell around the B_{12} icosahedron without affecting the overall symmetry of the structure. However, the cell edges of the unit cells of the perhalo salts would be considerably longer.

Table XXV illustrates the decrease in energy of the fundamentals of the different icosahedral salts studied with the increase in mass of the atoms of the outer icosahedron. It is apparent that frequencies decrease in the anticipated manner:

$$[B_{12}H_{12}]^{2-} > [B_{12}D_{12}]^{2-} > [B_{12}Cl_{12}]^{2-} > [B_{12}Br_{12}]^{2-} > [B_{12}I_{12}]^{2-}$$

Force constants for the totally symmetric B-H and B-B stretching vibrations can be estimated with reasonable accuracy from the equation of simple harmonic motion (Eq. 93). This is only applicable if the coupling between molecular vibrations is small and the atoms involved are either small or of quite different masses.

$$k = 4\pi M_1 C^2 \bar{\nu}^2 \mu \qquad (93)$$

where k is the force constant in mdyn Å^{-1}, M_1 is 1/16 of the mass of an ^{16}O atom (1.66×10^{-24} g), C is the velocity of light

TABLE XXV: Fundamental modes of the various icosahedral dodecaborate ions (cm^{-1})

Vib. no. and symmetry	$[B_{12}H_{12}]^{2-}$	$[B_{12}D_{12}]^{2-}$	$[B_{12}Cl_{12}]^{2-}$ [d]	$[B_{12}Br_{12}]^{2-}$ [d]	$[B_{12}I_{12}]^{2-}$ [d]	Assignment
ν_1, $\underline{a}_g$	2517	1910	~1070 [b,e]	(~950) [c]	(~900) [c]	B-X [a] cage breath.
ν_2, $\underline{a}_g$	746	718	301	199	146	B-B cage breath.
ν_3, $\underline{t}_{1u}$	2480	1882	1032	1000	930	B-X str.
ν_4, $\underline{t}_{1u}$	1070	932	541	443	380	B-B str. and B-X bend. (cage def.)
ν_5, $\underline{t}_{1u}$	720	596	160 [b]	——	——	B-B-X bend.
ν_6, $\underline{h}_g$	2472	1864	1005? [e]	(~950) [c]	(~900) [c]	B-X str.
ν_7, $\underline{h}_g$	954	896	490? [e]	——	——	B-B str.
ν_8, $\underline{h}_g$	774	622	~300	~200	~150	B-B str. and B-X def.
ν_9, $\underline{h}_g$	582	542	~130	~90	~71	B-B-B bend.

[a] X = H, D, Cl, Brand I

[b] Ref. 111

[c] Expected approximate values are in parentheses.

[d] Values for the perhalogens were obtained from the Cs^+ salts; splittings due to isotopic effects or crystal field effects were not considered.

[e] Very weak bands.

(2.99776×10^{10} cm sec^{-1}), $\bar{\nu}$ is the frequency of the vibration under consideration in cm^{-1}, and $\mu = \frac{M_1 M_2}{M_1+M_2}$ is the reduced mass of the two atoms involved in the vibration.

Molecular orbital calculations for the $[B_{12}H_{12}]^{2-}$ icosahedron have shown that the outer shell of hydrogen atoms is not appreciably coupled with the B_{12} skeletal cage. In view of this, the conditions for the simple oscillator are fulfilled and the totally symmetric breathing modes (ν_1 and ν_2) of the icosahedron can be considered as a result of only B-H stretching and only B-B stretching, respectively. Application of Eq. 93 for $[B_{12}H_{12}]^{2-}$ gave 3.41 and 1.78 mdyn $Å^{-1}$ for the B-H and B-B stretching force constants, respectively. The most realistic force field model postulated by Weber and Thorpe[111], that gave fundamental frequencies very close to the experimental values, possessed the following primary force constants: 3.05 (B-H stretching) and 0.65 (B-B stretching) mdyn $Å^{-1}$. It is evident from these force constants that the outward B-H forces are much stronger than the intra icosahedral forces. This was reflected in the ir and Raman spectra of the $[B_{12}H_{12}]^{2-}$ ion by the extremely intense B-H stretching modes and by their high frequencies.

An interesting point which arises from this study is that solid $Cs_2B_{12}H_{12}$ was originally believed to belong to the Fm3m (O_h^5)[73]. From this, it would follow that O_h is a subgroup of the I_h point group and this is certainly incorrect. The more recent X-ray diffraction study, however, shows that

the Cs^+ salt is isostructural with $K_2B_{12}H_{12}$ [Fm3 (T_h^3)]. Thus, the factor group analysis should be the same for both salts. Consequently, this analysis was not repeated for the Cs^+ salt; instead, this salt was analyzed assuming that the originally assigned space group was correct. This procedure was carried out mainly for the purpose of comparing the number of optically-active bands predicted for the two space groups. It is of interest that the spectral predictions were essentially identical.

CHAPTER V SUGGESTIONS FOR FUTURE WORK

Some of the many possible extensions of this thesis are listed below:

1. Far-ir measurements could be utilized to locate the lattice modes of the different dodecaborate salts studied, and also to determine frequencies for the ν_5 bending modes of the perhalogen derivatives.

2. Vibrational studies on the molten salts would be of interest to determine whether or not the icosahedral geometry is preserved in the melts.

3. Analogous systems such as $[CB_{11}H_{12}]^-$ (I_h), $C_2B_{10}H_{12}$ (I_h), $[B_{10}H_{10}]^{2-}$ (D_{4d}), $[B_8H_8]^{2-}$ (D_{3d}) and B_8H_8 (D_{2d}) have high symmetries and could also be studied on the same basis.

4. Ferrocene-type sandwich compounds involving polyhedral cages instead of pentagonal rings e.g., metalocarboranes $M(CB_{10}H_{11})_2$, $M(C_2B_9H_{11})_2$ and metalothioboranes $M(SB_{10}H_{11})_2$ could be spectroscopically analyzed and their spectra compared with those of the parent cages.

5. Normal coordinate calculations should prove interesting because they would yield further information about the precise nature of the normal modes and subsequently could help in assigning combinations, overtones, and satellite bands, etc.

6. The Raman technique of oriented single crystals could be very valuable in assigning the various modes of the $Cs_2B_{12}H_{12}\cdot CsCl$ double salt since the crystalline compound possesses a D_{2h} symmetry and thus its three crystallographic axes are distinguishable.

7. X-ray diffraction studies are needed to establish the crystal structures of the $M_2B_{12}X_{12}$ perhalogen derivatives.

8. The vibrational spectra of the different forms of elementary boron (all of which possess icosahedral B_{12} units) still await further investigation. The spectra of these compounds could be compared with those of the simpler $[B_{12}H_{12}]^{2-}$ icosahedral units. This approach could also be applied in studying molecular vibrations of the icosahedral polymeric compounds such as alloys, viruses, complexes and synthetic inorganic polymers.

APPENDIX I: THE GROUP THEORETICAL CALCULATIONS

In this section, several group theoretical treatments are presented. These will illustrate the principles and uses of the procedure. The first example is the calculation of normal modes for the icosahedral $[B_{12}H_{12}]^{2-}$ ion. Second, we will calculate the contributions of the different internal coordinates of the $[B_{12}H_{12}]^{2-}$ anion to the total molecular vibrations. An example of how to determine the symmetries of combinations and overtones is then given. Finally, factor group calculations for solid $K_2B_{12}H_{12}$ and $Cs_2B_{12}H_{12}$ are described.

A. CALCULATION OF NORMAL MODES FOR THE $[B_{12}H_{12}]^{2-}$ ION

The normal modes that belong to each species are obtained by applying the "magic formula":

$$n(a_g) = \frac{1}{120}[72 \times 1 \times 1 + 6.472 \times 1 \times 12 + (-2.472) \times 1 \times 12 + 8 \times 1 \times 15] = 2$$

$$n(t_{1g}) = \frac{1}{120}[72 \times 3 \times 1 + 6.472 \times 1.618 \times 12 + (-2.472) \times (-0.618) \times 12 + 8 \times -1 \times 15] = 2$$

TABLE XXVI: Normal modes for the $[B_{12}H_{12}]^{2-}$ ion

I_h [a,b]	E	$15C_3$	$20C_3$	$12C_5$	$12C_5^2$	i	15σ	$20S_6$	$12S_{10}$	$12S_{10}^3$	n_i	Activity
A_g (S_g)	1	1	1	1	1	1	1	1	1	1	2	Raman
T_{1g} (F_{1g})	3	-1	0	x[c]	y[c]	3	-1	0	x	y	2	
T_{2g} (F_{2g})	3	-1	0	y	x	3	-1	0	y	x	0	
G_g (U_g)	4	0	1	-1	-1	4	0	1	-1	-1	2	
H_g (V_g)	5	1	-1	0	0	5	1	-1	0	0	4	Raman
A_u (S_u)	1	1	1	1	1	-1	-1	-1	-1	-1	0	
T_{1u} (F_{1u})	3	-1	0	x	y	-3	1	0	-x	-y	4	ir
T_{2u} (F_{2u})	3	-1	0	y	x	-3	1	0	-y	-x	2	
G_u (U_u)	4	0	1	-1	-1	-4	0	-1	1	1	2	
H_u (V_u)	5	1	-1	0	0	-5	-1	1	0	0	2	
χ_j	24	0	0	4	4	0	8	0	0	0		
m_j	3	-1	0	1.618	-0.618	-3	1	0	-1.618	-0.382		
$m_j\chi_j$	72	0	0	6.472	-2.472	0	8	0	0	0		

[a] The symbols shown in parentheses are those used for the old nomenclature system of labelling irreducible representations[75].

[b] Order of the group, g = 120

[c] $x = \frac{1 + \sqrt{5}}{3} = 1.618$, $y = \frac{1 - \sqrt{5}}{2} = -0.618$

$$n(\underline{t}_{2g}) = \frac{1}{120}[72 \times 3 \times 1 + 6.472 \times (-0.618) \times 12 + (-2.472) \times 1.618 \times 12 + 8 \times -1 \times 15] = 0$$

$$n(\underline{g}_{g}) = \frac{1}{120}[72 \times 4 \times 1 + 6.472 \times -1 \times 12 + -2.472 \times -1 \times 12 + 0] = 2$$

$$n(\underline{h}_{g}) = \frac{1}{120}[72 \times 5 \times 1 + 0 + 0 + 8 \times 1 \times 15] = 4$$

$$n(\underline{a}_{u}) = \frac{1}{120}[72 \times 1 \times 1 + 6.472 \times 1 \times 12 + (-2.472) \times 1 \times 12 + 8 \times -1 \times 15] = 0$$

$$n(\underline{t}_{1u}) = \frac{1}{120}[72 \times 3 \times 1 + 6.472 \times 1.618 \times 12 + (-2.472) \times (-0.618) \times 12 + 8 \times 1 \times 15] = 4$$

$$n(\underline{t}_{2u}) = \frac{1}{120}[72 \times 3 \times 1 + 6.472 \times (-0.618) \times 12 + (-2.472) \times 1.618 \times 12 + 8 \times 1 \times 15] = 2$$

$$n(g_u) = \frac{1}{120}[72 \times 4 \times 1 + 6.472 \times 1 \times 12 + (-2.472) \times -1 \times 12 + 0] = 2$$

$$n(h_u) = \frac{1}{120}[72 \times 5 \times 1 + 0 + 0 + 8 \times -1 \times 15] = 2$$

These modes are shown in the right-hand side of Table XXV.

B. CONTRIBUTIONS OF THE INTERNAL COORDINATES

There are five internal coordinates for the $[B_{12}H_{12}]^{2-}$ icosahedron. These are the changes in the two bond lengths (B-H and B-B) and changes in the three interbond angles (B-$\hat{B}$-H, B-$\hat{B}$-B (60°) and B-$\hat{B}$-B (108°)]. The characters for these coordinates are shown in the following table.

TABLE XXVII: Characters of internal coordinates for $[B_{12}H_{12}]^{2-}$

I_h	E	$15C^2$	$20C_3$	$12C_5$	$12C_5^2$	i	15σ	$20S_6$	$12S_{10}$	$12S_{10}^3$
B-H	12	0	0	2	2	0	4	0	0	0
B-B	30	2	0	0	0	0	4	0	0	0
B-$\hat{B}$-H	60	0	0	0	0	0	4	0	0	0
$\hat{B}BB$(60°)	60	0	0	0	0	0	4	0	0	0
$\hat{B}BB$(108°)	60	0	0	0	0	0	4	0	0	0

Using the magic formula, we arrive at the irreducible representations (normal modes) for the different symmetry species.

1. B-H Stretching Modes

$$n(\underline{a}_g) = \frac{1}{120}[12 \times 1 \times 1 + 2 \times 12 \times 1 + 2 \times 12 \times 1 + 4 \times 15 \times 1] = 1$$

$$n(\underline{t}_{1g}) = \frac{1}{120}[12 \times 1 \times 3 + 2 \times 12 \times (\frac{1 + \sqrt{5}}{2}) + 2 \times 12 \times (\frac{1 - \sqrt{5}}{2}) + 4 \times 15 \times -1] = 0$$

$$n(\underline{t}_{2g}) = \frac{1}{120}[12 \times 1 \times 3 + 2 \times 12 \times (\frac{1 - \sqrt{5}}{2}) + 2 \times 12 \times (\frac{1 - \sqrt{5}}{2}) + 4 \times 15 \times -1] = 0$$

$$n(\underline{g}_g) = \frac{1}{120}[12 \times 1 \times 4 + 2 \times 12 \times -1 + 2 \times 12 \times -1 + 0] = 0$$

$$n(\underline{h}_g) = \frac{1}{120}[12 \times 1 \times 5 + 0 + 0 + 4 \times 1 \times 15] = 1$$

$$n(\underline{a}_u) = \frac{1}{120}[12 \times 1 \times 1 + 2 \times 12 \times 1 + 2 \times 12 \times 1 + 4 \times 15 \times -1] = 0$$

$$n(\underline{t}_{1u}) = \frac{1}{120}[12 \times 1 \times 3 + 2 \times 12 \times (\frac{1 + \sqrt{5}}{2}) + 2 \times 12 \times (\frac{1 - \sqrt{5}}{2}) + 4 \times 15 \times 1] = 1$$

$$n(\underline{t}_{2u}) = \frac{1}{120}[12 \times 1 \times 3 + 2 \times 12 \times (\frac{1 - \sqrt{5}}{2}) + 2 \times 12 \times (\frac{1 + \sqrt{5}}{2}) + 4 \times 15 \times 1] = 1$$

$$n(\underline{g}_u) = \frac{1}{120}[12 \times 1 \times 4 + 2 \times 12 \times -1 + 2 \times 12 \times -1 + 0] = 0$$

$$n(\underline{h}_u) = \frac{1}{120}[12 \times 1 \times 5 + 0 + 0 + 4 \times 15 \times -1] = 0$$

$$\Big\lceil^{I_h}_{B\text{-}H} = \underline{a}_g + \underline{h}_g + \underline{t}_{1u} + \underline{t}_{2u} \qquad (94)$$

2. B-B Stretching Modes

$$n(\underline{a}_g) = \frac{1}{120}[30 \times 1 \times 1 + 2 \times 15 \times 1 + 4 \times 15 \times 1] = 1$$

$$n(\underline{t}_{1g}) = \frac{1}{120}[30 \times 3 \times 1 + 2 \times 15 \times -1 + 4 \times 15 \times -1] = 0$$

$$n(\underline{t}_{2g}) = \frac{1}{120}[30 \times 3 \times 1 + 2 \times 15 \times -1 + 4 \times 15 \times -1] = 0$$

$$n(\underline{g}_{g}) = \frac{1}{120}[30 \times 4 \times 1 + 2 \times 15 \times 0 + 4 \times 15 \times 0] = 1$$

$$n(\underline{h}_{g}) = \frac{1}{120}[30 \times 5 \times 1 + 2 \times 15 \times 1 + 4 \times 15 \times 1] = 2$$

$$n(\underline{a}_{u}) = \frac{1}{120}[30 \times 1 \times 1 + 2 \times 15 \times 1 + 4 \times 15 \times -1] = 0$$

$$n(\underline{t}_{1u}) = \frac{1}{120}[30 \times 3 \times 1 + 2 \times 15 \times -1 + 4 \times 15 \times 1] = 1$$

$$n(\underline{t}_{2u}) = \frac{1}{120}[30 \times 3 \times 1 + 2 \times 15 \times -1 + 4 \times 15 \times 1] = 1$$

$$n(\underline{g}_{u}) = \frac{1}{120}[30 \times 4 \times 1 + 2 \times 15 \times 0 + 4 \times 15 \times 0] = 1$$

$$n(\underline{h}_{u}) = \frac{1}{120}[30 \times 5 \times 1 + 2 \times 15 \times 1 + 4 \times 15 \times -1] = 1$$

$$\Big\lceil^{I_h}_{B-B} = \underline{a}_g + \underline{g}_g + 2\underline{h}_g + \underline{t}_{1u} + \underline{t}_{2u} + \underline{g}_u + \underline{h}_u \qquad (95)$$

3. Contributions of the Interbond Angles

$$n(\underline{a}_g) = \frac{1}{120}[60 \times 1 \times 1 + 4 \times 15 \times 1] = 1$$

$$n(\underline{t}_{1g}) = \frac{1}{120}[60 \times 3 \times 1 + 4 \times 15 \times -1] = 1$$

$$n(\underline{t}_{2g}) = \frac{1}{120}[60 \times 3 \times 1 + 4 \times 15 \times -1] = 1$$

$$n(\underline{g}_g) = \frac{1}{120}[60 \times 4 \times 1 + 0] = 2$$

$$n(\underline{h}_g) = \frac{1}{120}[60 \times 5 \times 1 + 4 \times 15 \times 1] = 3$$

$$n(\underline{a}_u) = \frac{1}{120}[60 \times 1 \times 1 + 4 \times 15 \times -1] = 0$$

$$n(\underline{t}_{1u}) = \frac{1}{120}[60 \times 3 \times 1 + 4 \times 15 \times 1] = 2$$

$$n(\underline{t}_{2u}) = \frac{1}{120}[60 \times 3 \times 1 + 4 \times 15 \times 1] = 2$$

$$n(\underline{g}_u) = \frac{1}{120}[60 \times 4 \times 1 + 0] = 2$$

$$n(\underline{h}_u) = \frac{1}{120}[60 \times 5 \times 1 + 4 \times 15 \times -1] = 2$$

$$\Gamma_{B\text{-}\hat{B}\text{-}H} = \Gamma_{\substack{B\text{-}B\text{-}B \\ (60°)}} = \Gamma_{\substack{B\text{-}B\text{-}B \\ (108°)}} = \underline{a}_g + \underline{t}_{1g} + \underline{t}_{2g} + 2\underline{g}_g + 3\underline{h}_g + 2\underline{t}_{1u} + 2\underline{t}_{2u} + 2\underline{g}_u + 2\underline{h}_u \quad (96)$$

C. COMBINATIONS AND OVERTONES

In order to determine whether or not a combination or overtone is optically allowed, we multiply the characters of the corresponding species, then reduce the resulting representation in the usual way. If any of the resulting species has optical activity, then the combination or overtone is active. The $\underline{h}_g + \underline{t}_{1u}$ combination is used as an example and other combinations or overtones can be dealt with in a similar manner.

TABLE XXVIII: Examples of obtaining the characters of overtones for $[B_{12}H_{12}]^{2-}$

I_h	E	$12C_5$	$12C_5^2$	$20C_3$	$15C_2$	i	$12S_{10}$	$12S_{10}^3$	$20S_6$	15σ
H_g	5	0	0	-1	1	5	0	0	-1	1
T_{1u}	3	$\frac{1+\sqrt{5}}{2}$	$\frac{1-\sqrt{5}}{2}$	0	-1	-3	$\frac{\sqrt{5}-1}{2}$	$\frac{-\sqrt{5}-1}{2}$	0	1
$\underline{h}_g \times \underline{t}_{1u}$	15	0	0	0	-1	-15	0	0	0	1

$$n(A_g) = \frac{1}{120}[15 - 15 - 15 + 15] = 0$$

$$n(T_{1g}) = \frac{1}{120}[45 + 15 - 45 - 15] = 0$$

$$n(T_{2g}) = \frac{1}{120}[45 + 15 - 45 - 15] = 0$$

$$n(G_g) = \frac{1}{120}[60 + 0 - 60 + 0] = 0$$

$$n(H_g) = \frac{1}{120}[75 - 15 - 75 + 15] = 0$$

$$n(A_u) = \frac{1}{120}[15 - 15 + 15 - 15] = 0$$

$$n(T_{1u}) = \frac{1}{120}[45 + 15 + 45 + 15] = 1$$

$$n(T_{2u}) = \frac{1}{120}[45 + 15 + 45 + 15] = 1$$

$$n(G_u) = \frac{1}{120}[60 + 0 + 60 + 0] = 1$$

$$n(H_u) = \frac{1}{120}[75 - 15 + 75 - 15] = 1$$

$$\underline{t}_{1u} + \underline{h}_g = T_{1u} + T_{2u} + G_u + H_u \qquad (97)$$

Therefore, the $\underline{t}_{1u} + \underline{h}_g$ combination is ir-active since the product contains the T_{1u} species*.

---

*It should be pointed out that throughout this thesis, we have adopted the modern system of labelling the symmetry species of normal modes, i.e., lower-case letters such as $\underline{t}_{1u}$. For overtones and combinations, upper-case letters are used, e.g., T_{1u}.

D. CONTRIBUTION OF THE TWO SETS OF EQUIVALENT ATOMS OF THE $[B_{12}H_{12}]^{2-}$ ION TO THE MOLECULAR VIBRATIONS

TABLE XXVIX: Characters of the sets of equivalent atoms of $[B_{12}H_{12}]^{2-}$

I_h	E	$12C_2$	$20C_3$	$12C_5$	$12C_5^2$	i	15σ	$20S_6$	$12S_{10}$	$12S_{10}^3$
$\chi_j(H_{12})$	36	0	0	2	2	0	4	0	0	0
$\chi_j(B_{12})$	36	0	0	2	2	0	4	0	0	0

$$n(\underline{a}_g) = \frac{1}{120}[36 + 38.832 - 14.832 + 60] = 1$$

$$n(\underline{t}_{1g}) = \frac{1}{120}[108 + 62.75 + 9.25 - 60] = 1$$

$$n(\underline{t}_{2g}) = \frac{1}{120}[108 - 24 - 24 - 60] = 0$$

$$n(\underline{g}_g) = \frac{1}{120}[144 - 38.832 + 14.832 + 0] = 1$$

$$n(\underline{h}_g) = \frac{1}{120}[180 + 0 + 0 + 60] = 2$$

$$n(\underline{a}_u) = \frac{1}{120}[36 + 38.832 - 14.832 - 60] = 0$$

$$n(\underline{t}_{1u}) = \frac{1}{120}[108 + 62.75 + 9.25 + 60] = 2$$

$$n(\underline{t}_{2u}) = \frac{1}{120}[108 - 24 - 24 + 60] = 1$$

$$n(\underline{g}_u) = \frac{1}{120}[144 - 38.832 + 14.832 + 0] = 1$$

$$n(\underline{h}_u) = \frac{1}{120}[180 + 0 + 0 - 60] = 1$$

Therefore

$$\Gamma_{H_{12}} = \Gamma_{B_{12}} = \underline{a}_g + \underline{t}_{1g} + \underline{g}_g + 2\underline{h}_g + 2\underline{t}_{1u} + \underline{t}_{2u} + \underline{g}_u + \underline{h}_u \qquad (98)$$

E. FACTOR GROUP ANALYSIS

Factor group procedures for solid $K_2B_{12}H_{12}$ under the T_h^3 symmetry are outlined in Table VIII and the calculation is quite straight forward because of the simplicity of the T_h character table. A similar case is the factor group treatment

for solid $Cs_2B_{12}H_{12}$ under the O_h^5 symmetry which is shown in Table XV. The calculation of the normal modes for the latter is presented below.

TABLE XXX: Examples of factor group calculations for $Cs_2B_{12}H_{12}$

O_h[a]	E	$8C_3$	$3C_2$	$6C_4$	$6C_2'$	i	$8S_6$	$3\sigma_h$	$6S_4$	$6\sigma_d$
$[\chi_j\ (N)]$	78	0	-2	0	-4	0	0	8	-2	6
$[\chi_j\ (n_i)]$	66	0	2	-2	-2	0	0	8	0	4

[a]Taken from Table XV, p. 147.

1. Calculation of Total Modes (N)

$$n(a_{1g}) = \frac{1}{48}[78 - 6 - 24 + 24 - 12 + 36] = 2$$

$$n(a_{2g}) = \frac{1}{48}[78 - 6 + 24 + 24 + 12 - 36] = 2$$

$$n(a_{1u}) = \frac{1}{48}[78 - 6 - 24 - 24 + 12 - 36] = 0$$

$$n(\underline{a}_{2u}) = \frac{1}{48}[78 - 6 + 24 - 24 - 12 + 36] = 2$$

$$n(\underline{e}_g) = \frac{1}{48}[156 - 12 + 42] = 4$$

$$n(\underline{e}_u) = \frac{1}{48}[156 - 12 - 48] = 2$$

$$n(\underline{t}_{1g}) = \frac{1}{48}[234 + 6 + 24 - 24 - 12 - 36] = 4$$

$$n(\underline{t}_{2g}) = \frac{1}{48}[234 + 6 - 24 - 24 + 12 + 36] = 5$$

$$n(\underline{t}_{1u}) = \frac{1}{48}[234 + 6 + 24 + 24 + 12 + 36] = 7$$

$$n(\underline{t}_{2u}) = \frac{1}{48}[234 + 6 - 24 + 24 - 12 + 36] = 4$$

$$\Gamma^{O_h}_{\text{total}} = 2\underline{a}_{1g} + 2\underline{a}_{2g} + 2\underline{a}_{2u} + 4\underline{e}_g + 2\underline{e}_u + 4\underline{t}_{1g} + 5\underline{t}_{2g} + 7\underline{t}_{1u} + 4\underline{t}_{2u} \qquad (99)$$

2. Calculation of Internal Modes (n_i)

$$n(\underline{a}_{1g}) = \frac{1}{48}[66 + 6 - 12 - 12 + 24 + 24] = 2$$

$$n(\underline{a}_{2g}) = \frac{1}{48}[66 + 6 + 12 + 12 + 24 - 24] = 2$$

$$n(\underline{a}_{1u}) = \frac{1}{48}[66 + 6 - 12 - 12 - 24 - 24] = 0$$

$$n(\underline{a}_{2u}) = \frac{1}{48}[66 + 6 + 12 + 12 - 24 + 24] = 2$$

$$n(\underline{e}_{g}) = \frac{1}{48}[132 + 12 + 48] = 4$$

$$n(\underline{e}_{u}) = \frac{1}{48}[132 + 12 - 48] = 2$$

$$n(\underline{t}_{1g}) = \frac{1}{48}[198 - 6 - 12 + 12 - 24 - 24] = 3$$

$$n(\underline{t}_{2g}) = \frac{1}{48}[198 - 6 + 12 - 12 - 24 + 24] = 4$$

$$n(\underline{t}_{1u}) = \frac{1}{48}[198 - 6 - 12 + 12 + 24 + 24] = 5$$

$$n(\underline{t}_{2u}) = \frac{1}{48}[198 - 6 + 12 - 12 + 24 - 24] = 4$$

$$\Gamma^{O_h}_{(n_i)} = 2\underline{a}_{1g} + 2\underline{a}_{2g} + 2\underline{a}_{2u} + 4\underline{e}_g + 2\underline{e}_u + 3\underline{t}_{1g} + 4\underline{t}_{2g} + 5\underline{t}_{1u} + \underline{4}_{2u} \qquad (100)$$

The calculation of the translational or rotational modes is performed exactly as described above using the characters of the reducible representations shown in Table XV (p.147).

APPENDIX II: APPLICATION OF THE TELLER-REDLICH PRODUCT RULE

Vibrational frequencies of isotopic molecules can provide additional information of use in assigning the various internal modes. This has been formulated in the Teller-Redlich product rule[109] which states that the product of the (ω^i/ω) values for all vibrations of a given symmetry depends only on the masses of the atoms involved and the symmetry of the molecule, but is independent of the potential constants. The rule can be expressed by the general equation.

$$\omega_1^i/\omega_1 \cdot \omega_2^i/\omega_2 \cdot \omega_3^i/\omega_3 \cdots \omega_f^i/\omega_f = \tag{101}$$

$$(m_1/m_1^i)^{\alpha} \cdot (m_2/m_2^i)^{\beta} \cdots (M^i/M)^t \cdot (I_x^i/I_x)^{\delta x} \cdot (I_y^i/I_y)^{\delta y} \cdot (I_z^i/I_z)^{\delta z}.$$

where all quantities having the superscript (i) refer to the isotopic molecule; ω_1, ω_2, $\ldots\omega_f$ are the zero-order frequencies of the f genuine vibrations of the symmetry type considered; m_1, $m_2\ldots$ are the masses of the atoms representing various sets of equivalent atoms (those atoms which are transformed into one another by the symmetry operations of the molecule); α, $\beta,\ldots$ are the number of vibrations each set contributes to the symmetry species considered; M is the total mass of the molecule; t is the number of translations included in the symmetry species; I_x, I_y, I_z are the moments of inertia through

the centre of mass about the x, y, z axes; δ_x, δ_y, δ_z are 1 or 0 depending on whether or not the rotation about the x, y, z axis is a non-genuine vibration of the symmetry species considered.

Application of the product rule yields information about which atoms are involved in a particular vibration since larger isotopic shifts reflect greater amplitudes for the vibrating atoms. In our calculations, observed fundamentals (ν_i) are used instead of the zero-order frequencies (ω_i). This is usually believed to introduce about a 4% error in the calculations[109].

A. CASE OF THE $[B_{12}H_{12}]^{2-}$ ION

From group theoretical calculations, we arrive at the number of optically-active normal modes for the anion, viz., $2a_g(R) + 3t_{1u}(ir) + 4h_g(R)$. All nine frequencies are observed and the assignment to a_g and h_g modes are made on the basis of Raman polarization studies. There are two sets of equivalent atoms in this anion, viz., (H_{12}) and (B_{12}). The isotopic shift calculations are discussed in terms of a_g, t_{1u} and h_g symmetry species.

1. a_g modes

There are two vibrations (ν_1 and ν_2) that belong to this species. Both vibrations are genuine, i.e., there are no

rotational or translational modes: $t=\delta_x=\delta_y=\delta_z=0$. The hydrogen atom movements [the (H_{12}) set] contribute one vibration to this species: $\alpha=1$. The boron atom movements [the (B_{12}) set] contribute the other vibration, i.e., $\beta=1$. Applying the product rule, we obtain:

$$(\nu_1^i/\nu_1)^2 \cdot (\nu_2^i/\nu_2)^2 = m_H/m_D \cdot m_B/m_B \qquad (102)$$

$$(\frac{1910}{2517})^2 \cdot (\frac{718}{746})^2 = m_H/m_D \qquad (103)$$

$$0.58 \quad x \quad 0.93 \quad = \quad 0.53 \text{ (theor. } 0.50) \qquad (104)$$

2. $\underline{t_{1u}}$ modes

There are four vibrations of this symmetry species. Three vibrations are genuine (ν_3, ν_4 and ν_5) and one is a non-genuine translation ($t=1$). There are no rotations, i.e., $\delta_x=\delta_y=\delta_z=0$. The hydrogen atom movements contribute two vibrations ($\alpha=2$), while the boron atom movements contribute one vibration ($\beta=1$) after excluding a translational mode.

$$(\nu_3^i/\nu_3)^2 \quad (\nu_4^i/\nu_4)^2 \quad (\nu_5^i/\nu_5)^2 = (m_H/m_D)^2 \cdot (m_B/m_B) \cdot M^i/M \qquad (105)$$

$$\left(\frac{1882}{2480}\right)^2 \left(\frac{932}{1070}\right)^2 \left(\frac{596}{720}\right)^2 = \left(\tfrac{1}{2}\right)(1)\left(\frac{153.9}{141.8}\right) \qquad (106)$$

$$0.57 \times 0.76 \times 0.68 = 0.30 \text{ (theor. } 0.27) \qquad (107)$$

3. h_g modes

There are four normal vibrations, all of which are genuine: $t=\delta_x=\delta_y=\delta_z=0$. Both the (B_{12}) and (H_{12}) sets contribute two vibrations each to this species $(\alpha=\beta=2)$.

$$(\nu_6^i/\nu_6)^2 (\nu_7^i/\nu_7)^2 (\nu_8^i/\nu_8)^2 (\nu_9^i/\nu_9)^2 = (m_H/m_D)^2 (m_B/m_B)^2 \qquad (108)$$

$$\left(\frac{1864}{2472}\right)^2 \left(\frac{896}{954}\right)^2 \left(\frac{622}{774}\right)^2 \left(\frac{542}{582}\right)^2 = \left(\tfrac{1}{2}\right)^2 \qquad (109)$$

$$0.57 \times 0.88 \times 0.65 \times 0.87 = 0.28 \text{ (theor. } 0.25) \qquad (110)$$

Vibrations having the $\left(\frac{\nu^i}{\nu}\right)^2$ ratio square near unity are due to movements of boron atoms, e.g., ν_2, ν_7 and ν_9. Vibrations having $\left(\frac{\nu^i}{\nu}\right)^2$ values aroung 0.5 are mainly attributed to hydrogen atom movements such as the ν_1, ν_3 and ν_6 fundamentals. If the $\left(\frac{\nu^i}{\nu}\right)^2$ values are intermediate between 0.5 and

1, the vibrations are then considered as the result of the movements of both the boron and the hydrogen atoms (vide supra, Table VII).

B. CASE OF THE $K_2B_{12}H_{12}$ SALT

The product rule is applied to this salt and its deuterated analogue as discussed previously for the $[B_{12}H_{12}]^{2-}$ and $[B_{12}D_{12}]^{2-}$ ions. The only difference is that the h_g mode of the free ion could be split into e_g and t_g modes in the spectra of the solids. Since we do not have any way of differentiating between the e_g and t_g modes, their frequencies are combined and averaged prior to the application of the Teller-Redlich rule. The calculations for the various species are summarized below and the results are given in Table XII.

1. a_g modes

$$\left(\frac{1905}{2521}\right)^2_{\nu_1} \cdot \left(\frac{721}{757}\right)^2_{\nu_2} = \frac{m_H}{m_D} \cdot \frac{m_B}{m_B} \qquad (111)$$

$$0.57 \quad x \quad 0.90 \quad = \quad 0.52 \text{ (theor. } 0.50) \qquad (112)$$

2. t_u modes

$$\left(\frac{1876}{2471}\right)^2_{\nu_3} \cdot \left(\frac{928}{1074}\right)^2_{\nu_4} \cdot \left(\frac{597}{715}\right)^2_{\nu_5} = \left(\frac{m_H}{m_D}\right)^2 \cdot \frac{m_B}{m_B} \cdot \frac{M_{BD}}{M_{BH}} \qquad (113)$$

$$0.58 \quad x \quad 0.74 \quad x\ 0.7 \quad = \quad 0.30 \text{ (theor. } 0.27) \qquad (114)$$

3. $\underline{e_g} + \underline{t_g}$ modes

Here the average of the $\underline{e_g} + \underline{t_g}$ doublet is used in the calculation.

$$\left(\frac{1878}{2495}\right)^2_{\nu_6} \cdot \left(\frac{892}{960}\right)^2_{\nu_7} \cdot \left(\frac{621}{766}\right)^2_{\nu_8} \cdot \left(\frac{547}{585}\right)^2_{\nu_9} = \left(\frac{m_H}{m_D}\right)^2 \cdot \left(\frac{m_B}{m_B}\right)^2 \qquad (115)$$

$$0.57 \text{ x } 0.87 \text{ x } 0.65 \text{ x } 0.87 \quad = \quad 0.28 \text{ (theor. } 0.25) \qquad (116)$$

REFERENCES

1. F.A. Cotton, Chemical Application of Group Theory, Wiley-Interscience, New York, 1971.
2. E.L. Muetterties, The Chemistry of Boron and its Compounds, Wiley, New York, 1967.
3. G.S. Zhdanov and N.G. Sevast'yanov, Compt. Rend. Acad. Sci. USSR, 32, 432 (1941).
4. B.F. Decker and J.S. Kasper, Acta Cryst. 12, 503 (1959); L.V. McCarty, J.S. Kasper, F.N. Horn, B.F. Decker and E. A.E. Newkirk, J. Am. Chem. Soc., 80, 2592 (1958).
5. J.L. Hoard, R.E. Hughes and D.E. Sands, J. Am. Chem. Soc., 80, 4507 (1958).
6. H. Becher, in Boron Vol. 2, G.K. Gaulé, ed., Plenum Press, New York, 1965.
7. C.P. Talley, S. LaPlaca and B. Frost, Acta Cryst., 13, 271 (1960).
8. D.E. Sands and J.L. Hoard, J. Am. Chem. Soc., 79, 5582 (1957); R.E. Hughes, C.H.L. Kennard, D.B. Sullenger, H.A. Weakleim, D.E. Sands and J.L. Hoard, J. Am. Chem. Soc., 85, 361 (1963).
9. K. Wade, Chem. in Britain, 177 (1975).
10. A. Zalkin, J.D. Forester and D.H. Templeton, J. Chem. Phys., 39, 2881 (1963).
11. E.L. Muetterties and C.M. Wright, Quat. Rev. (London), 21, 109 (1967).
12. N.V. Mani and S. Ramasesham, Z. Krist., 114, 200 (1960).
13. J.L. Hoard and W.B. Vincent, J.Am.Chem.Soc., 62, 3126 (1940).

14. K. Wade, Electron Deficient Compounds, Nelson, London, 1971.

15. D.L. Kasper and A. Klug, Symp. Qual. Biol., 27, 1 (1962).

16. E.L. Muetterties and W.H. Knoth, Polyhedral Boranes, Marcel Dekker, New York, 1968.

17. H.K. Clark and J.L. Hoard, J. Am. Chem. Soc., 65, 2115 (1943).

18. G.S. Zhdanov, G.A. Meerson, N.N. Zhuralev, and G.V. Samsonov, Zhur. Fiz. kim., 28, 1076 (1954).

19. B. Magnusson and C. Brosset, Acta Chem. Scand., 16, 449 (1962).

20. V.I. Matkovich, J. Am. Chem. Soc., 83, 1804 (1961).

21. L.H. Spinar and C.C. Wang, Acta Cryst., 15, 1048 (1962).

22. R.A. Pasternack, Acta Cryst., 12, 612 (1959).

23. Ben Post, in R.M. Adams, Ed., Boron, Metalo-Boron Compounds and Boranes, Interscience, New York, 1964

24. G. Will, J. Am. Chem. Soc., 85, 2335 (1963).

25. V.I. Matkovich, J. Economy and R.F. Giese, Jr., J. Am. Chem. Soc., 86, 2337 (1964).

26. J.A. Kohn, W.F. Nye and G.K. Gaulé, Eds, Boron Vol. 1 (Synthesis, Structure and Properties), Plenum Press, New York, 1960.

27. H.J. Becker, Z. Anorg. Allg Chemie., 306, 266 (1960).

28. D.E. Sands, C.F. Cline, A. Zalkin and C.L. Hoenig, Acta Cryst., 14, 309 (1961).

29. B.F. Decker and J.S. Kasper, Acta Cryst., 13, 1030 (1960).

30. R.W. Johnson and A.H. Daane, J. Chem. Phys., 38, 425 (1963); S.M. Richards and J.S. Kasper, Abstracts, American Crystallographic Association Meeting, Gatlinburg, Tenn., June 27-July 2, 1965, p. 72.

31. S. LaPlaca in Boron, Metalo-Boron Compounds and Boranes, R.M. Adams, ed., Interscience, New York, 1964.

32. P.K. Smith and P.W. Gilles, J. Inorg. Nucl. Chem., 26, 1465 (1964).

33. L. Lavine and W.N. Lipscomb, J. Chem. Phys., 22, 614 (1954).

34. F.L. Hirshfeld, K. Eriks, R.E. Dickerson, E.L. Lippert, Jr. and W.N. Lipscomb, J. Chem. Phys., 28, 56 (1958).

35. P.G. Simpson and W.N. Lipscomb, J. Chem. Phys., 35, 1340 (1961).

36. J.S. Kasper, C.M. Lucht, and D. Harker, Acta Cryst., 3, 436 (1950).

37. V.D. Aflandilian, H.C. Miller, G. W. Parshall and E.L. Muetterties, Inorg. Chem., 1, 734 (1962).

38. W.N. Lipscomb, Boron Hybrides, Benjamin, New York, 1963.

39. E.L. Muetterties and W.H. Knoth, Chem. Eng. News, May 9 (1966), p. 88.

40. P.G. Simpson and W.N. Lipscomb, Proc. Natl. Acad. Sci. U.S., 48, 1490 (1962).

41. J.H. Enemark, L.B. Friedman, J.A. Hartsuck, and W.N. Lipscomb, J. Am. Chem. Soc., 88, 3659 (1966).

42. R.J. Wiersema and R.L. Middough, J. Am. Chem. Soc., 89, 5078 (1967); R.J. Wiersema and R.L. Middough, Inorg. Chem., 8, 2074 (1969).

43. F.A. Cotton and G. Wilkinson, Advanced Inorganic Chemistry, 2nd edition, Interscience, New York, 1966. p. 284; J.A. Potenza and W.N. Lipscomb, Proc. Natl. Acad. Sci. U.S., 56, 1917 (1966).

44. H. Schroeder, J. Reiner, R.P. Alexander and T.L. Heying, Inorg. Chem., 3, 1464 (1964); H. Schroeder, T.L. Heying and J. Reiner, Inorg. Chem., 2, 1092 (1963).

45. J.A. Potenza and W.M. Lipscomb, Inorg. Chem., 3, 1673 (1964); D. Voet and W.N. Lipscomb, Inorg. Chem., 3, 1679 (1964).

46. W.H. Knoth, J. Am. Chem. Soc., 89, 1274 (1967).

47. W.R. Hertler, F. Klanberg and E.L. Muetterties, Inorg. Chem., 6, 1696 (1967).

48. M.F. Hawthorne, Endeavour, 25, 146 (1966).

49. M.F. Hawthorne and T.D. Andrews, Chem. Commun., 443 (1965).

50. W.H. Knoth, J. Am. Chem. Soc., 89, 3342 (1967).

51. R.W. Rudolph, R.L. Voorkees and R.E. Cockoy, J. Am. Chem. Soc., 92, 3351 (1970).

52. K. Wade, Electron Deficient Compounds, ref. 14, p. 169.

53. J.L. Little, J.T. Moran and J.J. Todd, J. Am. Chem. Soc., 89, 5495 (1967).

54. R.E. Rundle, J. Am. Chem. Soc., 73, 4172 (1951).

55. B.D. James and M.G.H. Wallbridge, in Progress in Inorganic Chemistry VII, S.J. Lippard, ed., Wiley, London, 1970, p. 99; B.D. James, R.K. Nauda and M.G.H. Wallbridge, J. Chem. Soc. A, 182 (1966).

56. E.B. Hunt'jun, R.E. Rundle, and A.J. Stosick, Acta Cryst., 7, 106 (1954).

57. A. Rosenheim, V. Samter and J. Davidsohn, Z. Anorg. Chem., 35, 424 (1903).

58. S. Scavnicar and B. Prodic, Acta Cryst., 18, 698 (1965).

59. F.M. Jaeger and F.A. Van Melle, Prod. Acad. Sci. (Amsterdam), 31, 651 (1928).

60. F.C. Frank and J. Kasper, Acta Cryst., 11, 184 (1958).

61. B. Aronsson, T. Lundström and S. Rundqvist, Borides, Silicides and Phosphides, Methuen Press, London, 1965.

62. A.R. Pitochelli and M.F. Hawthorne, J. Am. Chem. Soc., 82, 3228 (1960).

63. H.C. Miller, N.E. Miller and E.L. Muetterties, J. Am. Chem. Soc., 85, 3885 (1963).

64. I.A. Ellis, D.F. Gaines and R. Schaeffer, J. Am. Chem. Soc., 85, 3885 (1963).

65. N.N. Greenwood and G.H. Morris, Proc. Chem. Soc., 338 (1963).

66. C. Harzdorf, H. Niederprüem and H. Odenbach, Z. Naturforsch, B 25, 6 (1970).

67. H.C. Miller, N.E. Miller and E.L. Muetterties, Inorg. Chem., 3, 1456 (1964).

68. R.M. Adams, A.R. Siedle and I. Grant, Inorg. Chem. 3, 461 (1964).

69. E.L. Muetterties, J.H. Balthis, Y.T. Chia, W.H. Knoth and H.C. Miller, Inorg. Chem., 3, 444 (1964).

70. A. Kaczmarczyk and M. Collins, Inorg. Chem, 14, 207 (1975).

71. L.J. Todd, in Progress in Boron Chemistry, Vol. 2, R.J. Brotherton and H. Steinberg, eds., Pergamon Press, Oxford, 1970.

72. J.A. Wunderlich and W.N. Lipscomb, J. Am. Chem. Soc., 82, 4427 (1960).

73. S.I. Uspenskaya, K.A. Solntsev and N.T. Kuznetsov, Zh. Strukt. Kim, 14, 166 (1973).

74. S.I. Uspenskaya, K.A. Solntsev and N.T. Kuznetsov, ibid., 16, 482 (1975).

75. H.C. Longuet-Higgins and M. de V. Roberts, Proc. Roy. Soc. (London) A230, 110 (1955).

76. N. Nakamto, Infrared Spectra of Inorganic Coordination Compounds, Wiley-Intersicence, New York, 1970.

77. E.L. Muetterties, Boron Hybride Chemistry, Academic Press, New York, 1975.

78. A. Kaczmarczyk and G.B. Kolski, Inorg. Chem., 4, 655 (1965).

79. E.L. Muetterties, R.E. Merrifield, H.C. Miller, W.H. Knoth and J.R. Downing, J. Am. Chem. Soc., 84, 2506 (1962).

80. R. Hoffmann and W.N. Lipscomb, J. Chem. Phys., 37, 2872 (1962).

81. W.H. Knoth, H.C. Miller, J.C. Sauer, J.H. Balthis, Y.T. Chia and E.L. Muetterties, Inorg. Chem., 3, 159 (1964).

82. W.H. Knoth, J.C. Sauer, H.C. Miller and E.L. Muetterties, J. Am. Chem. Soc., 86, 115 (1964).

83. W.H. Knoth, J. C. Sauer, J.H. Balthis, H.C. Miller and E.L. Muetterties, J. Am. Chem. Soc., 89, 4842 (1967); W.H. Knoth, J. Am. Chem. Soc., 88, 935 (1966).

84. W.R. Hertler, W.H. Knoth, and E.L. Muetterties, Inorg. Chem., 4, 288 (1965).

85. W.H. Knoth, J.C. Sauer, D.C. England, W.R. Hertler and E.L. Muetterties, J. Am. Chem. Soc., 86, 3973 (1964).

86. W.R. Hertler and M.S. Raasch, J. Am. Chem. Soc., 86, 3661 (1964).

87. W.R. Hertler, Inorg. Chem., 3, 1195 (1964).

88. A.B. Harmon and K.M. Harmon, J. Am. Chem. Soc., 88, 4093 (1966).

89. H.C. Miller, W.R. Hertler, E.L. Muetterties, W.H. Knoth and N.E. Miller, Inorg. Chem., 4, 1216 (1965).

90. S. Trofimenko and H.N. Cripps, J. Am. Chem. Soc., 87, 653 (1965).

91. A.B. Harmon and K.M. Harmon, J. Am. Chem. Soc., 88, 4093 (1966).

92. J.H. Bigelow U.S. Patent 238,480, March 27, 1972.

93. W. Drinkard, U.S. Patent 3,361,541, January 2, 1968.

94. A.H. Soloway, 'Boron Compounds in Cancer Therapy', in Progress in Boron Chemistry, Vol. I, H. Steinberg and A. L. McCloskey, eds., McMillan, New York, 1964, p. 203.